Royal Norwegian Council
for Scientific and Industrial Research
(NTNF)

NORSAR

NORSAR Scientific Report No. 1-89/90

Semiannual Technical Summary

1 April — 30 September 1989

Kjeller, December 1989

UNCLASSIFIED
SECURITY CLASSIFICATION OF THIS PAGE

REPORT DOCUMENTATION PAGE

Form Approved
OMB No. 0704-0188

1a. REPORT SECURITY CLASSIFICATION UNCLASSIFIED	1b. RESTRICTIVE MARKINGS NOT APPLICABLE
2a. SECURITY CLASSIFICATION AUTHORITY NOT APPLICABLE	3. DISTRIBUTION/AVAILABILITY OF REPORT APPROVED FOR PUBLIC RELEASE DISTRIBUTION UNLIMITED
2b. DECLASSIFICATION/DOWNGRADING SCHEDULE NOT APPLICABLE	
4. PERFORMING ORGANIZATION REPORT NUMBER(S) Scientific Rep. 1-89/90	5. MONITORING ORGANIZATION REPORT NUMBER(S) – Scientific Rep. 1-89/90
6a. NAME OF PERFORMING ORGANIZATION NTNF/NORSAR 6b. OFFICE SYMBOL (If applicable)	7a. NAME OF MONITORING ORGANIZATION HQ/AFTAC/TTS
6c. ADDRESS (City, State, and ZIP Code) Post Box 51 N-2007 Kjeller, Norway	7b. ADDRESS (City, State, and ZIP Code) Patrick AFB, FL 32925-6001
8a. NAME OF FUNDING/SPONSORING ORGANIZATION Defence Advanced Research Projects Agency 8b. OFFICE SYMBOL (If applicable) NMRO	9. PROCUREMENT INSTRUMENT IDENTIFICATION NUMBER Contract No. F08606-89-C-0005
8c. ADDRESS (City, State, and ZIP Code) 1400 Wilson Blvd. Arlington, VA 22209-2308	10. SOURCE OF FUNDING NUMBERS PROGRAM ELEMENT NO.: R&D PROJECT NO.: NORSAR PHASE 3 TASK NO: SOW TASK 5.0 WORK UNIT ACCESSION NO.: SEQUENCE No. 003A2
11. TITLE (Include Security Classification) SEMIANNUAL TECHNICAL SUMMARY, 1 APRIL - 30 SEPTEMBER 1989 (UNCLASSIFIED)	
12. PERSONAL AUTHO L.B. Loughran (ed.)	
13a. TYPE OF REPORT SCIENTIFIC SUMMARY 13b. TIME COVERED FROM 1 Apr TO 30 Sep 89	14. DATE OF REPORT (Year, Month, Day) December 1989 15. PAGE COUNT 129
16. SUPPLEMENTARY NOTATION NOT APPLICABLE	
17. COSATI CODES FIELD: 8 / GROUP: 11 / SUB-GROUP:	18. SUBJECT TERMS (Continue on reverse if necessary and identify by block number) NORSAR, NORWEGIAN SEISMIC ARRAY

19. ABSTRACT (Continue on reverse if necessary and identify by block number)

(Please see reverse side)

20. DISTRIBUTION/AVAILABILITY OF ABSTRACT ☐ UNCLASSIFIED/UNLIMITED ☒ SAME AS RPT ☐ DTIC USERS	21. ABSTRACT SECURITY CLASSIFICATION UNCLASSIFIED
22a. NAME OF RESPONSIBLE INDIVIDUAL MR. LEE BRIDGES	22b. TELEPHONE (Include Area Code) (407) 494-7765 22c. OFFICE SYMBOL AFTAC/TTS

DD Form 1473, JUN 86 *Previous editions are obsolete* SECURITY CLASSIFICATION OF THIS PAGE

Abstract

This Semiannual Technical Summary describes the operation, maintenance and research activities at the Norwegian Seismic Array (NORSAR), the Norwegian Regional Seismic Array (NORESS) and the Arctic Regional Seismic Array (ARCESS), for the period 1 April - 30 September 1989.

The NORSAR Detection Processing system has been operated throughout the period with an average uptime of 94.9 as compared to 98.2 for the previous reporting period. A total of 1908 seismic events have been reported in the NORSAR monthly seismic bulletin. The performance of the continuous alarm system and the automatic bulletin transfer by telex to AFTAC has been satisfactory. Processing of requests for full NORSAR/NORESS data on magnetic tapes has progressed according to established schedules.

The satellite link for transmitting NORESS data in real time to the U.S. has had an average uptime of 97.8% as compared to 99.9% for the previous period. On-line detection processing and data recording at the NORSAR Data Center (NDPC) of NORESS and ARCESS data have been conducted throughout the period, with an average uptime of 92.1% for NORESS and 92.2% for ARCESS.

Field maintenance activity has included regular preventive maintenance at all array sites and occasional corrective actions when required. All the NORSAR communications systems have been checked during the period, and although there have been some irregularities in connection with 01A, 02C and 06C, the performance has been satisfactory. Modcomp problems began at the end of August and fault finding continued throughout the rest of the reporting period.

Various alternatives for a possible future upgrade of the NORSAR system have been considered during the period. The NORSAR Detection Processing has been transferred to a more powerful IBM computer which became available after moving NORESS to a SUN-system. There have been no changes in the routine processing of NORSAR events.

The routine detection processing of NORESS is running satisfactorily on a dedicated SUN-3/280. Event processing, which can be performed on any of the SUN workstations, is performed in two steps: (i) Phase estimation, and (ii) plot and epicenter determination. The routine detection processing of ARCESS is also running satisfactorily on a separate SUN-3/280. Event processing for ARCESS is identical to that of NORESS.

The "generalized beamforming" method, which has been developed at NORSAR and represents a new approach to associate detected seismic phases from a regional or global network, has been further tested. A data base of 77 regional and local seismic events recorded by NORESS and ARCESS has been used, and the results have been compared to output of the Assess procedure in the Intelligent Monitoring System (IMS). We have found that the generalized beamforming method matches or exceeds the Assess results as far as phase grouping is concerned and that the epicenter determinations are also quite accurate. It is concluded that the new method would be useful to supplement expert systems techniques. The recommended approach is to use it as a pre-processor, and subsequently invoke rule-based and script-based algorithms in order to further refine the solutions.

NORSAR RMS Lg magnitude measurements as published in previous Semiannual reports have been compared to yield data recently published by Soviet scientists for Shagan River explosions. The correspondence appears to be excellent, and considerably better than the correspondence between world-wide m_b and these yield estimates. However, only a few large events have been available for this study and more data will be needed before firm conclusions may be drawn. Based on these same yield data, and analyzing the smallest explosions available, it appears that during normal noise conditions the NORSAR P-wave detection threshold for fully coupled Semipalatinsk explosions is below 1 kt, even at the single sensor level. Additional significant improvement would be obtainable through array processing of these data.

The stability of RMS Lg magnitudes of Semipalantinsk explosions as a function of azimuth and distance has been further studied by analyzing data from the China Digital Seismograph Network (CDSN). Data from the stations WMQ and HIA have been processed for a total of 12 explosions and compared to NORSAR M(Lg). The resulting scatter in the magnitude measurements is very small, and indicates that single station M(Lg) may be measured with an accuracy (one standard deviation) of 0.03–0.04 magnitude units. This corroborates previous results comparing data from NORSAR and IRIS stations in the Soviet Union. Furthermore, Lg detectability is excellent for these two CDSN stations. Thus the station WMQ, which is situated at 960 km from Semipalatinsk, has an Lg detection threshold estimated at 2 magnitude units lower than that of NORSAR.

A new data acquisition system for the FINESA array in Finland has been developed at NORSAR, and installed in cooperation with the University of Helsinki. This system enables real time acquisition and processing of data from the 15 SPZ seismometers of the array both at Helsinki and at the NORSAR data center. Initial on-line processing has been established both in Finland and Norway, and data quality appears very satisfactory. The FINESA data are currently being prepared for integration into the Intelligent Monitoring

System, along with data from NORESS, ARCESS and the GERESS system under development. Initially, the beam deployment for FINESA has been adapted from the NORESS/ARCESS deployments, and the real time processing methodology is essentially identical.

A project to establish a mining explosion data base for Fennoscandia and adjacent regions has been initiated. A questionnaire requesting information on mine locations, charge sizes, firing practices as well as details of individual explosions after 1984 has initially been submitted to 67 organizations and companies known to conduct mining activities. So far, responses have been obtained from 16 companies, and the available information is being compiled into a data base conforming to the 2.8 CSS format. The data base will be continually updated and expanded as more information is obtained, and the aim is to map mining activity in Fennoscandia as well as Central Europe and Western USSR. This knowledge will ultimately be of great value in the regular analysis of array data, and will also be the basis for addressing a range of interesting and important topics within seismological verification research.

A study has been conducted modelling the transverse components of Lg waves and relating the synthetic seismograms to refraction data observed at NORSAR. It is shown that an upper crust with a uniform distribution of microcracks aligned in the regional stress field can account for transverse components of Lg waves induced by explosions. The preferred model to explain this in terms of upper crustal anisotropy is a distribution of liquid-filled cracks in the upper 10 km of the crust with a crack density larger than 0.02 and most favorably around 0.05. This model is consistent with previously published observations of shear wave splitting in northern Scandinavia.

A study addressing statistical procedures for seismic signal detection and estimation using small-array data has been undertaken. A generalization of Capon's maximum likelihood technique for detection and estimation of seismic signals is introduced. By using multidimensional autoregressive approximation of array seismic noise, Capon's group filter can be implemented for on-line processing. Such autoregressive adaptation to the current noise matrix power spectrum yields good suppression of mutually correlated array noise processes. An example is shown of this technique as applied to detection of a small underground explosion (Semipalatinsk, December 28, 1988) recorded at the ARCESS array.

AFTAC Project Authorization	: T/9141/B/PKP
ARPA Order No.	: 4138 AMD # 16
Program Code No.	: 0F10
Name of Contractor	: Royal Norwegian Council for Scientific and Industrial Research
Effective Date of Contract	: 1 Oct 1988
Contract Expiration Date	: 30 Sep 1989
Project Manager	: Frode Ringdal (06) 81 71 21
Title of Work	: The Norwegian Seismic Array (NORSAR) Phase 3
Amount of Contract	: $ 1,902,447
Contract Period Covered by Report	: 1 Apr - 30 Sep 1989

This research was supported by the Advanced Research Projects Agency of the Department of Defense and was monitored by AFTAC, Patrick AFB, FL 32925, under contract no. F08606-89-C-0005.

NORSAR Contribution No. 414

Contents

1 Summary

This Semiannual Technical Summary describes the operation, maintenance and research activities at the Norwegian Seismic Array (NORSAR), the Norwegian Regional Seismic Array (NORESS) and the Arctic Regional Seismic Array (ARCESS) for the period 1 April – 30 September 1989.

The NORSAR Detection Processing system has been operated throughout the period with an average uptime of 94.9 as compared to 98.2 for the previous reporting period. A total of 1908 seismic events have been reported in the NORSAR monthly seismic bulletin. The performance of the continuous alarm system and the automatic bulletin transfer by telex to AFTAC has been satisfactory. Processing of requests for full NORSAR/NORESS data on magnetic tapes has progressed according to established schedules.

The satellite link for transmitting NORESS data in real time to the U.S. has had an average uptime of 97.8% as compared to 99.9% for the previous period. On-line detection processing and data recording at the NORSAR Data Center (NDPC) of NORESS and ARCESS data have been conducted throughout the period, with an average uptime of 92.1% for NORESS and 92.2% for ARCESS.

Various alternatives for upgrading the NORSAR system have been considered during the period. The Nanometrics system used at Yellowknife and Hagfors in Sweden has features which seem to make it suitable for an upgrade of the NORSAR array. The NORSAR Detection Processing has been transferred to a more powerful IBM computer which became available after moving NORESS to a SUN-system. There have been no changes in the routine processing of NORSAR events.

The routine detection processing of NORESS is running satisfactorily on a dedicated SUN-3/280. Event processing, which can be performed on any of the Sun workstations, is performed in two steps: Phase estimation, and plot and epicenter determination. The routine detection processing of ARCESS is also running satisfactorily on a separate SUN-3/280. Event processing for ARCESS is identical to that of NORESS.

The research activity is summarized in Section 7. Section 7.1 presents a performance test of the generalized beamforming method applied to a data base of regional events. Section 7.2 discusses NORSAR P-wave detection and yield estimation of selected Semipalatinsk explosions. Section 7.3 presents an analysis of data from the Chinese Digital Seismograph Network for Soviet nuclear explosions. Section 7.4 describes a new data acquisition system for FINESA. Establishment of a mining explosion data base is presented in section 7.5. In section 7.6, transverse components of explosion-induced Lg waves and upper crustal anisotropy are discussed. Section 7.7 discusses statistically optimal event detection using small array data.

2 Operation of all Systems

2.1 Detection Processor (DP) Operation

There have been 93 breaks in the otherwise continuous operation of the NORSAR online system within the current 6-month reporting interval. The uptime percentage for the period is 94.9 as compared to 98.2 for the previous period.

Fig. 2.1.1 and the accompanying Table 2.1.1 both show the daily DP downtime for the days between 1 April and 30 September 1989. The monthly recording times and percentages are given in Table 2.1.2.

The breaks can be grouped as follows:

a)	Hardware failure	46
b)	Stops related to program work or error	2
c)	Hardware maintenance stops	11
d)	Power jumps and breaks	0
e)	TOD error correction	20
f)	Communication lines	14

The total downtime for the period was 225 hours and 46 minutes. The mean-time-between-failures (MTBF) was 1.9 days, as compared to 1.8 for the previous period.

J. Torstveit

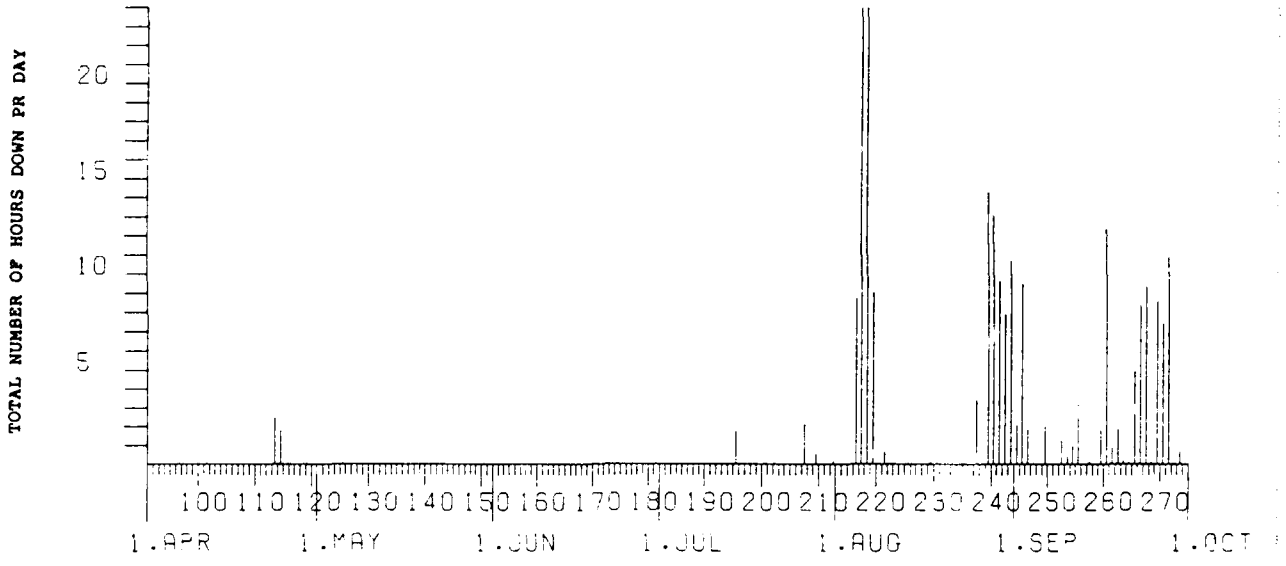

Fig. 2.1.1 Detection Processor downtime in the period 1 April – 30 September 1989.

LIST OF BREAKS IN DP PROCESSING THE LAST HALF-YEAR

DAY	START		STOP		COMMENTS.....
93	10	34	10	35	TOD RETARED 14MS
101	6	11	6	12	TOD RETARED 22MS
113	6	6	8	29	2701 FAILURE
113	9	34	9	42	2701 FAILURE
114	10	45	12	36	2701 FAILURE
118	6	0	6	1	TOD RETARED 20MS
122	6	40	6	41	LINE FAILURE
122	7	48	7	49	LINE FAILURE
123	12	5	12	6	LINE FAILURE
128	6	4	6	5	TOD RETARED 22MS
132	6	1	6	2	TOD RETARED 12MS
139	6	3	6	4	TOD RETARED 12MS
145	6	1	6	2	TOD RETARED 22MS
153	6	1	6	2	TOD RETARED 11MS
157	6	12	6	13	TOD RETARED 12MS
163	6	27	6	28	TOD RETARED 22MS
172	9	24	9	25	LINE FAILURE
172	11	6	11	10	TOD RETARED 20MS
174	6	10	6	12	LINE FAILURE
174	9	55	9	57	LINE FAILURE
177	6	54	6	55	TOD RETARED 25MS
177	7	24	7	25	LINE FAILURE
180	9	42	9	43	TOD RETARED 23MS
186	5	10	5	11	LINE FAILURE
187	5	9	5	10	LINE FAILURE
187	6	1	6	2	TOD RETARED 23MS
195	6	0	7	45	LINE FAILURE
207	15	7	17	15	CE MAINTENANCE
209	7	31	8	5	MACHINE ERROR
212	8	41	8	42	TOD RETARED 30MS
212	8	49	8	54	LINE FAILURE
212	8	58	9	4	LINE FAILURE
212	9	10	9	12	LINE FAILURE
216	15	15	24	0	MODCOMP FAILURE
217	0	0	24	0	MODCOMP FAILURE
218	0	0	24	0	MODCOMP FAILURE
219	0	0	9	0	MODCOMP FAILURE
219	9	48	9	52	LINE FAILURE
221	13	42	14	21	MODCOMP FAILURE
222	7	50	7	53	TOD RETARED 22MS
228	6	9	6	11	TOD RETARED 13MS
229	7	44	8	15	CE MAINTENANCE
230	8	55	9	3	CPU FAILURE
234	6	6	6	8	TOD RETARED 23MS
237	3	41	7	4	MODCOMP FAILURE
239	5	38	19	33	MODCOMP FAILURE
239	23	36	24	0	MODCOMP FAILURE
240	0	0	6	34	MODCOMP FAILURE
240	9	20	10	55	MODCOMP FAILURE
240	19	2	24	0	MODCOMP FAILURE
241	0	0	5	22	MODCOMP FAILURE
241	6	31	9	40	MODCOMP FAILURE
241	11	47	12	55	MODCOMP FAILURE
242	3	28	5	16	MODCOMP FAILURE
242	11	53	12	15	MODCOMP FAILURE
242	12	45	12	51	MODCOMP FAILURE
242	17	10	18	9	MODCOMP FAILURE
242	18	30	19	0	MODCOMP FAILURE
242	19	49	24	0	MODCOMP FAILURE
243	0	0	10	43	MODCOMP FAILURE
244	21	53	24	0	MODCOMP FAILURE
245	0	0	9	30	MODCOMP FAILURE
246	16	0	17	53	MODCOMP FAILURE
247	11	2	11	3	TEST DISK
247	12	15	12	18	TEST DISK
249	10	5	12	5	CE SERVICE MODC.
251	6	10	6	11	TOD RETARED 23MS
252	14	18	15	10	MODCOMP FAILURE
252	22	1	22	26	MODCOMP FAILURE
253	17	51	18	15	MODCOMP FAILURE
254	6	3	6	36	MODCOMP FAILURE
254	15	45	16	10	MODCOMP FAILURE
255	0	22	2	30	MODCOMP FAILURE
255	5	8	6	7	MODCOMP FAILURE
255	8	5	8	11	CE SERVICE MODC.
257	9	4	9	12	MODCOMP FAILURE
259	22	9	24	0	MODCOMP FAILURE
260	0	0	12	24	MODCOMP FAILURE
261	15	10	15	51	MODCOMP FAILURE
261	17	11	17	22	MODCOMP FAILURE
262	5	15	5	50	MODCOMP FAILURE
262	7	0	7	34	MODCOMP FAILURE
262	11	54	12	37	CE SERVICE MODC.
263	6	1	6	3	TOD RETARED 28MS
263	15	53	16	4	MODCOMP FAILURE
264	12	47	12	52	CE SERVICE MODC.
265	19	0	24	0	MODCOMP FAILURE
266	0	0	8	30	MODCOMP FAILURE
267	0	10	8	10	MODCOMP FAILURE
267	10	36	12	0	MODCOMP FAILURE
268	12	38	12	55	CE SERVICE MODC.
269	2	22	4	8	MODCOMP FAILURE
269	12	13	12	49	MODCOMP FAILURE
269	13	13	13	43	MODCOMP FAILURE
269	13	57	14	18	MODCOMP FAILURE
269	15	5	16	40	CE SERVICE MODC.
269	20	8	24	0	MODCOMP FAILURE
270	0	0	6	17	MODCOMP FAILURE
270	8	48	9	7	CE SERVICE MODC.
270	20	7	20	59	MODCOMP FAILURE
271	8	34	19	30	CE SERVICE MODC.
272	9	18	9	23	CE SERVICE CPU
273	23	16	23	59	MODCOMP FAILURE

Table 2.1.1 Daily DP downtime in the period 1 April - 30 September 1989.

Month	DP uptime hours	DP uptime %	No. of DP breaks	No. of days with breaks	DP MTBF* (days)
APR	715.60	99.4	6	5	4.3
MAY	743.88	99.9	7	6	3.9
JUN	719.75	99.9	10	7	2.7
JUL	741.27	99.4	10	6	2.8
AUG	617.67	83.0	21	16	1.2
SEP	630.10	87.5	39	26	0.7
		94.9	93	66	1.9

*Mean-time-between-failures = total uptime/no. of up intervals.

Table 2.1.2 Online system performance, 1 April - 30 September 1989.

2.2 Array communications

General

Table 2.2.1 reflects the performance of the communications system throughout the reporting period.

The comm. adapter 2701 SDAII failed in April, causing "garbled" data between the IBM 4341 and the Modcomp. Already the next day (24 April) the fault was found and the systems were started again. Although irregularities in connection with 01A, 02C and 06C occurred, the performance of the comm. systems may be characterized as most satisfactory.

In May 02B power problems started in connection with lightning in the area. NTA carrier systems affected 01B, 03C, 04C and 06C.

June was characterized by many outages. Specially 02B and 06C were affected. 02B lost power after lightning, and 06C had SLEM problems. Besides, NTA transmission system (in Oslo) affected all subarrays.

Also in July most subarrays were affected (-01A, 01B), 02B by lightning (as usual), 02C by a broken cable. 03C, 04C and 06C were affected by NTA cable work (planned).

Modcomp problems started in August (25), and 02B had been down since 28 July due to power outages. Estimated comm. error figures were calculated while the Modcomp was down.

In September Modcomp fault findings continued. 01A was affected by a broken comm. cable (week 38). 02C was affected week 39, and 06C by excessive error rate (week 36). Estimated average error figures for each comm. system were calculated during Modcomp stops.

Detailed summary

April (weeks 14-17), 3-30.4.89

Week 16 01A and 02C were affected by comm. line irregularities. 06C was down week 17, reason not stated. 23 April the comm. adapter IBM 2701 SDAII failed causing "garbled" data transfer between the IBM 4341 and the Modcomp. 24 April a bad card was found and the system started again.

May (weeks 18-22), 1.5-4.6.89

02B power affected after lightning (week 19). Local power company repaired the damage 19 May. 22 May the subarray was visited by NMC staff and the SLEM was reset. 01B, 04C and 06C were also affected week 20, 01B by 3.6%, 04C and 06C approx. 10.7%. NTA carrier equipment was the probable reason.

An increasing number of resynchronizations were observed over several days. NTA/Lillestrøm confirmed carrier equipment instability and the problem was solved (week 21). 25 May the same problem was observed, and all subarrays were affected. NTA found a 60-channel group in Oslo was faulty. 1 June a coaxial cable carrying 03C and 04C data was damaged. 06C and the satellite control line between Eik earth station and NORESS were also affected. NTA/Hamar switched 03C,04C comm. paths to a spare coax carrier system.

June (weeks 23-26), 5.6-2.7.89

02B was out of operation from 5 June, and resumed operation 14 June after SLEM reset. Faulty transmission system in Oslo affected all comm. systems 11 June. A faulty transmission system between Oslo and Hamar affected 02B, 03C, 04C and 06C 23 June. 02B was down approx. 20 hours between 21 and 22 June, and went down again 30 June. It remained down throughout the week (26). 22 June we lost contact with the subarray. 29 June the subarray resumed operation.

July (weeks 27-30), 3-30.7.89

02B, which went down 30 June due to lightning in the area, was turned on 5 July after SLEM reset. 28 July the subarray was affected again by a power outage, caused by lightning, and remained down throughout the month. 02C was affected 4 July due to a broken cable. 03C,04C and 06C were affected 5 and 6 July in connection with planned NTA/Hamar cable work.

August (weeks 31-35), 31.7-3.9.89

02B was turned on 2 August after having been down since 28 July. The Modcomp reliability was reduced since 25 August, with many stops. Per 31 August TM-data, responsible for corrective/preventive maintenance of the machine, had not been able to find the items causing the stops. The performance of the comm. systems (excl. the Modcomp) was in the period most satisfactory, and estimated average error figures for the systems while Modcomp was stopped were calculated.

September (weeks 36-39), 4.9-1.10.89

Modcomp fault finding continued in September in spite of TM-data's efforts to solve the problem. The next step will be to analyze the CPU microcodes. As far as comm. systems are concerned, 01A was affected by a broken comm. cable week 38. 02C was down week 39 of unknown reason. Excessive error rate could be observed week 36 in connection with 06C. During the Modcomp stop periods, estimated average error figures were calculated for each subarray comm. system.

O.A. Hanson

Sub-arrays	Apr (4) 3-30.4	May (5) 1.5-4.6	Jun (4) 5.6-2.7	Jul (4) 3-30.7	Aug (5) 31.7-3.9	Sep (4) 4.9-1.10	Average 1/2 Year
01A	*0.5100	0.030	*1.370	0.020	0.007	[10]*0.050	0.330
01B	0.0002	*0.770	*1.390	*0.060	0.002	0.001	0.370
02B	0.0040	[1]*0.004	[2]*N/A	[4]*0.020	[9]*0.003	0.004	[13]0.007
02C	*0.4400	0.030	*0.930	[5]*0.020	0.003	[11]*0.002	0.240
03C	0.0040	0.390	*6.730	[6]*0.020	0.007	0.003	1.190
04C	0.0010	*2.540	*2.710	[7]*0.030	0.004	0.002	0.630
06C	0.1600	*2.950	[3]N/A	[8]*1.230	0.002	[12]*0.060	[14]0.880
AVER	0.1600	0.960	2.630	0.200	0.004	0.020	0.560
Less			02B,06C				

*See Section 2.2 regarding figures preceded by an asterisk.

Figures representing error rate (in per cent) preceded by a number 1), 2), etc., are related to legend below.

1) Power outages weeks 19-22
2) Power outages weeks 23-26
3) Outages weeks 23-26 (faulty SLEM)
4) Average 2 weeks (28,29), 27,30 N/A
5–8) Average 3 weeks (28,29,30), 27 N/A
9) Average 4 weeks (32-35), 31 N/A
10) Average 3 weeks (36-38), 39 N/A
11) Average 3 weeks (36-38), 39 N/A
12) Average 3 weeks (36-38), 39 N/A
13) Average 5 months, weeks 23-26 N/A
14) Average 5 months, weeks 23-26 N/A

Table 2.2.1 Communications performance. The numbers represent error rates in per cent based on total transmitted frames/week (1 April – 30 September 1989).

2.3 Event Detection operation

In Table 2.3.1 some monthly statistics of the Detection and Event Processor operation are given. The table lists the total number of detections (DPX) triggered by the on-line detector, the total number of detections processed by the automatic event processor (EPX) and the total number of events accepted after analyst review (Teleseismic phases, core phases and total).

	Total	Total	Accepted events			
	DPX	EPX	P-phases	Core phases	Sum	Daily
Apr 89	8900	1203	302	62	364	12.1
May 89	8250	1217	291	92	383	12.4
Jun 89	7325	1286	222	55	277	9.2
Jul 89	7350	1070	244	53	297	9.6
Aug 89	5800	980	254	60	314	10.1
Sep 89	9450	1412	221	52	273	9.1
			1534	374	1908	10.4

Table 2.3.1. Detection and Event Processor statistics, 1 April - 30 September 1989.

B.Kr. Hokland

3 Operation of NORESS and ARCESS

3.1 Satellite transmission of NORESS data to the U.S.

The satellite transmission of data to the U.S. from the NORESS field installation was interrupted on 16 occasions, as shown in Table 3.3.1. Only one outage period was due to failure of the ground station equipment.

25	May	1649	to	1713	Power failure due to thunderstorm
1	Jun	1055	to	1145	Control lines down
7	Jun	0202	to	0416	Power failure
9	Jun	0844	to	0945	Power failure
13	Jun	2235	to 14 Jun	0152	Power failure
21	Jun	0930	to	1225	Power failure due to thunderstorm
21	Jun	2227	to	2229	Control lines down
22	Jun	2332	to	2334	Control lines down
23	Jun	2046	to 24 Jun	0810	Satellite modem down
29	Jun	0926	to	1059	Power failure due to thunderstorm
29	Jun	1616	to	1834	Power failure due to thunderstorm
29	Jun	1900	to	1941	Power failure due to thunderstorm
23	Jul	1611	to 26 Jul	1118	Power failure due to thunderstorm
26	Jul	1229	to	1339	Repair work due to thunderstorm
31	Jul	2004	to	2151	Control lines down
1	Aug	0136	to	0139	Control lines down

Table 3.1.1 Outage periods for NORESS satellite transmission system April - September 1989.

The total uptime for the NORESS Earth Station for satellite transmission of data to the U.S. was 97.8% as compared to 99.9% for the previous period.

The ground station for continuous transmission of NORESS data to the U.S. was closed down on 1 October 1989. From this date, NORESS and ARCESS data can be obtained in the U.S. at the Center for Seismic Studies (CSS), using the new dedicated satellite link established between NDPC and CSS.

3.2 Recording of NORESS data at NDPC, Kjeller

Table 3.2.1 lists the main outage times and reasons. As can be seen, the main reasons for the outage are power failures at the HUB and line failures.

The average recording time was 92.1% as compared to 98.5% for the previous period.

Date	Time	Cause
25 May	1654-1817	Power failure HUB due to thunderstorm
7 Jun	0208-0549	Power failure HUB due to thunderstorm
9 Jun	0553-0601	Power failure HUB due to thunderstorm
9 Jun	0852-0915	Power failure HUB due to thunderstorm
13 Jun	2243-	Power failure HUB due to thunderstorm
14 Jun	-0608	Power failure HUB due to thunderstorm
20 Jun	0726-0736	Transmission line failure
21 Jun	0931-1447	Power failure HUB due to thunderstorm
23 Jun	0832-0909	Transmission line failure
29 Jun	0531-0542	Power failure HUB
29 Jun	0935-1148	Power failure HUB
29 Jun	1440-1606	Power failure HUB
30 Jun	0706-0720	Transmission line failure
3 Jul	0501-1238	Power failure HUB
4 Jul	0855-1225	Transmission line failure
7 Jul	1334-	Transmission line failure
8 Jul	-1223	Transmission line failure
13 Jul	1105-1234	Transmission line failure
16 Jul	0949-1336	Power failure HUB
19 Jul	0611-0622	Transmission line failure
23 Jul	1655-	Power failure HUB due to thunderstorm
3 Aug	-1628	Power failure HUB due to thunderstorm
18 Aug	1231-1255	Hardware failute at NDPC
3 Sep	0626-0831	Power failure HUB
20 Sep	1255-1333	Hardware maintenance at NDPC
20 Sep	1621-1732	Transmission line failure

Table 3.2.1 Interruptions in NORESS recordings at NDPC, April–September 1989.

Monthly uptimes for the Noress on-line data recording task, taking into account all factors (field installations, transmissions line, data center opera-

tion) affecting this task were as follows:

April	:	99.6%
May	:	99.8%
June	:	96.8%
July	:	68.2%
August	:	88.5%
September	:	99.4%

Fig. 3.2.1 shows the uptime for the data recording task, or equivalently, the availability of NORESS data in our tape archive, on a day-by-day basis, for the reporting period.

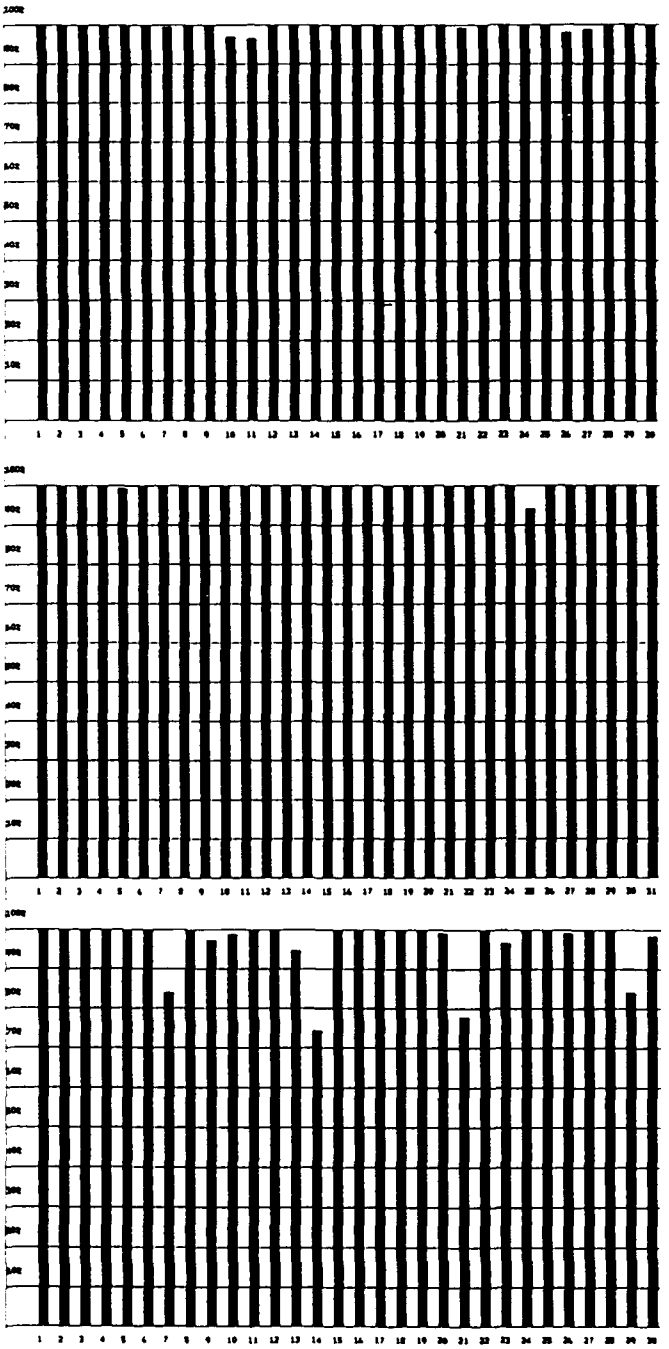

Fig. 3.2.1 NORESS data recording uptime for April (top), May (middle) and June (bottom) 1989.

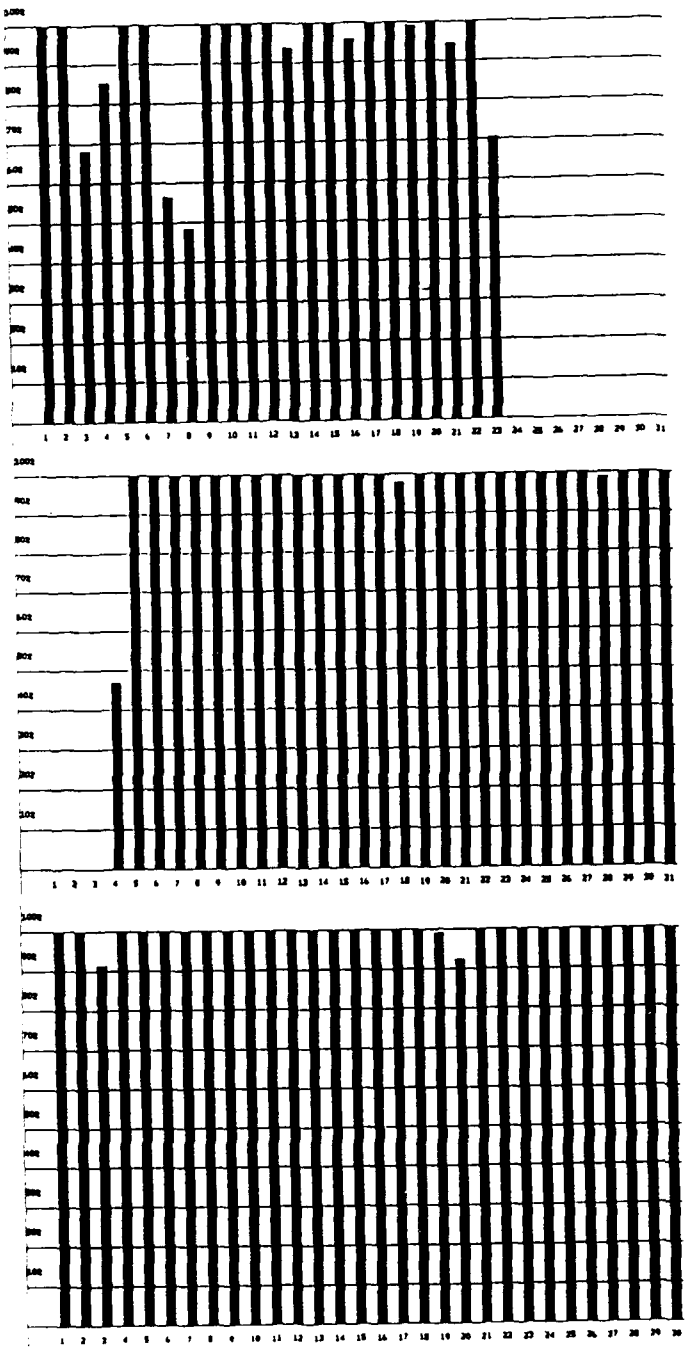

Fig. 3.2.1 NORESS data recording uptime for July (top), August (middle) and September (bottom) 1989.

3.3 Recording of ARCESS data at NDPC, Kjeller

The main reasons causing most of the ARCESS outage in the period are: Hardware failure at NDPC, transmission failure, and maintenance work. A bad cable was found causing most of the hardware failures at NDPC in the period.

The average recording time was 92.2% as compared to 98.5% for the previous period.

Date	Time	Duration	Cause
18 Apr	0209-0508		Hardware failure at NDPC
18 Apr	2100-		Hardware failure at NDPC
19 Apr	-0517		Hardware failure at NDPC
1 May	1040-1122		Hardware failure at NDPC
3 May	0600-0725		Hardware failure at NDPC
18 May	0720-1603		Hardware work at NDPC
18 May	1618-1658		Maintenance at NDPC
30 May	0904-1334		Change of transmission satelite
2 Jun	1200-1252		Maintenance at HUB
9 Jun	0646-0707		Maintenance at HUB
13 Jun	0016-0517		Hardware failure at NDPC
17 Jun	2245-		Transmission line failure
18 Jun	-0057		Transmission line failure
19 Jun	0358-0505		Hardware failure at NDPC
6 Jul	1418-		Hardware failure at NDPC
7 Jul	-0608		Hardware failure at NDPC
11 Jul	0537-0627		Hardware failure at NDPC
11 Jul	0719-0739		Hardware failure at NDPC
12 Jul	2205-		Transmission line failure
13 Jul	-0434		Transmission line failure
13 Jul	0627-0643		Hardware failure at NDPC
15 Jul	0540-		Satellite modem failure
21 Jul	-0141		Satellite modem failure
28 Jul	0741-0902		Hardware failure at NDPC
4 Aug	1301-1358		Hardware failure at NDPC
10 Aug	0317-0529		Hardware failure at NDPC
16 Aug	0844-0904		Hardware failure at NDPC
16 Aug	0929-0944		Hardware failure at NDPC
16 Aug	2015-2031		Hardware failure at NDPC
16 Aug	2054-		Hardware failure at NDPC
17 Aug	-0504		Hardwarw failure at NDPC

17 Aug	0717-0736	Hardware failure at NDPC
24 Aug	0040-0520	Hardware failure at NDPC
24 Aug	1627-	Hardware failure at NDPC
25 Aug	-0516	Hardware failure at NDPC
26 Aug	0936-	Transmission line failure
27 Aug	-1909	Transmission line failure
4 Sep	1250-1332	Maintenance at HUB
8 Sep	1233-1704	Maintenance at NDPC
12 Sep	0653-	Maintenance at antenna at NDPC
13 Sep	-0638	Maintenance at antenna at NDPC
13 Sep	0837-1009	Maintenance at antenna at NDPC
13 Sep	1355-1433	Maintenance at antenna at NDPC
14 Sep	0720-1540	Maintenance at antenna at NDPC
15 Sep	1023-1106	Adjusting the antenna at NDPC
17 Sep	0324-1136	Hardware failure at NDPC
24 Sep	1036-1200	Hardware failure at NDPC

Table 3.3.1 The main interruptions in ARCESS recordings at NDPC, April-September 1989.

Monthly uptimes for the ARCESS on-line data recording task, taking into account all factors (field installations, transmissions line, data center operation) affecting this task were as follows:

April	:	98.4%
May	:	97.8%
June	:	98.7%
July	:	77.8%
August	:	89.3%
September	:	91.3%

Fig. 3.3.1 shows the uptime for the data recording task, or equivalently, the availability of ARCESS data in our tape archive, on a day-by-day basis, for the reporting period.

J. Torstveit

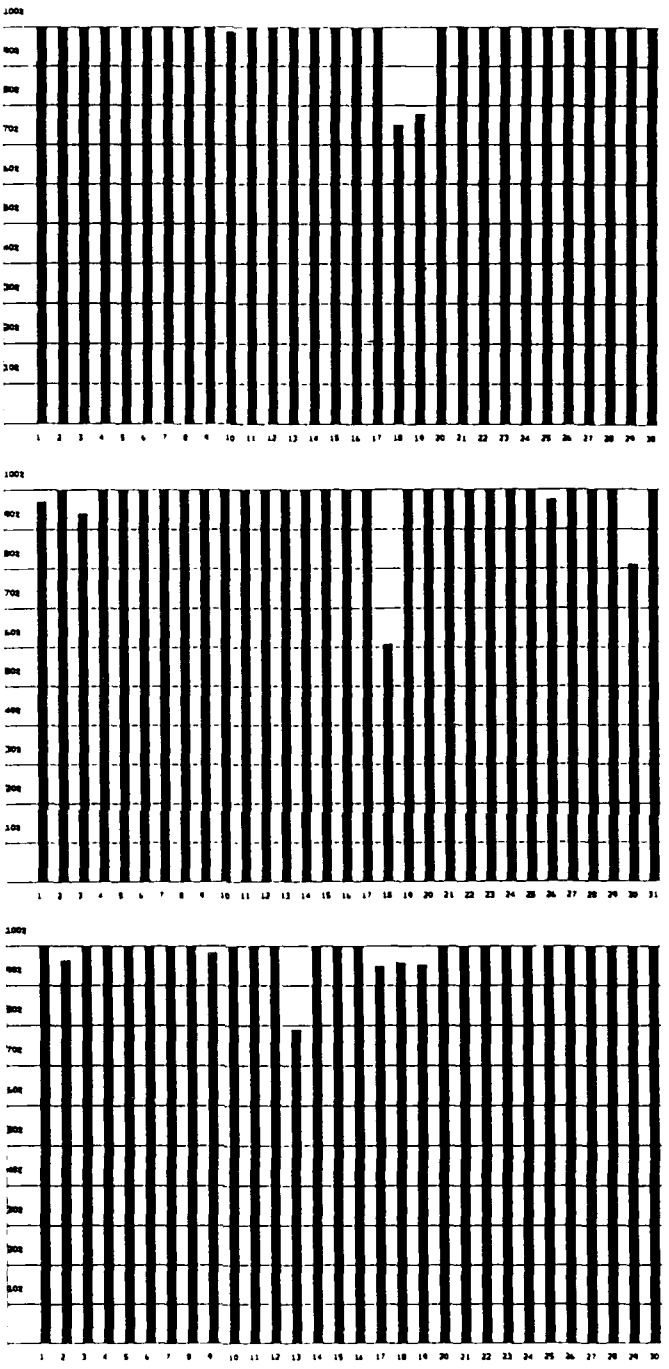

Fig. 3.3.1 ARCESS data recording uptime for April (top), May (middle) and June (bottom) 1989.

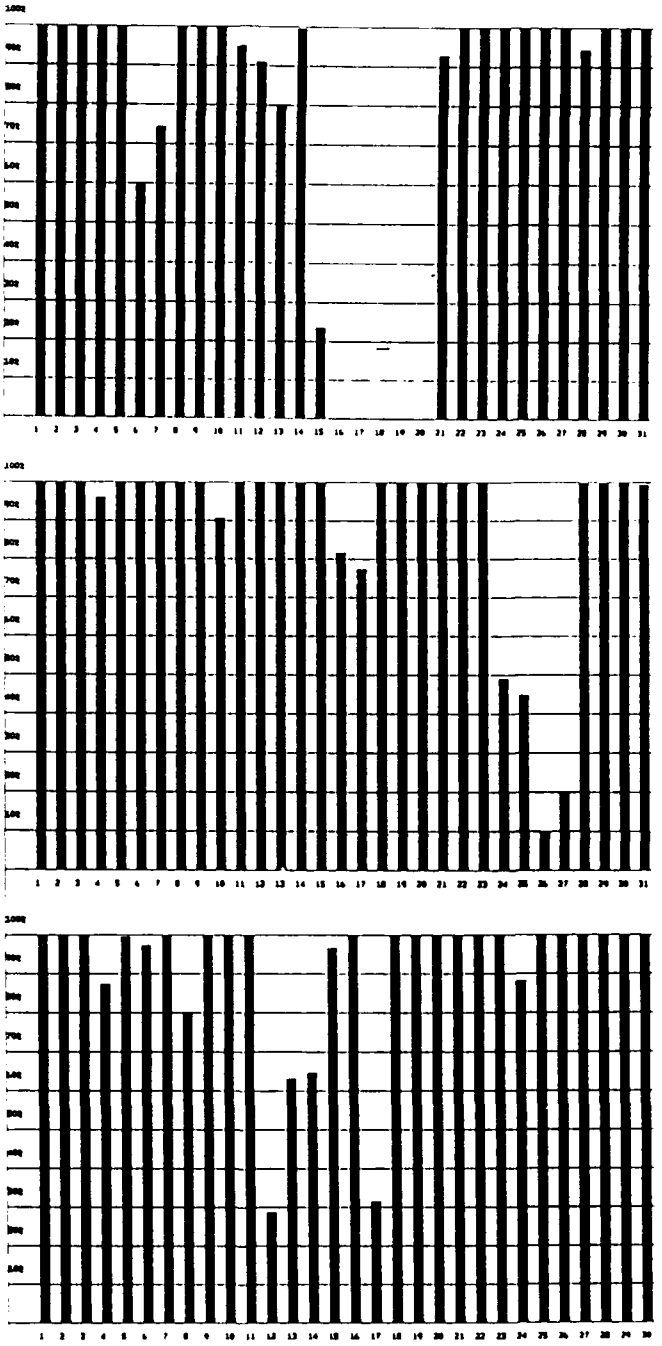

Fig. 3.3.1 ARCESS data recording uptime for July (top), August (middle) and September (bottom) 1989.

3.4 Event detection operation

NORESS detections

The number of detections (phases) reported during day 091, 1989 through day 273,1989 was 38803, giving an average of 246 detections per processed day. During this period, 25 days were not processed due to NORESS downtime (see paragraph 2.2).

Table 3.4.1 shows daily and hourly distribution of detections for NORESS.

Events automatically located by NORESS

During days 091 through 273, 2166 local and regional events were located by NORESS, based on automatic association of P- and S-type arrivals. This gives an average of 13.7 events per processed day (158 days processed). 66 % of these events are within 300 km, and 87 % of these events are within 1000 km.

ARCESS detections

The number of detections (phases) reported during day 091, 1989 through day 273,1989 was 56375, giving an average of 348 detections per processed day. During this period, 21 days were not processed (see paragraph 2.3).

Table 3.4.2 shows daily and hourly distribution of detections for ARCESS.

Events automatically located by ARCESS

During days 091 through 273, 2732 local and regional events were located by ARCESS, based on automatic association of P- and S-type arrivals. This gives an average of 16.9 events per processed day (162 days processed). 45 % of these events are within 300 km, and 78 % of these events are within 1000 km.

J. Fyen

NRS .FKX Hourly distribution of detections

Day	00	01	02	03	04	05	06	07	08	09	10	11	12	13	14	15	16	17	18	19	20	21	22	23	Sum	Date		
91	6	4	11	5	7	4	2	1	6	5	10	2	0	1	2	0	2	5	0	0	2	5	10	7	97	Apr 01	Saturday	
92	5	6	6	5	4	13	7	2	2	4	5	4	0	1	0	0	2	7	0	1	6	26	8	19	133	Apr 02	Sunday	
93	9	21	20	38	11	9	6	3	2	3	5	5	7	12	18	8	2	15	4	21	0	1	2	17	239	Apr 03	Monday	
94	6	13	9	7	4	6	10	1	13	15	6	19	12	10	11	10	9	7	6	7	7	0	4	32	224	Apr 04	Tuesday	
95	2	11	16	14	5	5	4	4	1	11	11	25	10	9	14	13	4	12	8	3	0	2	7	23	214	Apr 05	Wednesday	
96	8	3	16	13	5	2	17	3	11	5	4	14	10	15	10	10	0	6	4	7	0	3	6	22	194	Apr 06	Thursday	
97	6	0	10	8	0	2	1	2	4	9	11	4	7	16	4	11	1	8	6	8	2	5	0	22	147	Apr 07	Friday	
98	15	10	12	10	9	4	2	7	4	15	14	3	0	2	4	7	9	11	1	9	1	0	3	3	155	Apr 08	Saturday	
99	4	0	8	3	12	6	2	5	1	17	8	1	1	2	2	4	1	18	4	3	1	5	2	13	123	Apr 09	Sunday	
100	1	5	18	3	4	2	0	7	5	7	12	9	11	4	7	6	10	8	4	5	2	5	3	10	148	Apr 10	Monday	
101	0	6	11	0	17	3	1	12	9	7	9	6	3	12	17	16	5	8	4	2	4	2	5	5	164	Apr 11	Tuesday	
102	23	2	7	3	1	3	2	3	4	2	16	36	17	12	3	13	9	11	12	13	3	2	5	31	233	Apr 12	Wednesday	
103	2	11	13	1	16	5	0	10	8	9	10	13	29	20	16	15	4	19	9	12	4	1	6	33	266	Apr 13	Thursday	
104	2	6	10	4	2	2	6	8	5	10	11	14	18	21	4	13	3	13	12	11	2	3	1	42	223	Apr 14	Friday	
105	6	16	25	11	17	20	23	21	26	6	5	26	18	23	23	27	25	29	32	44	53	67	53	61	657	Apr 15	Saturday	
106	68	74	52	47	46	36	19	11	14	12	9	9	9	9	8	11	9	8	4	3	11	3	3	8	483	Apr 16	Sunday	
107	4	4	7	1	0	6	2	6	7	2	21	7	13	8	5	17	0	15	4	6	3	2	2	33	175	Apr 17	Monday	
108	5	2	14	5	2	5	3	9	12	14	9	10	15	14	8	35	9	24	9	25	12	10	15	42	308	Apr 18	Tuesday	
109	19	14	20	24	10	10	2	14	5	15	11	17	19	11	20	40	24	24	29	32	24	36	35	48	503	Apr 19	Wednesday	
110	40	42	43	37	27	23	15	12	19	13	21	23	30	14	31	24	9	33	35	26	27	36	46	49	675	Apr 20	Thursday	
111	52	42	47	52	23	10	13	6	22	23	15	19	22	19	28	38	19	28	31	33	46	40	32	50	710	Apr 21	Friday	
112	39	47	43	47	30	38	45	36	27	29	46	42	35	39	35	37	41	44	53	66	49	58	56	56	1038	Apr 22	Saturday	
113	66	71	70	69	62	53	55	13	14	12	8	11	15	6	11	11	14	19	14	17	12	13	10	18	664	Apr 23	Sunday	
114	5	8	5	13	1	1	1	0	9	4	4	5	7	13	0	7	1	11	6	3	2	6	8	18	138	Apr 24	Monday	
115	9	5	18	11	6	2	4	7	5	4	8	4	5	7	19	8	23	15	5	4	2	1	5	27	204	Apr 25	Tuesday	
116	2	4	7	2	6	3	3	7	3	6	8	4	18	7	10	7	3	12	4	7	0	2	4	21	150	Apr 26	Wednesday	
117	4	1	19	1	6	3	1	4	10	4	20	20	19	23	6	21	2	4	5	6	9	3	1	28	220	Apr 27	Thursday	
118	1	6	9	1	5	2	0	5	8	15	8	21	8	9	10	19	6	15	9	12	11	11	7	30	228	Apr 28	Friday	
119	4	7	10	3	4	3	6	5	4	0	6	5	2	3	4	5	3	5	0	3	2	3	4	4	95	Apr 29	Saturday	
120	6	3	3	3	7	11	4	2	25	6	5	6	0	14	2	6	2	5	0	3	3	1	4	4	125	Apr 30	Sunday	
121	5	2	2	4	3	4	5	6	6	7	7	3	10	6	4	3	11	8	3	3	0	5	1	9	117	May 01	Monday	Første
122	2	4	12	1	0	1	6	8	4	7	3	4	4	23	4	8	2	7	2	3	3	5	1	25	139	May 02	Tuesday	
123	6	2	11	5	3	10	18	13	9	11	7	12	16	19	16	9	5	10	8	13	6	8	7	19	242	May 03	Wednesday	
124	27	25	36	36	19	27	6	5	4	13	16	17	4	7	7	12	2	3	9	2	4	1	3	7	292	May 04	Thursday	Kristi
125	1	0	4	3	4	10	4	3	3	3	9	5	11	4	5	2	17	20	9	9	2	1	2	13	144	May 05	Friday	
126	5	2	10	4	4	0	3	2	5	6	9	14	8	3	5	3	4	7	3	8	8	19	4	12	148	May 06	Saturday	
127	7	8	9	12	12	8	13	3	6	5	14	6	6	11	6	20	25	15	9	5	4	8	10	14	236	May 07	Sunday	
128	6	9	3	9	3	4	6	7	8	8	14	14	15	10	15	11	7	11	12	7	19	11	12	32	253	May 08	Monday	
129	23	22	26	24	8	6	2	7	13	1	18	8	3	9	14	7	6	6	3	3	4	2	2	7	224	May 09	Tuesday	
130	7	3	9	7	1	4	1	7	2	4	7	9	12	3	8	6	10	9	1	7	4	1	3	17	142	May 10	Wednesday	
131	1	0	8	9	2	18	1	4	14	10	17	17	6	23	12	5	10	6	17	6	14	7	4	6	217	May 11	Thursday	
132	24	6	18	8	1	4	1	14	2	9	10	15	23	14	7	4	13	9	14	9	15	8	9	12	249	May 12	Friday	
133	21	8	7	11	13	3	2	6	4	3	11	5	2	2	4	3	11	13	2	5	2	2	1	2	143	May 13	Saturday	
134	2	11	7	2	3	2	5	5	6	13	4	9	7	9	7	1	7	14	3	1	1	1	3	1	124	May 14	Sunday	Første
135	2	2	7	2	11	2	5	11	13	15	21	5	14	8	2	3	10	17	11	15	8	12	7	18	221	May 15	Monday	Annen
136	1	1	12	2	5	3	2	2	3	11	8	11	19	11	15	10	22	36	21	2	8	9	1	6	221	May 16	Tuesday	
137	22	3	0	0	1	5	5	9	37	13	9	13	10	14	9	1	7	11	5	1	2	1	1	0	179	May 17	Wednesday	Sytten
138	4	3	22	12	1	8	5	6	11	11	15	18	24	19	10	17	11	3	5	3	5	4	8	1	226	May 18	Thursday	
139	25	0	13	6	4	13	15	11	21	2	10	22	11	8	6	26	1	5	8	10	3	1	3	22	246	May 19	Friday	
140	2	2	10	1	5	4	3	6	3	8	8	8	5	9	5	6	7	3	7	3	20	8	5	4	142	May 20	Saturday	
141	4	3	2	10	4	11	5	18	14	4	3	16	0	7	1	1	1	4	9	3	2	3	9	11	145	May 21	Sunday	
142	7	6	32	19	15	5	3	4	6	11	17	21	33	7	10	8	10	19	12	12	12	3	2	30	304	May 22	Monday	
143	2	4	9	5	1	4	25	9	16	22	8	24	17	16	17	13	8	11	3	2	2	7	5	6	236	May 23	Tuesday	
144	9	3	22	15	0	3	8	10	8	12	14	20	10	15	11	29	8	9	6	10	8	2	1	2	235	May 24	Wednesday	
145	20	10	7	4	9	8	5	8	16	15	14	19	16	19	10	7	18	10	7	13	6	5	3	22	271	May 25	Thursday	
146	1	4	11	1	8	4	4	6	11	15	7	16	7	7	12	22	1	7	8	10	5	2	6	5	180	May 26	Friday	

Table 3.4.1 Daily and hourly distribution of NORESS detections. For each day is shown the number of detections within each hour of the day, and the number of detections for that day. The statistics at the end of the table give total number of detections for each hour and the total sum of detections during the period. The averages show number of processed days, hourly distribution and average per processed day.

147	5	1	15	25	6	5	5	0	3	9	17	10	2	4	8	1	4	7	7	8	19	12	14	14	201	May	27	Saturday
148	11	18	9	12	11	8	5	1	3	5	5	1	5	7	4	8	3	12	1	1	4	6	9	17	166	May	28	Sunday
149	15	16	25	11	13	9	15	5	8	11	10	10	22	5	6	11	17	18	18	10	18	10	22	29	334	May	29	Monday
150	18	12	23	17	15	23	17	12	9	21	13	29	17	30	25	14	17	11	31	9	24	14	19	25	445	May	30	Tuesday
151	14	15	14	13	15	11	10	9	5	11	12	10	21	9	17	11	11	8	28	7	20	3	4	11	289	May	31	Wednesday
152	5	13	11	4	4	6	19	19	16	10	31	20	22	15	15	10	14	25	29	17	26	16	18	16	381	Jun	01	Thursday
153	19	20	32	20	14	7	15	20	14	21	25	22	35	6	8	17	23	20	30	25	17	23	21	29	483	Jun	02	Friday
154	25	32	43	31	28	23	28	20	12	15	13	22	31	16	16	26	23	15	12	22	29	30	19	22	553	Jun	03	Saturday
155	23	29	21	23	18	15	8	3	6	1	2	8	5	2	4	20	9	18	3	6	1	6	6	15	252	Jun	04	Sunday
156	9	4	14	4	1	5	13	12	8	10	15	7	37	17	16	10	13	26	31	6	33	16	33	30	370	Jun	05	Monday
157	42	59	58	56	31	11	23	30	16	11	10	13	23	20	18	21	22	26	17	27	25	40	29	43	671	Jun	06	Tuesday
158	45	48	4	0	20	18	16	35	17	17	28	41	29	16	21	13	21	30	27	38	38	26	37	40	625	Jun	07	Wednesday
159	41	38	39	45	31	13	10	12	18	20	14	23	37	17	12	15	23	36	17	3	15	0	2	6	487	Jun	08	Thursday
160	4	1	4	2	6	0	8	10	12	13	16	6	16	14	3	3	9	12	5	9	10	3	3	15	184	Jun	09	Friday
161	1	4	11	3	4	0	1	4	4	0	4	13	2	1	8	6	0	-8	5	6	2	6	2	3	98	Jun	10	Saturday
162	3	1	5	5	6	4	4	4	5	6	6	7	5	12	15	10	4	10	4	1	3	3	13	12	148	Jun	11	Sunday
163	10	9	16	1	2	3	7	2	2	2	5	26	16	15	12	18	8	12	20	11	18	3	10	5	233	Jun	12	Monday
164	6	6	10	2	1	1	3	3	2	6	3	11	23	22	7	13	20	9	6	4	21	7	12	0	198	Jun	13	Tuesday
165	0	7	24	20	11	21	7	5	8	12	8	7	12	17	21	9	7	15	25	13	14	15	17	16	311	Jun	14	Wednesday
166	20	18	23	17	9	9	4	14	18	12	10	19	28	10	17	25	24	27	16	31	20	1	10	8	390	Jun	15	Thursday
167	8	1	7	1	4	9	8	10	11	6	12	16	24	14	8	10	8	15	12	13	21	5	6	23	252	Jun	16	Friday
168	14	17	11	20	10	9	6	7	13	12	24	9	8	9	22	16	30	20	24	19	24	29	21	23	397	Jun	17	Saturday
169	12	14	11	16	21	17	9	22	8	13	7	6	9	16	16	21	14	14	8	15	16	15	11	16	327	Jun	18	Sunday
170	22	5	20	2	7	5	15	1	3	6	8	10	16	10	15	13	23	11	13	17	35	20	38	21	336	Jun	19	Monday
171	15	21	29	16	8	10	9	9	13	9	13	8	28	13	22	14	23	19	23	26	35	39	31	40	473	Jun	20	Tuesday
172	27	28	32	18	20	11	14	25	26	9	0	0	0	0	2	25	14	16	18	25	23	13	19	24	389	Jun	21	Wednesday
173	37	26	19	23	19	3	25	17	11	11	21	22	16	16	22	17	18	13	24	14	23	18	6	12	433	Jun	22	Thursday
174	15	6	17	14	14	2	13	4	5	9	6	29	18	10	6	5	11	9	13	8	25	3	4	7	253	Jun	23	Friday
175	9	2	12	8	5	7	7	1	9	3	31	9	11	4	5	11	2	3	2	5	1	2	5	4	158	Jun	24	Saturday
176	5	3	4	2	4	4	5	4	1	9	7	7	9	11	10	14	14	10	2	2	9	2	2	9	149	Jun	25	Sunday
177	7	3	6	7	2	4	3	5	6	14	9	7	18	4	6	13	2	2	8	0	13	7	3	5	154	Jun	26	Monday
178	17	6	10	4	7	2	1	6	13	4	22	16	17	11	5	3	10	15	10	1	9	0	4	11	204	Jun	27	Tuesday
179	9	14	9	2	0	3	2	4	8	8	17	4	23	16	7	12	10	10	8	4	15	6	6	8	205	Jun	28	Wednesday
180	10	4	10	2	7	7	8	5	9	4	0	19	23	9	8	16	3	0	0	0	0	0	0	0	144	Jun	29	Thursday
181	0	0	0	0	0	0	0	0	0	0	0	0	0	2	47	0	0	0	0	0	0	0	0	0	49	Jun	30	Friday
182	0	0	0	0	0	0	0	0	0	0	0	0	0	0	0	0	0	0	0	0	0	0	0	0	0	Jul	01	Saturday
183	0	0	0	0	0	0	0	0	0	0	0	0	0	0	0	0	0	0	0	0	0	0	0	0	0	Jul	02	Sunday
184	0	0	0	0	0	0	0	0	0	0	0	0	0	0	0	0	0	0	0	0	0	0	0	0	0	Jul	03	Monday
185	0	0	0	0	0	0	0	0	0	21	10	2	8	10	11	0	8	17	10	7	20	6	4	11	145	Jul	04	Tuesday
186	23	9	5	7	2	1	4	10	10	10	6	6	1	22	15	6	9	9	12	6	35	0	5	5	218	Jul	05	Wednesday
187	3	8	17	5	8	3	11	19	7	2	4	18	12	15	9	11	8	25	7	4	23	4	2	17	242	Jul	06	Thursday
188	3	9	11	2	8	11	11	1	11	7	7	14	13	1	0	0	0	5	8	5	17	4	4	16	168	Jul	07	Friday
189	1	3	9	0	0	0	0	0	4	5	6	8	1	5	2	7	4	2	5	5	4	2	1	4	78	Jul	08	Saturday
190	6	6	8	15	6	9	2	3	2	6	4	3	3	1	3	14	4	8	5	3	2	3	2	11	129	Jul	09	Sunday
191	2	9	5	4	4	5	6	8	4	12	9	12	15	6	11	7	6	14	11	7	4	3	5	5	174	Jul	10	Monday
192	4	6	15	1	1	3	3	8	13	9	7	12	23	8	4	13	6	12	2	1	0	3	9	3	166	Jul	11	Tuesday
193	2	4	9	2	5	8	8	29	3	14	4	17	17	8	7	7	7	9	5	4	1	1	4	5	180	Jul	12	Wednesday
194	8	9	11	3	7	10	12	8	14	10	5	0	9	13	7	3	11	6	3	2	8	2	3	11	175	Jul	13	Thursday
195	4	4	14	5	2	4	15	12	15	6	8	7	3	9	4	8	11	11	6	3	8	9	4	17	189	Jul	14	Friday
196	10	0	13	1	0	3	11	3	1	3	7	13	9	4	4	3	5	8	1	0	4	1	6	1	111	Jul	15	Saturday
197	5	5	7	3	6	5	0	5	5	2	5	102	0	0	0	0	0	0	0	0	5	4	12	7	178	Jul	16	Sunday
198	6	6	10	6	2	2	7	1	9	9	12	6	19	6	7	9	11	10	0	10	1	7	5	10	171	Jul	17	Monday
199	11	8	12	1	4	4	16	4	9	6	4	16	9	8	3	7	14	12	2	6	2	3	5	15	181	Jul	18	Tuesday
200	8	4	7	3	2	12	9	7	6	9	16	11	16	16	11	12	12	10	2	2	1	1	9	11	197	Jul	19	Wednesday
201	3	13	15	1	7	20	12	3	13	9	6	12	34	31	5	2	23	35	41	14	3	1	7	9	319	Jul	20	Thursday
202	15	15	20	19	3	2	13	15	24	18	20	2	9	0	11	10	15	9	5	6	6	1	6	22	266	Jul	21	Friday
203	2	1	13	2	0	17	13	3	7	5	8	3	4	8	5	5	5	6	3	8	5	7	4	5	139	Jul	22	Saturday
204	0	3	1	3	2	5	9	8	11	25	1	5	5	0	5	15	1	0	0	0	0	0	0	0	99	Jul	23	Sunday
205	0	0	0	0	0	0	0	0	0	0	0	0	0	0	0	0	0	0	0	0	0	0	0	0	0	Jul	24	Monday
206	0	0	0	0	0	0	0	0	0	0	0	0	0	0	0	0	0	0	0	0	0	0	0	0	0	Jul	25	Tuesday

Table 3.4.1 (cont.)

207	0	0	0	0	0	0	0	0	0	0	0	0	0	0	0	0	0	0	0	0	0	0	0	0	0	Jul	26	Wednesday
208	0	0	0	0	0	0	0	0	0	0	0	0	0	0	0	0	0	0	0	0	0	0	0	0	0	Jul	27	Thursday
209	0	0	0	0	0	0	0	0	0	0	0	0	0	0	0	0	0	0	0	0	0	0	0	0	0	Jul	28	Friday
210	0	0	0	0	0	0	0	0	0	0	0	0	0	0	0	0	0	0	0	0	0	0	0	0	0	Jul	29	Saturday
211	0	0	0	0	0	0	0	0	0	0	0	0	0	0	0	0	0	0	0	0	0	0	0	0	0	Jul	30	Sunday
212	0	0	0	0	0	0	0	0	0	0	0	0	0	0	0	0	0	0	0	0	0	0	0	0	0	Jul	31	Monday
213	0	0	0	0	0	0	0	0	0	0	0	0	0	0	0	0	0	0	0	0	0	0	0	0	0	Aug	01	Tuesday
214	0	0	0	0	0	0	0	0	0	0	0	0	0	0	0	0	0	0	0	0	0	0	0	0	0	Aug	02	Wednesday
215	0	0	0	0	0	0	0	0	0	0	0	0	0	0	0	0	0	0	0	0	0	0	0	0	0	Aug	03	Thursday
216	0	0	0	0	0	0	0	0	0	0	0	0	0	0	0	0	0	0	0	0	0	0	0	0	0	Aug	04	Friday
217	0	0	0	0	0	0	0	0	0	0	0	0	0	0	0	0	0	0	0	0	0	0	0	0	0	Aug	05	Saturday
218	0	0	0	0	0	0	0	0	0	0	0	0	0	0	0	0	0	0	0	0	0	0	0	0	0	Aug	06	Sunday
219	0	0	0	0	0	0	0	0	0	0	0	0	0	0	0	0	0	0	0	0	0	0	0	0	0	Aug	07	Monday
220	0	0	0	0	0	0	0	0	0	0	0	0	0	0	0	0	0	0	0	0	0	0	0	0	0	Aug	08	Tuesday
221	0	0	0	0	0	0	0	0	0	0	0	0	0	0	0	0	0	0	0	0	0	0	0	0	0	Aug	09	Wednesday
222	0	0	0	0	0	0	0	0	0	0	0	0	0	0	0	0	0	0	0	0	0	0	0	0	0	Aug	10	Thursday
223	0	0	0	0	0	0	0	0	0	0	0	0	0	0	0	0	0	0	0	0	0	0	0	0	0	Aug	11	Friday
224	0	0	0	0	0	0	0	0	0	0	0	0	0	0	0	0	0	0	0	0	0	0	0	0	0	Aug	12	Saturday
225	0	0	0	0	0	0	0	0	0	0	0	0	0	0	0	0	0	0	0	0	0	0	0	0	0	Aug	13	Sunday
226	0	0	0	0	0	0	0	0	0	0	0	0	0	0	0	0	0	0	0	0	0	0	0	0	0	Aug	14	Monday
227	0	0	0	0	0	0	0	0	0	0	19	9	15	12	12	10	13	13	10	10	11	11	11	12	168	Aug	15	Tuesday
228	17	14	15	11	10	4	12	28	11	12	6	6	10	15	5	14	15	13	6	5	9	9	10	11	268	Aug	16	Wednesday
229	11	14	20	21	10	6	6	11	3	9	10	11	14	22	12	12	22	17	15	7	9	16	13	14	305	Aug	17	Thursday
230	16	17	18	11	10	8	9	17	16	13	32	12	12	26	17	14	22	25	22	22	27	19	15	30	430	Aug	18	Friday
231	14	26	25	22	24	27	23	19	21	19	17	15	11	18	25	19	15	18	21	19	24	26	24	31	503	Aug	19	Saturday
232	34	14	24	14	10	2	6	14	2	3	10	20	7	13	8	11	4	11	20	9	4	5	4	6	255	Aug	20	Sunday
233	7	10	7	3	2	8	3	13	25	11	20	10	22	8	0	13	9	8	18	2	12	3	6	11	231	Aug	21	Monday
234	9	2	10	6	7	6	8	1	13	4	5	6	10	8	17	8	8	4	9	3	15	9	7	3	178	Aug	22	Tuesday
235	4	7	10	2	3	4	10	9	8	5	9	8	8	15	8	11	18	17	11	13	14	2	6	2	204	Aug	23	Wednesday
236	4	5	29	5	0	1	12	7	19	2	7	6	15	10	10	12	12	17	12	11	10	2	4	26	238	Aug	24	Thursday
237	5	7	19	10	5	7	6	19	17	13	17	15	13	9	2	4	21	17	8	5	21	2	4	12	258	Aug	25	Friday
238	7	3	20	5	3	12	7	2	7	10	2	5	5	5	4	2	5	5	6	3	9	4	1	1	133	Aug	26	Saturday
239	0	7	1	8	4	10	0	5	3	1	1	1	1	3	1	20	2	19	2	2	6	1	3	18	119	Aug	27	Sunday
240	8	5	11	3	1	4	6	8	5	5	1	13	16	11	14	7	10	6	8	3	10	0	7	6	168	Aug	28	Monday
241	1	5	9	2	9	1	5	5	10	8	12	25	19	7	12	7	19	8	6	0	18	1	3	11	203	Aug	29	Tuesday
242	8	8	12	5	8	2	8	11	9	16	10	17	33	24	18	23	8	10	10	8	13	5	9	15	290	Aug	30	Wednesday
243	5	4	22	5	0	2	4	1	14	10	5	8	6	0	0	0	0	0	0	0	0	0	0	0	86	Aug	31	Thursday
244	2	1	10	3	0	4	4	6	5	8	8	19	21	4	12	5	13	18	13	19	0	2	2	9	188	Sep	01	Friday
245	12	4	18	2	6	2	11	6	2	11	7	7	1	5	9	7	3	14	5	4	2	5	3	5	151	Sep	02	Saturday
246	5	10	4	5	3	9	2	0	3	6	5	2	2	1	4	16	4	21	9	4	0	6	5	16	142	Sep	03	Sunday
247	3	11	14	1	1	5	5	5	8	7	5	9	12	22	7	6	10	9	8	3	19	3	3	15	191	Sep	04	Monday
248	9	3	18	5	6	4	13	7	19	3	16	14	17	34	12	9	10	11	11	7	14	5	5	3	255	Sep	05	Tuesday
249	3	9	14	12	2	3	5	6	13	13	19	31	10	12	20	8	11	20	21	2	15	2	2	8	261	Sep	06	Wednesday
250	2	10	9	2	2	5	7	6	16	1	24	7	31	24	21	5	20	14	2	1	13	1	6	13	242	Sep	07	Thursday
251	3	9	16	11	2	3	13	13	26	19	13	21	17	18	14	15	6	8	15	23	10	8	3	15	301	Sep	08	Friday
252	2	6	25	1	6	3	4	4	5	4	7	4	7	20	5	2	9	8	7	6	7	2	3	3	150	Sep	09	Saturday
253	2	1	3	9	3	7	2	5	5	5	4	2	5	8	9	18	10	14	2	19	5	13	7	10	168	Sep	10	Sunday
254	16	4	21	1	6	6	13	2	15	10	3	21	10	30	17	15	19	39	5	1	11	5	15	20	305	Sep	11	Monday
255	15	7	16	5	3	6	6	15	29	8	9	25	9	8	22	5	18	16	5	5	14	0	11	2	259	Sep	12	Tuesday
256	12	2	16	7	10	8	7	12	20	15	11	15	12	35	23	15	12	9	2	4	12	8	11	4	282	Sep	13	Wednesday
257	6	4	11	2	4	13	4	3	18	10	9	15	25	16	8	6	11	7	13	17	3	1	6	7	219	Sep	14	Thursday
258	4	6	16	3	1	5	13	10	11	19	10	13	9	7	6	12	16	6	13	4	17	1	6	6	214	Sep	15	Friday
259	3	4	34	15	9	13	8	5	2	4	10	16	4	22	42	5	5	11	6	3	1	0	3	13	238	Sep	16	Saturday
260	7	36	13	11	10	10	13	2	7	11	0	2	9	3	7	17	12	14	5	4	2	4	6	5	210	Sep	17	Sunday
261	11	0	14	4	4	8	11	3	4	5	8	7	18	14	11	12	7	12	2	2	13	8	6	15	199	Sep	18	Monday
262	5	9	20	6	15	0	6	5	16	11	8	10	16	22	9	11	12	18	6	1	16	5	4	12	243	Sep	19	Tuesday
263	13	3	11	3	9	13	0	9	21	5	11	12	12	6	15	15	2	5	9	0	11	0	6	7	198	Sep	20	Wednesday
264	7	3	7	0	1	2	4	6	6	13	6	7	13	20	5	11	12	14	9	6	8	1	8	11	180	Sep	21	Thursday
265	4	4	15	5	10	1	7	7	13	19	11	17	11	10	6	3	5	10	11	12	18	4	0	10	213	Sep	22	Friday
266	0	2	17	1	3	12	1	2	5	3	2	6	2	7	6	5	1	5	13	6	2	1	3	1	106	Sep	23	Saturday

Table 3.4.1 (cont.)

267	5	2	2	5	6	1	0	8	21	3	6	9	6	13	13	4	20	4	10	0	0	15	6	3	162	Sep 24	Sunday
268	12	5	11	11	2	4	3	17	0	7	21	10	8	9	12	13	6	27	16	3	7	3	2	3	212	Sep 25	Monday
269	6	6	8	12	3	11	2	11	4	8	7	5	9	18	19	19	15	13	9	17	2	24	0	11	239	Sep 26	Tuesday
270	9	9	2	13	4	5	5	10	1	10	9	11	18	23	22	5	4	20	12	5	5	9	4	8	223	Sep 27	Wednesday
271	4	6	8	19	4	5	6	5	7	12	8	7	14	27	19	13	3	9	13	4	1	9	10	6	219	Sep 28	Thursday
272	19	11	2	10	6	9	0	3	3	10	7	14	17	20	12	2	4	15	4	8	12	7	1	3	199	Sep 29	Friday
273	10	7	1	15	4	5	6	8	6	1	4	2	4	3	12	5	0	5	7	3	3	4	0	6	121	Sep 30	Saturday
NRS	*00*	*01*	*02*	*03*	*04*	*05*	*06*	*07*	*08*	*09*	10	11	12	13	14	15	16	17	18	19	20	21	22	23			
Sum	1552		1514		1158		1274		1443		1978		1877		1737		2026		1368		1220		2281				
	1655		2296		1183		1225		1514		1640		2037		1696		1582		1583		1677		1287		38803	Total sum	
158	10	10	15	10	7	7	8	8	10	9	10	13	13	12	11	11	10	13	10	9	11	8	8	14	246	Total average	
126	9	8	13	8	5	5	6	7	9	8	10	12	14	12	10	10	9	12	10	8	10	6	7	14	221	Average workdays	
57	10	10	12	10	9	9	7	6	7	7	8	9	6	7	7	8	7	9	6	7	7	8	7	10	192	Average weekends	

Table 3.4.1 (cont.)

FRS .FKX Hourly distribution of detections

Day	00	01	02	03	04	05	06	07	08	09	10	11	12	13	14	15	16	17	18	19	20	21	22	23	Sum	Date		
91	17	6	8	5	27	6	1	4	6	6	15	10	12	14	3	0	4	7	9	8	1	16	23	7	215	Apr 01	Saturday	
92	3	11	6	3	1	0	0	0	0	0	0	0	0	0	0	0	0	0	0	0	0	0	0	0	24	Apr 02	Sunday	
93	0	0	0	0	0	2	4	3	6	2	2	2	6	7	12	12	1	10	8	12	8	7	12	14	130	Apr 03	Monday	
94	4	5	2	6	5	10	6	12	16	25	8	24	15	8	12	11	8	6	10	5	6	6	9	0	219	Apr 04	Tuesday	
95	3	5	2	5	1	4	7	12	2	4	13	19	18	11	12	12	6	21	9	5	1	7	19	7	205	Apr 05	Wednesday	
96	10	6	8	7	2	6	12	1	14	17	13	16	2	11	10	9	14	20	3	15	11	3	13	5	228	Apr 06	Thursday	
97	13	0	7	5	2	10	2	18	14	5	8	17	20	16	5	7	7	14	5	6	10	13	21	3	228	Apr 07	Friday	
98	13	10	1	13	7	1	2	11	15	17	11	21	2	2	5	9	7	1	4	3	5	2	9	2	173	Apr 08	Saturday	
99	5	1	6	4	10	11	1	4	1	10	7	13	17	3	4	6	5	6	10	6	10	2	22	3	167	Apr 09	Sunday	
100	3	3	3	3	1	4	3	2	7	8	9	6	16	22	6	4	3	3	13	12	6	5	10	6	158	Apr 10	Monday	
101	4	7	4	5	12	9	2	23	7	35	9	9	9	13	12	15	1	1	−8	7	4	6	17	0	219	Apr 11	Tuesday	
102	3	6	9	16	27	8	9	8	4	4	15	32	21	3	11	4	3	3	9	8	7	2	19	3	234	Apr 12	Wednesday	
103	1	10	4	7	16	15	6	20	7	4	11	13	7	6	12	7	11	14	6	6	2	6	14	8	213	Apr 13	Thursday	
104	6	6	4	1	1	6	6	14	16	19	15	24	25	20	12	18	19	9	8	13	3	5	20	15	285	Apr 14	Friday	
105	4	9	5	2	2	2	12	3	22	9	23	29	2	7	8	6	1	4	8	3	10	24	7	5	207	Apr 15	Saturday	
106	7	6	1	1	7	11	20	10	22	4	8	9	7	14	1	5	10	2	8	7	20	15	29	17	241	Apr 16	Sunday	
107	15	17	26	6	3	8	14	9	2	4	10	21	13	13	5	12	5	14	5	4	12	25	29	35	307	Apr 17	Monday	
108	36	25	3	0	0	6	5	12	18	6	6	16	35	16	6	4	11	39	13	17	4	0	0	0	278	Apr 18	Tuesday	
109	0	0	0	0	0	5	5	24	8	10	23	20	11	15	9	4	4	9	4	7	8	5	16	9	196	Apr 19	Wednesday	
110	36	38	19	15	1	2	2	12	6	7	5	13	11	7	8	7	8	5	14	3	20	9	18	9	275	Apr 20	Thursday	
111	5	0	8	3	6	10	0	6	9	26	29	44	19	12	10	3	2	2	4	6	8	6	14	25	257	Apr 21	Friday	
112	14	13	16	6	4	3	1	15	5	14	50	9	17	18	5	3	6	8	47	38	63	47	30	3	435	Apr 22	Saturday	
113	12	9	18	14	2	7	8	8	7	3	4	4	4	4	1	4	2	10	4	12	5	7	25	2	176	Apr 23	Sunday	
114	8	10	2	7	1	7	6	13	5	5	10	10	8	11	4	6	5	14	8	5	12	14	10	7	188	Apr 24	Monday	
115	38	55	41	23	8	8	7	5	9	10	9	7	7	7	14	4	12	12	9	4	9	8	10	11	327	Apr 25	Tuesday	
116	4	41	48	13	2	1	3	14	10	15	7	10	11	12	10	8	3	11	6	2	8	6	11	2	258	Apr 26	Wednesday	
117	5	9	6	2	8	7	4	9	13	12	15	19	17	14	4	9	8	2	5	11	7	10	10	5	211	Apr 27	Thursday	
118	4	4	6	2	3	3	2	5	14	10	9	22	7	11	10	6	6	12	2	10	10	10	12	6	186	Apr 28	Friday	
119	4	9	3	8	2	5	10	6	13	7	10	19	3	7	7	10	2	1	7	3	8	9	6	3	162	Apr 29	Saturday	
120	12	10	14	6	5	18	7	0	12	11	4	1	2	4	1	8	13	1	8	1	8	1	7	12	166	Apr 30	Sunday	
121	20	14	18	4	10	6	4	1	7	4	1	0	4	1	6	3	5	5	8	6	1	3	12	4	147	May 01	Monday	Første
122	3	3	2	2	6	6	8	4	3	14	6	4	2	3	1	4	1	3	9	1	5	10	12	2	114	May 02	Tuesday	
123	5	3	4	7	3	8	0	1	4	6	11	11	4	7	10	7	5	11	8	4	8	5	10	3	145	May 03	Wednesday	
124	5	4	5	6	6	11	5	6	11	9	11	19	9	10	7	5	4	1	12	5	5	2	17	6	181	May 04	Thursday	Kristi
125	3	3	8	3	3	12	7	8	5	9	16	9	12	7	15	5	4	18	19	4	10	5	16	3	204	May 05	Friday	
126	7	4	6	8	11	0	7	4	7	13	21	19	9	1	3	4	2	1	7	5	8	9	11	3	170	May 06	Saturday	
127	10	5	5	8	2	2	4	5	5	9	9	5	8	6	3	19	28	26	7	22	11	6	25	10	240	May 07	Sunday	
128	3	2	8	8	2	1	5	8	10	16	6	17	6	9	20	5	4	7	8	4	3	13	22	7	194	May 08	Monday	
129	1	0	5	1	1	3	7	2	1	2	16	6	11	5	5	4	1	3	3	5	6	8	19	6	121	May 09	Tuesday	
130	5	2	3	8	2	2	5	7	11	16	34	30	15	21	22	19	20	21	8	14	12	9	30	3	319	May 10	Wednesday	
131	5	13	5	22	8	32	21	15	16	25	36	82	11	26	22	30	19	33	10	16	24	7	24	10	512	May 11	Thursday	
132	17	7	5	8	3	10	15	14	29	16	18	47	23	19	27	12	18	8	6	12	13	16	24	9	376	May 12	Friday	
133	10	3	9	13	8	26	9	11	24	20	49	15	10	15	16	13	2	1	6	13	16	7	8	4	308	May 13	Saturday	
134	5	21	5	0	3	8	7	7	12	22	17	15	16	5	11	16	11	9	8	7	7	4	15	6	237	May 14	Sunday	Første
135	7	6	1	2	11	29	6	7	8	10	7	32	23	14	31	20	8	0	0	0	0	0	0	0	222	May 15	Monday	Annen
136	0	0	0	0	0	0	0	0	0	0	0	36	38	8	20	11	7	14	4	8	7	14	18	12	197	May 16	Tuesday	
137	1	9	10	12	3	10	7	15	22	15	11	32	19	17	23	21	31	25	18	2	8	3	16	6	336	May 17	Wednesday	Sytten
138	8	13	13	25	13	21	24	15	0	0	0	0	0	0	0	0	19	53	24	13	21	12	24	5	303	May 18	Thursday	
139	7	5	15	12	2	12	24	15	19	18	22	33	23	23	24	5	17	9	9	19	12	2	19	3	349	May 19	Friday	
140	6	17	3	10	9	18	8	13	12	16	21	26	21	22	13	17	16	6	19	14	13	4	19	2	325	May 20	Saturday	
141	2	2	6	2	11	4	8	10	2	1	5	6	11	9	9	24	11	6	36	14	13	5	27	2	226	May 21	Sunday	
142	9	9	26	25	21	29	18	28	31	21	36	32	37	20	14	9	9	7	16	15	11	9	17	3	452	May 22	Monday	
143	4	8	9	10	5	14	13	22	20	36	36	57	48	40	32	31	24	15	19	17	14	12	24	17	532	May 23	Tuesday	
144	10	7	12	12	2	43	30	31	27	20	27	29	31	25	16	20	19	24	15	13	8	13	21	6	461	May 24	Wednesday	
145	10	12	9	11	4	39	30	30	39	35	28	46	29	39	26	16	9	23	19	17	9	6	19	13	518	May 25	Thursday	
146	7	12	14	3	24	25	15	39	26	46	34	35	40	30	20	17	25	38	11	6	7	9	14	6	503	May 26	Friday	

Table 3.4.2 Daily and hourly distribution of ARCESS detections. For each day is shown the number of detections within each hour of the day, and the number of detections for that day. The statistics at the end of the table give total number of detections for each hour and the total sum of detections during the period. The averages show number of processed days, hourly distribution and average per processed day.

147	8	7	6	10	15	8	7	15	16	16	26	44	16	16	19	20	8	4	16	9	29	8	19	3	345	May	27	Saturday
148	13	4	7	11	6	7	8	1	0	0	0	0	0	0	0	0	0	0	0	0	0	0	0	0	57	May	28	Sunday
149	0	0	0	0	0	0	0	0	27	50	49	58	48	45	42	10	12	8	15	15	7	12	18	7	423	May	29	Monday
150	2	5	8	8	8	45	41	60	47	0	0	0	0	11	27	7	3	9	12	1	6	19	13	9	341	May	30	Tuesday
151	11	5	6	5	37	31	33	36	29	51	58	51	47	48	43	19	19	28	6	27	9	10	10	3	622	May	31	Wednesday
152	1	5	6	7	11	43	29	37	27	19	34	17	21	29	12	21	14	27	19	18	0	0	0	0	397	Jun	01	Thursday
153	0	0	0	0	0	0	0	0	0	0	0	0	2	30	25	12	29	18	15	8	11	25	25	19	219	Jun	02	Friday
154	15	5	23	14	5	23	6	19	17	14	91	159	0	0	0	0	0	0	0	0	0	0	0	0	391	Jun	03	Saturday
155	0	0	0	0	0	0	0	0	0	8	11	17	5	16	10	11	14	20	8	12	13	6	32	11	194	Jun	04	Sunday
156	7	6	5	9	20	37	36	34	35	19	27	37	49	36	32	22	13	19	6	13	7	12	16	1	498	Jun	05	Monday
157	5	9	4	9	30	96	204	33	38	58	43	57	42	30	49	34	15	24	17	21	27	23	27	10	905	Jun	06	Tuesday
158	9	12	21	16	7	21	32	56	44	41	55	56	58	29	52	27	25	29	13	16	5	30	24	14	692	Jun	07	Wednesday
159	8	12	10	19	40	27	57	26	36	24	55	41	1	0	0	0	0	0	0	0	0	0	0	0	356	Jun	08	Thursday
160	0	0	0	0	0	0	0	0	0	0	0	0	0	0	0	0	0	0	0	0	0	0	0	0	0	Jun	09	Friday
161	0	0	0	0	0	0	0	0	0	0	0	0	0	0	0	0	0	0	0	0	0	0	0	0	0	Jun	10	Saturday
162	0	0	0	0	0	0	17	19	14	13	12	29	25	11	27	10	12	14	21	14	7	4	16	4	269	Jun	11	Sunday
163	6	7	3	19	2	0	0	0	0	0	0	0	0	0	0	0	0	0	0	0	0	0	0	0	37	Jun	12	Monday
164	0	0	0	0	0	5	8	17	10	31	24	20	32	22	27	24	13	17	21	11	18	9	11	12	332	Jun	13	Tuesday
165	21	6	3	21	28	14	10	33	29	36	38	29	23	19	17	13	24	29	29	14	3	17	22	14	492	Jun	14	Wednesday
166	12	4	9	23	18	24	16	19	19	19	18	23	22	27	21	14	19	12	6	11	7	14	19	21	397	Jun	15	Thursday
167	12	5	8	11	30	14	18	42	39	20	30	42	41	21	18	13	10	38	5	13	13	15	27	20	505	Jun	16	Friday
168	8	9	2	16	8	8	13	13	15	24	47	38	6	16	18	15	6	14	11	19	8	7	8	0	329	Jun	17	Saturday
169	1	6	5	10	6	13	9	7	11	6	15	11	6	12	16	3	9	17	8	10	10	12	13	4	220	Jun	18	Sunday
170	6	11	10	8	0	14	22	18	34	26	31	45	41	42	28	29	22	21	21	3	9	19	26	9	495	Jun	19	Monday
171	9	14	19	21	22	16	23	30	11	35	21	30	21	12	34	31	20	24	33	13	10	36	26	11	522	Jun	20	Tuesday
172	9	8	8	25	17	19	21	43	41	34	25	28	35	45	31	33	21	21	17	13	11	0	0	0	505	Jun	21	Wednesday
173	0	0	0	0	0	0	0	0	0	0	0	0	0	0	0	0	0	0	0	0	0	23	27	9	59	Jun	22	Thursday
174	7	8	18	25	17	28	24	51	43	22	20	61	27	9	23	9	13	13	6	8	9	3	3	6	453	Jun	23	Friday
175	9	21	6	7	2	20	21	18	18	21	25	21	13	11	14	9	4	6	25	13	15	14	6	12	331	Jun	24	Saturday
176	10	11	8	6	18	16	26	18	26	11	19	23	23	13	12	9	11	9	18	10	18	20	15	5	355	Jun	25	Sunday
177	1	6	14	21	16	28	26	26	31	27	42	42	43	34	40	18	30	6	18	26	8	8	14	15	540	Jun	26	Monday
178	14	3	13	21	18	24	31	36	53	36	43	32	36	19	38	23	14	12	9	11	17	18	21	5	547	Jun	27	Tuesday
179	9	4	11	22	20	17	25	29	32	43	48	47	50	8	34	20	13	12	14	17	11	14	24	8	532	Jun	28	Wednesday
180	12	7	6	28	17	16	25	29	24	43	27	26	25	40	34	30	5	0	0	0	0	0	0	0	394	Jun	29	Thursday
181	0	0	0	0	0	0	5	34	30	33	31	17	0	0	0	0	0	0	0	0	0	0	0	0	150	Jun	30	Friday
182	0	0	0	0	0	0	0	0	0	0	0	0	18	27	15	15	13	9	14	5	4	7	11	2	140	Jul	01	Saturday
183	15	2	1	0	9	9	24	22	15	19	14	23	27	12	23	8	13	16	15	13	8	7	4	4	303	Jul	02	Sunday
184	4	3	10	15	20	12	22	16	29	27	35	20	22	19	18	19	9	35	25	33	6	12	20	5	436	Jul	03	Monday
185	0	3	5	10	11	11	19	35	35	32	44	36	37	13	0	0	0	0	0	0	0	0	0	0	291	Jul	04	Tuesday
186	0	0	0	0	0	25	37	30	40	48	37	55	29	42	24	33	30	24	20	7	13	9	15	5	523	Jul	05	Wednesday
187	5	5	6	37	11	0	17	22	31	19	33	44	53	18	6	0	0	0	0	0	0	0	0	0	307	Jul	06	Thursday
188	0	0	0	0	0	0	0	9	27	30	22	34	0	11	20	17	15	0	0	0	0	0	0	0	185	Jul	07	Friday
189	6	11	1	12	4	19	12	27	24	31	41	37	17	14	19	9	9	9	14	9	10	4	16	10	365	Jul	08	Saturday
190	5	4	9	17	12	13	4	11	13	17	33	36	21	13	13	19	16	14	15	19	19	30	5	4	362	Jul	09	Sunday
191	3	10	1	28	23	21	21	18	31	26	32	61	47	35	45	33	35	25	17	14	24	4	11	6	571	Jul	10	Monday
192	8	2	12	11	30	15	19	32	29	46	35	39	29	35	29	26	39	12	14	20	8	20	14	2	526	Jul	11	Tuesday
193	1	6	5	10	7	13	23	26	53	42	22	50	27	19	30	21	23	16	5	31	10	17	1	0	458	Jul	12	Wednesday
194	0	0	0	0	3	22	10	26	44	35	26	38	30	37	37	37	30	28	10	39	6	22	25	11	516	Jul	13	Thursday
195	6	7	17	9	32	16	26	33	39	48	51	59	29	5	34	36	18	28	31	15	15	19	13	12	598	Jul	14	Friday
196	8	7	9	10	10	8	0	0	0	0	0	0	0	0	0	0	0	0	0	0	0	0	0	0	52	Jul	15	Saturday
197	0	0	0	0	0	0	0	0	0	0	0	0	0	0	0	0	0	0	0	0	0	0	0	0	0	Jul	16	Sunday
198	0	0	0	0	0	0	0	0	0	0	0	0	0	0	0	0	0	0	0	0	0	0	0	0	0	Jul	17	Monday
199	0	0	0	0	0	0	0	0	0	0	0	0	0	0	0	0	0	0	0	0	0	0	0	0	0	Jul	18	Tuesday
200	0	0	0	0	0	0	0	0	0	0	0	0	0	0	0	0	0	0	0	0	0	0	0	0	0	Jul	19	Wednesday
201	0	0	0	0	0	0	0	0	0	0	0	0	0	0	0	0	0	0	0	0	0	0	0	0	0	Jul	20	Thursday
202	5	2	3	22	12	13	25	19	15	38	55	51	18	17	42	6	8	5	7	4	22	7	21	10	427	Jul	21	Friday
203	15	9	16	10	4	19	12	24	23	17	34	29	17	13	8	3	16	29	18	12	4	16	14	9	371	Jul	22	Saturday
204	4	9	9	5	8	5	26	8	19	28	26	22	16	7	13	19	8	24	7	8	24	10	4	18	327	Jul	23	Sunday
205	7	12	6	14	11	25	17	19	25	28	55	38	25	26	31	5	24	32	0	0	0	0	0	0	400	Jul	24	Monday
206	0	0	0	7	0	0	0	0	0	0	0	0	0	0	0	0	0	0	0	0	0	0	0	0	7	Jul	25	Tuesday

Table 3.4.2 (cont.)

207	0	0	0	0	0	0	0	0	0	0	0	0	0	0	0	0	0	0	0	0	0	0	0	0	0	Jul	26	Wednesday
208	0	0	0	0	0	0	0	0	0	0	0	0	0	0	0	0	0	0	0	0	0	0	0	0	0	Jul	27	Thursday
209	0	0	0	0	4	14	14	24	0	39	51	48	58	20	40	43	43	45	27	16	16	5	13	20	540	Jul	28	Friday
210	4	8	12	6	3	8	4	12	20	27	20	29	17	10	18	13	6	23	14	14	8	12	14	6	308	Jul	29	Saturday
211	6	9	12	12	12	8	20	19	17	18	34	17	13	9	12	7	14	14	27	40	20	16	10	5	371	Jul	30	Sunday
212	6	6	4	10	4	22	18	19	30	29	36	29	22	26	16	16	16	19	14	16	15	13	13	0	399	Jul	31	Monday
213	11	3	5	9	6	12	23	17	21	38	39	44	24	15	28	17	6	29	5	21	2	19	11	1	406	Aug	01	Tuesday
214	9	3	7	14	11	16	19	36	13	28	35	37	25	17	25	10	7	33	4	27	15	14	13	22	440	Aug	02	Wednesday
215	6	7	9	27	14	41	24	26	30	38	27	48	21	13	24	15	33	22	12	17	10	12	24	7	507	Aug	03	Thursday
216	1	9	9	9	3	0	0	0	0	0	0	0	42	1	21	12	14	26	15	18	22	11	11	4	228	Aug	04	Friday
217	19	8	13	8	9	20	25	23	16	36	46	53	14	19	17	9	4	17	15	19	12	3	11	5	421	Aug	05	Saturday
218	4	8	7	8	3	21	9	23	24	23	31	26	18	21	21	12	10	11	38	36	7	9	13	12	395	Aug	06	Sunday
219	18	23	9	11	17	33	31	19	38	45	49	45	59	41	39	44	30	32	28	20	13	33	13	9	699	Aug	07	Monday
220	17	12	16	22	25	28	34	27	49	57	40	62	46	31	51	22	30	32	28	28	22	26	19	17	741	Aug	08	Tuesday
221	0	0	0	0	0	0	0	0	0	56	49	51	48	32	31	40	58	21	15	18	30	8	25	6	488	Aug	09	Wednesday
222	14	10	12	2	0	9	35	34	32	40	49	44	37	28	42	28	11	24	9	15	12	15	11	16	529	Aug	10	Thursday
223	3	16	5	15	14	22	24	33	42	63	56	81	56	41	33	13	4	28	30	22	6	14	19	4	644	Aug	11	Friday
224	14	16	25	5	8	11	14	22	15	17	40	27	29	18	14	16	39	22	14	7	7	5	21	4	410	Aug	12	Saturday
225	8	6	4	3	6	20	12	21	28	14	27	16	4	29	11	5	10	15	14	13	18	11	11	4	310	Aug	13	Sunday
226	11	9	5	6	18	54	77	76	55	64	59	49	58	23	38	19	25	30	34	15	23	18	34	6	806	Aug	14	Monday
227	0	7	10	7	25	46	65	38	32	49	33	48	48	25	33	44	25	54	37	28	22	13	33	17	739	Aug	15	Tuesday
228	9	14	5	12	32	43	63	65	36	19	59	65	70	39	47	25	6	0	0	0	0	0	0	0	609	Aug	16	Wednesday
229	0	0	0	0	0	0	0	3	0	0	0	0	0	0	0	0	0	0	0	0	0	0	0	0	3	Aug	17	Thursday
230	0	0	0	0	0	0	0	0	0	0	0	0	0	0	0	0	0	0	0	0	0	0	0	0	0	Aug	18	Friday
231	0	0	0	0	0	0	0	0	0	0	0	0	0	0	0	0	0	0	0	0	0	0	0	0	0	Aug	19	Saturday
232	0	0	0	0	0	0	0	0	0	0	0	0	0	0	0	0	0	0	0	0	0	0	0	0	0	Aug	20	Sunday
233	0	0	0	0	0	0	0	41	36	35	29	31	22	0	0	0	0	0	0	0	0	0	0	0	194	Aug	21	Monday
234	0	0	0	0	0	0	0	0	0	0	0	0	0	0	0	0	0	0	0	0	0	0	0	0	0	Aug	22	Tuesday
235	0	0	0	0	0	0	0	0	0	0	0	0	0	0	0	0	0	0	0	0	0	0	0	0	0	Aug	23	Wednesday
236	0	0	0	0	0	0	0	0	0	0	0	0	0	0	0	0	0	0	0	0	0	0	0	0	0	Aug	24	Thursday
237	0	0	0	0	0	0	0	0	0	0	0	0	0	0	0	0	0	0	0	0	0	0	0	0	0	Aug	25	Friday
238	0	0	0	0	0	0	0	0	0	0	0	0	0	0	0	0	0	0	0	0	0	0	0	0	0	Aug	26	Saturday
239	0	0	0	0	0	0	0	0	0	0	0	0	0	0	0	0	0	0	0	0	0	0	0	0	0	Aug	27	Sunday
240	0	0	0	0	0	0	0	0	0	0	0	0	0	0	0	0	0	0	0	0	0	0	0	0	0	Aug	28	Monday
241	0	0	0	0	0	0	0	0	0	0	0	0	0	0	0	0	0	0	0	0	0	0	0	0	0	Aug	29	Tuesday
242	0	0	0	0	0	0	0	0	30	38	35	39	26	25	30	43	19	25	10	7	0	0	0	0	327	Aug	30	Wednesday
243	0	0	0	0	0	0	0	0	0	0	0	0	0	0	0	0	0	0	0	0	0	0	0	0	0	Aug	31	Thursday
244	3	12	16	4	3	24	25	51	34	44	36	24	39	34	39	28	33	17	11	10	12	10	14	5	528	Sep	01	Friday
245	3	8	5	2	5	12	19	21	26	53	37	31	22	3	42	22	11	11	9	6	8	5	13	1	375	Sep	02	Saturday
246	6	1	5	4	4	9	10	8	13	19	14	9	12	10	15	25	2	31	32	11	17	16	22	3	298	Sep	03	Sunday
247	12	3	1	3	16	37	18	18	36	36	32	23	55	12	23	24	26	13	16	13	15	6	23	17	478	Sep	04	Monday
248	5	4	8	6	9	9	25	37	21	27	20	50	27	27	25	20	9	17	13	20	5	12	18	2	416	Sep	05	Tuesday
249	21	1	15	7	13	21	26	14	14	0	0	33	17	16	10	25	28	18	13	15	2	13	20	6	348	Sep	06	Wednesday
250	23	0	3	0	0	26	18	28	28	30	35	48	41	45	21	5	27	26	20	7	7	13	18	4	473	Sep	07	Thursday
251	2	13	10	14	15	10	9	46	37	38	35	41	7	0	0	0	0	15	27	14	14	7	10	3	367	Sep	08	Friday
252	5	11	7	11	4	25	5	11	16	13	21	21	17	13	14	4	4	16	4	9	6	3	15	5	260	Sep	09	Saturday
253	10	1	4	12	8	9	5	5	17	19	14	7	14	10	19	4	20	21	18	10	14	38	27	4	310	Sep	10	Sunday
254	11	3	6	2	22	12	22	14	34	19	24	32	23	20	18	15	12	17	24	14	6	13	17	15	395	Sep	11	Monday
255	1	3	9	16	20	24	8	0	0	0	0	0	0	0	0	0	0	0	0	0	0	0	0	0	81	Sep	12	Tuesday
256	0	0	0	0	0	0	9	34	21	0	24	31	39	17	15	24	29	6	15	19	2	18	21	6	330	Sep	13	Wednesday
257	1	9	5	28	23	22	13	5	0	0	0	0	0	0	0	4	16	16	10	27	15	2	19	6	221	Sep	14	Thursday
258	16	20	8	9	6	26	22	32	10	41	25	20	21	19	18	20	26	13	23	26	6	15	12	7	441	Sep	15	Friday
259	9	8	23	17	10	19	9	13	12	13	29	29	14	14	27	23	12	4	13	4	4	2	13	10	331	Sep	16	Saturday
260	8	35	6	1	0	0	0	0	0	0	0	3	16	15	21	10	9	13	27	21	20	6	12	3	226	Sep	17	Sunday
261	4	4	3	22	14	19	27	10	20	12	16	46	12	14	34	10	25	21	23	16	17	25	18	13	425	Sep	18	Monday
262	3	13	4	11	7	13	20	19	25	25	18	45	15	25	9	18	23	23	9	13	4	20	21	5	388	Sep	19	Tuesday
263	7	3	2	14	3	25	25	13	9	17	18	30	19	17	12	9	9	12	12	10	4	14	14	7	305	Sep	20	Wednesday
264	12	7	6	10	12	15	7	26	26	19	40	30	27	27	21	26	13	12	16	6	9	8	11	3	389	Sep	21	Thursday
265	5	2	7	5	13	16	5	17	23	14	21	18	20	20	16	18	22	12	8	19	12	15	10	6	324	Sep	22	Friday
266	10	4	13	3	1	18	3	21	18	27	22	18	9	16	24	11	16	6	21	10	26	1	21	2	321	Sep	23	Saturday

Table 3.4.2 (cont.)

267	6	3	5	11	11	36	14	6	6	12	5	0	20	35	69	29	12	11	14	10	21	9	25	15	385	Sep 24	Sunday
268	6	5	15	35	76	15	20	19	20	10	16	26	137	106	82	90	15	10	15	10	16	7	40	61	852	Sep 25	Monday
269	97	41	10	15	128	30	15	11	17	9	114	93	64	111	13	28	31	8	18	12	11	4	14	14	908	Sep 26	Tuesday
270	4	10	2	14	19	14	20	25	7	13	12	24	35	5	5	12	10	14	0	11	8	6	6	14	290	Sep 27	Wednesday
271	7	14	3	6	6	11	17	22	9	19	12	25	30	23	47	59	79	10	10	11	12	6	15	14	467	Sep 28	Thursday
272	4	14	1	8	4	4	19	12	22	16	9	23	42	29	22	30	23	7	4	7	12	6	7	28	353	Sep 29	Friday
273	6	12	4	7	10	6	3	9	18	7	19	18	22	24	10	19	4	8	6	4	7	6	6	12	247	Sep 30	Saturday
FRS	00	01	02	03	04	05	06	07	08	09	10	11	12	13	14	15	16	17	18	19	20	21	22	23			
Sum	1245		1502		2361		2902		3344		4562		2894		2407		2315		1832		1594		1161				
	1243		1210		1640		2510		3032		3908		3597		3027		2166		1985		1591		2347		56375	Total sum	
162	8	8	7	9	10	15	15	18	19	21	24	28	22	18	19	15	13	14	12	11	10	10	14	7	348	Total average	
126	7	7	6	9	10	14	16	19	19	21	23	28	23	18	18	15	13	14	10	10	8	9	13	7	338	Average workdays	
57	7	7	7	6	6	10	8	10	12	13	18	19	11	11	12	10	8	9	12	9	10	8	12	5	241	Average weekends	

Table 3.4.2 (cont.)

4 Improvements and modifications

4.1 NORSAR

Data acquisition

No modification has been made to the NORSAR data acquisition system. The MODCOMP system, which communicates with the NORSAR subarrays and the IBM acquisition and processing system, has been very unstable.

Due to the many old parts in the system data flow, we have found no way to make partial replacements, like say replacing the MODCOMP. The only rational upgrade/replacement seems to be to replace all systems from A/D converters (today's SLEM) to central data recording.

An upgrade of the NORSAR system should include digital data transmission from seismometer to subarray vault, and the resulting dynamic range should be comparable to that of NORESS/GERESS (at least 21 bit dynamic range). The upgrade should include broadband seismometers and local recording at the subarray vault.

Depending on which system is chosen, cables between subarray vaults and seismometers may have to be replaced, due to power requirements and/or data transmission technique.

To use the NORESS/ARCESS technology, seven such systems would be required. Moreover, there may be a problem with cabling and power. Another problem may be time synchronization for array beamforming.

The Teledyne GERESS system has not yet been tested, but may also have too large power requirements to use existing cables.

The new FINESA system would make some improvement with less cost. However, data would still be limited to the dynamic range of the analog signals on the buried cables.

The Nanometrics system used at Yellowknife and Hagfors in Sweden has features that seem to fit very well for an upgrade of the NORSAR array. With acceptable dynamic range and 16 bit resolution, the system may use existing cabling to meet all other requirements. This system has local recording.

Detection processing

The NORSAR detection processor has been running satisfactorily on the IBM during this reporting period. Processing has been moved to a more powerful IBM computer, that became available after moving NORESS to a SUN-system.

Detection statistics are given in chapter 2.

Event processing

There are no changes in the routine processing of NORSAR events, using the IBM system. Full event processing on the SUN system is not yet implemented.

4.2 NORESS

Detection processing

The routine detection processing of NORESS is running satisfactorly on a SUN-3/280. From day 091:00 through day 103:08, the RONAPP beam set of 17 coherent beams and 3 incoherent beams was used. The detection processor recipe for this beam set was described in NORSAR Sci. Rep. No. 2-88/89. The beam set is given in Table 4.2.1.

From 1989, day 103:09, we have used a recipe with 66 coherent and 10 incoherent beams, which nearly doubled the number of detections per day. The beam list is shown in Table 4.2.2. This processing includes STA/LTA detection processing only, as the computer intensive f-k analysis for each detection is performed offline as part of the event processing. This detector gives two files per day, e.g., NRS89091.DPX, indicating detection processor report (.DPX) for NORESS (NRS), day 091, 1989, and NRS89091.REP, giving reports on the occurrence of spikes and otherwise data of bad quality.

We have tested the SUN-3/280 array data acquisition system with variable processing load and found that STA/LTA processing may be performed without disturbing acquisition or data serving. However, the added load of f-k analysis for this high number of detections is not advisable.

Event processing. Phase estimation

The NORESS event processing is performed in two steps. In step 1, all detections are subjected to broadband f-k, polarization, and onset analysis, called phase estimation. This analysis results in one file per day, e.g., NRS89091.FKX, indicating f-k analysis report (.FKX) for NORESS (NRS), day 091, 1989. The report files give onset time, detection beam, SNR, velocity, preliminary phase name, azimuth, coherency, quality of f-k, frequency, amplitude, detection STA and polarization results.

This processing may be performed on any of the SUN workstations.

Event processing. Plot and Epicenter determination

In step two of the automatic event processing, all phases from one array are

analyzed for association to events, as described in NORSAR Sci. Rep. 2-88/89. The location analysis results in one file per day, e.g., NRS89091.EPX, indicating event analysis report (.EPX) for NORESS (NRS), day 091, 1989. All 'interesting' phases are plotted on an Imagen postscript laser printer. These plots also give event location, origin time and magnitude. Where a minimum of two phases (at least one P and one S) have been associated, we have located the event with the TTAZLOC procedure.

4.3 ARCESS

Detection processing

The routine detection processing of ARCESS is running satisfactorly on a SUN-3/280. From day 091:00 through day 130:09, the RONAPP beam set of 17 coherent beams and 3 incoherent beams was used. The detection processor recipe for this beam set was described in NORSAR Sci. Rep. No. 2-88/89. The beam set is given in Table 4.3.1. From day 1989-130:09, we have used a recipe with 66 coherent and 10 incoherent beams, which nearly doubled the number of detections per day. The beam list is shown in Table 4.3.2. This processing include STA/LTA detection processing only, as the computer intensive f-k analysis for each detection is performed offline as part of the event processing. This detector give two file per day. E.g., FRS89091.DPX, indicating detection processor report (.DPX) for ARCESS (FRS,ARC), day 091, 1989, and FRS89091.REP, giving reports on the occurrence of spikes and otherwise data of bad quality

Event processing. Phase estimation

The ARCESS event processing is identical to that of NORESS. This processing results in one file per day, e.g., FRS89091.FKX, indicating f-k analysis report (.FKX) for ARCESS (FRS,ARC), day 091, 1989.

Event processing. Plot and Epicenter determination

In step two of the automatic event processing, all phases from one array are analyzed for association to events, as described in NORSAR Sci. Rep. No. 2-88/89. The location analysis results in one file per day, e.g., FRS89091.EPX, indicating event analysis report (.EPX) for ARCESS (FRS,ARC), day 091, 1989. All 'interesting' phases are plotted on an Imagen postscript laser printer. These plots also give event location, origin time and magnitude. Where a minimum of two phases (at least one P and one S) have been associated, we have located the event with the TTAZLOC procedure.

J. Fyen

BEAM	Velocity	Azimuth	Filter band	Threshold	Configuration	
NR01	99999.9	0.0	1.0 - 3.0	4.0	17	CD
NR02	99999.9	0.0	1.5 - 3.5	4.0	17	CD
NR03	99999.9	0.0	2.0 - 4.0	4.0	22	BCD
NR04	99999.9	0.0	2.5 - 4.5	4.0	13	BC
NR05	99999.9	0.0	3.0 - 5.0	4.0	13	BC
NR06	99999.9	0.0	4.0 - 8.0	5.0	9	AB
NR07	99999.9	0.0	8. - 16.0	5.0	9	AB
NR08	14.3	0.0	2.0 - 4.0	4.0	22	BCD
NR09	14.3	90.0	2.0 - 4.0	4.0	22	BCD
NR10	14.3	180.0	2.0 - 4.0	4.0	22	BCD
NR11	14.3	15.0	2.5 - 4.5	4.0	22	BCD
NR12	14.3	75.0	2.5 - 4.5	4.0	22	BCD
NR13	14.3	135.0	2.5 - 4.5	4.0	22	BCD
NR14	14.3	25.0	3.0 - 5.0	4.0	22	BCD
NR15	14.3	75.0	3.0 - 5.0	4.0	22	BCD
NR16	14.3	125.0	3.0 - 5.0	4.0	22	BCD
NR17	99999.9	0.0	2.0 - 4.0	4.0	13	BC
NI18	99999.9	0.0	1.0 - 2.0	2.5	17	C
NI19	99999.9	0.0	2.0 - 3.0	2.5	22	C
NI20	99999.9	0.0	2.0 - 4.0	2.1	13	D
IN18	99999.9	0.0	1.0 - 2.0	2.5	17	C
IN19	99999.9	0.0	2.0 - 3.0	2.5	22	C
IN20	99999.9	0.0	2.0 - 4.0	2.1	13	D

Table 4.2.1 NORESS 'RONAP' beam table. The table shows the name of beam, velocity (km/sec), azimuth (degrees), filter band (Hz), STA/LTA threshold, and configuration. The configuration is described with number of sensors and A,B,C or D-rings. Center A0 is always within the configuration. NI18 - NI20 are incoherent beams using vertical components. IN18 - IN20 are identical to NI18 - NI20. This beam set was used up to 1989, day 103:08.

BEAM	Velocity	Azimuth	Filter band			Threshold	Configuration
N011	99999.9	0.0	0.5	-	1.5	4.0	10	D
N021	99999.9	0.0	1.0	-	3.0	4.0	17	CD
N031	99999.9	0.0	1.5	-	3.5	4.0	17	CD
N032	11.0	30.0	1.5	-	3.5	4.0	17	CD
N033	11.0	90.0	1.5	-	3.5	4.0	17	CD
N034	11.0	150.0	1.5	-	3.5	4.0	17	CD
N035	11.0	210.0	1.5	-	3.5	4.0	17	CD
N036	11.0	270.0	1.5	-	3.5	4.0	17	CD
N037	11.0	330.0	1.5	-	3.5	4.0	17	CD
N038	15.8	80.0	1.5	-	3.5	3.5	17	CD
N039	10.0	30.0	1.5	-	3.5	3.5	17	CD
N041	99999.9	0.0	2.0	-	4.0	4.0	17	CD
N042	10.2	30.0	2.0	-	4.0	4.0	17	CD
N043	10.2	90.0	2.0	-	4.0	4.0	17	CD
N044	10.2	150.0	2.0	-	4.0	4.0	17	CD
N045	10.2	210.0	2.0	-	4.0	4.0	17	CD
N046	10.2	270.0	2.0	-	4.0	4.0	17	CD
N047	10.2	330.0	2.0	-	4.0	4.0	17	CD
N048	15.8	80.0	2.0	-	4.0	3.5	17	CD
N049	10.0	30.0	2.0	-	4.0	3.5	17	CD
N051	99999.9	0.0	2.5	-	4.5	4.0	22	BCD
N052	8.90	30.0	2.5	-	4.5	4.0	22	BCD
N053	8.90	90.0	2.5	-	4.5	4.0	22	BCD
N054	8.90	150.0	2.5	-	4.5	4.0	22	BCD
N055	8.90	210.0	2.5	-	4.5	4.0	22	BCD
N056	8.90	270.0	2.5	-	4.5	4.0	22	BCD
N057	8.90	330.0	2.5	-	4.5	4.0	22	BCD
N058	15.8	80.0	2.5	-	4.5	3.5	22	BCD
N059	10.0	30.0	2.5	-	4.5	3.5	22	BCD
N061	99999.9	0.0	3.0	-	5.0	4.0	22	BCD
N062	10.5	30.0	3.0	-	5.0	4.0	22	BCD
N063	10.5	90.0	3.0	-	5.0	4.0	22	BCD
N064	10.5	150.0	3.0	-	5.0	4.0	22	BCD
N065	10.5	210.0	3.0	-	5.0	4.0	22	BCD
N066	10.5	270.0	3.0	-	5.0	4.0	22	BCD
N067	10.5	330.0	3.0	-	5.0	4.0	22	BCD
N068	15.8	80.0	3.0	-	5.0	3.5	22	BCD
N069	10.0	30.0	3.0	-	5.0	3.5	22	BCD
N071	99999.9	0.0	3.5	-	5.5	4.0	13	BC
N072	11.1	30.0	3.5	-	5.5	4.0	13	BC
N073	11.1	90.0	3.5	-	5.5	4.0	13	BC
N074	11.1	150.0	3.5	-	5.5	4.0	13	BC
N075	11.1	210.0	3.5	-	5.5	4.0	13	BC

Table 4.2.2 NORESS beam table. The table shows the name of beam, velocity (km/sec), azimuth (degrees), filter band (Hz), STA/LTA threshold, and configuration. The configuration is described with number of sensors and A,B,C or D-rings. Center A0 is always within the configuration. NH01 - NH04 are incoherent beams using horizontal components of the A0,C2,C4 and C7 three-component stations. NV01 - NV04 are incoherent beams using vertical components. This beam set has been in operation since 1989, day 103:08.

N076	11.1	270.0	3.5 - 5.5	4.0	13	BC
N077	11.1	330.0	3.5 - 5.5	4.0	13	BC
N081	99999.9	0.0	4.0 - 8.0	4.0	13	BC
N082	9.5	30.0	4.0 - 8.0	4.0	13	BC
N083	9.5	90.0	4.0 - 8.0	4.0	13	BC
N084	9.5	150.0	4.0 - 8.0	4.0	13	BC
N085	9.5	210.0	4.0 - 8.0	4.0	13	BC
N086	9.5	270.0	4.0 - 8.0	4.0	13	BC
N087	9.5	330.0	4.0 - 8.0	4.0	13	BC
N091	99999.9	0.0	5.0 - 10.0	4.5	13	BC
N092	10.5	30.0	5.0 - 10.0	4.5	13	BC
N093	10.5	90.0	5.0 - 10.0	4.5	13	BC
N094	10.5	150.0	5.0 - 10.0	4.5	13	BC
N095	10.5	210.0	5.0 - 10.0	4.5	13	BC
N096	10.5	270.0	5.0 - 10.0	4.5	13	BC
N097	10.5	330.0	5.0 - 10.0	4.5	13	BC
N101	99999.9	0.0	8.0 - 16.0	4.5	9	AB
N102	9.9	30.0	8.0 - 16.0	4.5	9	AB
N103	9.9	90.0	8.0 - 16.0	4.5	9	AB
N104	9.9	150.0	8.0 - 16.0	4.5	9	AB
N105	9.9	210.0	8.0 - 16.0	4.5	9	AB
N106	9.9	270.0	8.0 - 16.0	4.5	9	AB
N107	9.9	330.0	8.0 - 16.0	4.5	9	AB
NH01	99999.9	0.0	2.0 - 4.0	2.4	22	AC_ne
NH02	99999.9	0.0	3.5 - 5.5	2.4	13	AC_ne
NH03	99999.9	0.0	5.0 - 10.0	2.4	13	AC_ne
NH04	99999.9	0.0	8.0 - 16.0	2.5	9	AC_ne
NV01	99999.9	0.0	0.5 - 1.5	2.5	17	D
NV02	99999.9	0.0	1.0 - 2.0	2.5	17	C
NV03	99999.9	0.0	1.5 - 2.5	2.5	17	C
NV04	99999.9	0.0	2.0 - 3.0	2.5	22	C
NV05	99999.9	0.0	2.0 - 4.0	2.4	22	C
NV06	99999.9	0.0	3.5 - 5.5	2.4	13	C

Table 4.2.2 (cont.)

BEAM	Velocity	Azimuth	Filter band	Threshold	Configuration
FR01	99999.9	0.0	1.0 - 3.0	4.0	17 CD
FR02	99999.9	0.0	1.5 - 3.5	4.0	17 CD
FR03	99999.9	0.0	2.0 - 4.0	4.0	22 BCD
FR04	99999.9	0.0	2.5 - 4.5	4.0	13 BC
FR05	99999.9	0.0	3.0 - 5.0	4.0	13 BC
FR06	99999.9	0.0	4.0 - 8.0	5.0	9 AB
FR07	99999.9	0.0	8.0 - 16.0	5.0	9 AB
FR08	14.3	0.0	2.0 - 4.0	4.0	22 BCD
FR09	14.3	90.0	2.0 - 4.0	4.0	22 BCD
FR10	14.3	180.0	2.0 - 4.0	4.0	22 BCD
FR11	14.3	15.0	2.5 - 4.5	4.0	22 BCD
FR12	14.3	75.0	2.5 - 4.5	4.0	22 BCD
FR13	14.3	135.0	2.5 - 4.5	4.0	22 BCD
FR14	14.3	25.0	3.0 - 5.0	4.0	22 BCD
FR15	14.3	75.0	3.0 - 5.0	4.0	22 BCD
FR16	14.3	125.0	3.0 - 5.0	4.0	22 BCD
FR17	99999.9	0.0	2.0 - 4.0	4.0	13 BC
IF18	99999.9	0.0	1.0 - 2.0	2.5	17 C
IF19	99999.9	0.0	2.0 - 3.0	2.5	22 C
IF20	99999.9	0.0	2.0 - 4.0	2.1	13 D
FI18	99999.9	0.0	1.0 - 2.0	2.5	17 C
FI19	99999.9	0.0	2.0 - 3.0	2.5	22 C
FI20	99999.9	0.0	2.0 - 4.0	2.1	13 D

Table 4.3.1 ARCESS 'RONAP' beam table. The table shows the name of beam, velocity (km/sec), azimuth (degrees), filter band (Hz), STA/LTA threshold, and configuration. The configuration is described with number of sensors and A,B,C or D-rings. Center A0 is always within the configuration. FI18 - FI20 are incoherent beams using vertical components. IF18 - IF20 are identical to FI18 - FI20. This beam set was used up to 1989, day 103:09.

BEAM	Velocity	Azimuth	Filter band	Threshold	Configuration
F011	99999.9	0.0	0.5 - 1.5	4.0	10 D
F021	99999.9	0.0	1.0 - 3.0	4.0	17 CD
F031	99999.9	0.0	1.5 - 3.5	4.0	17 CD
F032	11.0	30.0	1.5 - 3.5	4.0	17 CD
F033	11.0	90.0	1.5 - 3.5	4.0	17 CD
F034	11.0	150.0	1.5 - 3.5	4.0	17 CD
F035	11.0	210.0	1.5 - 3.5	4.0	17 CD
F036	11.0	270.0	1.5 - 3.5	4.0	17 CD
F037	11.0	330.0	1.5 - 3.5	4.0	17 CD
F038	15.8	80.0	1.5 - 3.5	3.5	17 CD
F039	10.0	30.0	1.5 - 3.5	3.5	17 CD
F041	99999.9	0.0	2.0 - 4.0	4.0	17 CD
F042	10.2	30.0	2.0 - 4.0	4.0	17 CD
F043	10.2	90.0	2.0 - 4.0	4.0	17 CD
F044	10.2	150.0	2.0 - 4.0	4.0	17 CD
F045	10.2	210.0	2.0 - 4.0	4.0	17 CD
F046	10.2	270.0	2.0 - 4.0	4.0	17 CD
F047	10.2	330.0	2.0 - 4.0	4.0	17 CD
F048	15.8	80.0	2.0 - 4.0	3.5	17 CD
F049	10.0	30.0	2.0 - 4.0	3.5	17 CD
F051	99999.9	0.0	2.5 - 4.5	4.0	22 BCD
F052	8.90	30.0	2.5 - 4.5	4.0	22 BCD
F053	8.90	90.0	2.5 - 4.5	4.0	22 BCD
F054	8.90	150.0	2.5 - 4.5	4.0	22 BCD
F055	8.90	210.0	2.5 - 4.5	4.0	22 BCD
F056	8.90	270.0	2.5 - 4.5	4.0	22 BCD
F057	8.90	330.0	2.5 - 4.5	4.0	22 BCD
F058	15.8	80.0	2.5 - 4.5	3.5	22 BCD
F059	10.0	30.0	2.5 - 4.5	3.5	22 BCD
F061	99999.9	0.0	3.0 - 5.0	4.0	22 BCD
F062	10.5	30.0	3.0 - 5.0	4.0	22 BCD
F063	10.5	90.0	3.0 - 5.0	4.0	22 BCD
F064	10.5	150.0	3.0 - 5.0	4.0	22 BCD
F065	10.5	210.0	3.0 - 5.0	4.0	22 BCD
F066	10.5	270.0	3.0 - 5.0	4.0	22 BCD
F067	10.5	330.0	3.0 - 5.0	4.0	22 BCD
F068	15.8	80.0	3.0 - 5.0	3.5	22 BCD
F069	10.0	30.0	3.0 - 5.0	3.5	22 BCD
F071	99999.9	0.0	3.5 - 5.5	4.0	13 BC
F072	11.1	30.0	3.5 - 5.5	4.0	13 BC
F073	11.1	90.0	3.5 - 5.5	4.0	13 BC
F074	11.1	150.0	3.5 - 5.5	4.0	13 BC
F075	11.1	210.0	3.5 - 5.5	4.0	13 BC

Table 4.3.2 ARCESS beam table. The table shows the name of beam, velocity (km/sec), azimuth (degrees), filter band (Hz), STA/LTA threshold, and configuration. The configuration is described with number of sensors and A,B,C or D-rings. Center A0 is always within the configuration. FH01 - FH04 are incoherent beams using horizontal components of the A0,C2,C4 and C7 three-component stations. FV01 - FV04 are incoherent beams using vertical components. This beam set has been in operation since 1989, day 103:09.

F076	11.1	270.0	3.5 - 5.5	4.0	13	BC
F077	11.1	330.0	3.5 - 5.5	4.0	13	BC
F081	99999.9	0.0	4.0 - 8.0	4.0	13	BC
F082	9.50	30.0	4.0 - 8.0	4.0	13	BC
F083	9.50	90.0	4.0 - 8.0	4.0	13	BC
F084	9.50	150.0	4.0 - 8.0	4.0	13	BC
F085	9.50	210.0	4.0 - 8.0	4.0	13	BC
F086	9.50	270.0	4.0 - 8.0	4.0	13	BC
F087	9.50	330.0	4.0 - 8.0	4.0	13	BC
F091	99999.9	0.0	5.0 - 10.0	4.5	13	BC
F092	10.5	30.0	5.0 - 10.0	4.5	13	BC
F093	10.5	90.0	5.0 - 10.0	4.5	13	BC
F094	10.5	150.0	5.0 - 10.0	4.5	13	BC
F095	10.5	210.0	5.0 - 10.0	4.5	13	BC
F096	10.5	270.0	5.0 - 10.0	4.5	13	BC
F097	10.5	330.0	5.0 - 10.0	4.5	13	BC
F101	99999.9	0.0	8.0 - 16.0	4.5	9	AB
F102	9.9	30.0	8.0 - 16.0	4.5	9	AB
F103	9.9	90.0	8.0 - 16.0	4.5	9	AB
F104	9.9	150.0	8.0 - 16.0	4.5	9	AB
F105	9.9	210.0	8.0 - 16.0	4.5	9	AB
F106	9.9	270.0	8.0 - 16.0	4.5	9	AB
F107	9.9	330.0	8.0 - 16.0	4.5	9	AB
FH01	99999.9	0.0	2.0 - 4.0	2.4	22	AC_ne
FH02	99999.9	0.0	3.5 - 5.5	2.4	13	AC_ne
FH03	99999.9	0.0	5.0 - 10.0	2.4	13	AC_ne
FH04	99999.9	0.0	8.0 - 16.0	2.5	9	AC_ne
FV01	99999.9	0.0	0.5 - 1.5	2.5	17	D
FV02	99999.9	0.0	1.0 - 2.0	2.5	17	C
FV03	99999.9	0.0	1.5 - 2.5	2.5	17	C
FV04	99999.9	0.0	2.0 - 3.0	2.5	22	C
FV05	99999.9	0.0	2.0 - 4.0	2.4	22	C
FV06	99999.9	0.0	3.5 - 5.5	2.4	13	C

Table 4.3.2 (cont.)

5 Maintenance Activities

5.1 Activities in the field and at the Maintenance Center

This section summarizes the activities in the field, at the Maintenance Center (NMC) Hamar and NDPC activities related to monitoring and control of the NORSAR, NORESS and ARCESS arrays.

Activities comprise preventive/corrective maintenance in connection with all the NORSAR subarrays, NORESS and ARCESS. Other activities are related to testing the NORSAR communications systems.

Cables have been pointed out (01A,02C) and spliced (04C,02B,01B,02C). SLEMs have been replaced/reset (02B,06C). LP seismometers and related equipment have been adjusted/replaced (02B,01B,03C).

NORESS

Power and fiber cables have been cut and spliced, buried and rerouted in three new trenches (NORESS, C3). Hub station power distribution and power supply at site D3 have been replaced after lightning. Electronics on remote sites A1,A3,B3,B5 were repaired. Satellite modem was replaced and broadband instrument KS36000 installed after repair.

ARCESS

A new NORSAT B antenna was erected. Ditches and roads were sown. Fiber optical links at all sites were adjusted.

Details are presented in Table 5.1.

Subarray/ area	Task	Date
NDPC	Daily check of SP/LP data and comm. systems. Check including NORESS and ARCESS data. Weekly calibrations of SP/LP instruments. Adjustment of MP/FP parameters when outside tolerances	April
01A	In connection with digging, SP05 pointed out to a farmer.	19 May
02B	SLEM reset after power outage. Cable work SP02.	22 May
04C	Cables splicing SP04.	24 May
NORESS:	Power and fiber cables to site C3 cut and spliced. Afterwards buried in a new trench	May
NDPC	Daily routine check of NORSAR, NORESS and ARCESS data. Weekly calibration of SP/LP instruments.	May
NORSAR:		
02C	Cable splicing SP05.	19,20 June
02B	Cable splicing SP02.	21,22 June
06C	Check of EW LP seismometer.	23 June
04C	Cable splicing SP04.	26 June
02B	Replaced MP motor (RCD) EW LP seismometer.	27 June
02B	Cable fault SP04.	28 June
06C	Digital Unit replaced (SLEM).	29 June
01B	Cable splicing SP02.	30 June
ARCESS:	Ditches and roads sown.	1-12 June
	Fiber opitical links at all sites adjusted.	11,12 June
NORESS:	Satellite transmitter modem, Hub and remote site (C3,D5,D2,D3) were still down due to lack of spare parts (from Sandia).	June
NORSAR:		
04C	Visit to SP02,03 and 00 in connection with repair after lightning.	6 July
01A	Cable work SP02.	24,26 July
01A	Cable work SP04.	27,28 July
02C	Cable splicing SP05.	25 July

Table 5.1 Activities in the field and the NORSAR Maintenance Center, including NDPC activities related to the NORSAR array, 1 April – 30 September 1989.

Subarray/ area	Task	Date
ARCESS:	Array visited by P.W. Larsen. Satellite modem was replaced.	18-20 July
NORESS:	Hub station power distribution replaced.	4 July
	Power supply site D3 replaced after lightning.	5 July
	HF supply faulty	17 July
	Lightning put the array out of operation and it remained so throughout the month.	24 July
NDPC:	Daily routine check of NORSAR, NORESS and ARCESS data.	July
NORSAR:		
06C	Replaced SLEM power supply.	1 Aug
06C	Cable splicing carried out SP03.	17 Aug
02C	Located faulty cable SP05.	31 Aug
NDPC:	Daily check of NORSAR, NORESS and ARCESS data.	Aug
	Calibration every week of NORSAR LP instruments. Measurements of Mass Pos. and Free Period, adjusted when outside tolerances.	Aug
ARCESS:	Installed broadband instrument KS36000 which has been in USA for repair. In addition, a new NORSAT B antenna erected.	1-7 Sep
NORESS:	Electronics on remote sites A1,A3,B3,B5 repaired, and cable D6 spliced.	12-15 Sep & 20 Sep
NORSAR:		
01A	Repaired damaged cable SP02.	18-19 Sep
01B	LP instruments adjusted.	22 Sep
02C	Repaired JB box SP05.	11 Sep
03C	SP/LP adjustments carried out.	25 Sep
04C	Test Gen. and Protection Card on SP04 replaced.	21 Sep
02B	(Telemetry) Station 2 was repaired.	26,27 Sep
06C	Broadband filter removed from ch. 05 and experiment terminated.	30 Sep
NDPC:	Daily check of NORSAR, NORESS and ARCESS data. In spite of a failing Modcomp we were able to calibrate and check the NORSAR array.	Sep

Table 5.1 (cont.)

5.2 Array status

Broadband filter experiment 06C SP ch 05 was terminated by the end of September 1989.

As of 30 Sep 1989 the following NORSAR channels deviated from tolerances.

01A 01 8 Hz filter
02 8 Hz filter
04 30 dB attenuator

O.A. Hansen

6 Documentation Developed

Hansen, R.A., H. Bungum and A. Alsaker (1989): Three recent larger earthquakes offshore Norway, *Terra Nova*, 3, 284-295.

Loughran, L.B. (ed.) (1989): *Semiannual Technical Summary, 1 October 1988 - 31 March 1989*, NORSAR Sci. Rep. 2-88/89, Kjeller, Norway.

Maupin, V. (1989): Surface wavs in weakly anisotropic structures: on the use of ordinary or quasi-degenerate perturbation methods, *Geophys. J.*, 98, 553-563.

Maupin, V. (1989): Numerical modelling of Lg wave propagation across the North Sea Central Graben, *Geophys. J. Int.*, 99, 273-283.

Mykkeltveit, S. (ed.) (1989): *NORSAR Basic Seismological Research, 1 Jan - 30 Sep 1989*, Annual Tech. Report, NORSAR, Kjeller, Norway.

7 Summary of Technical Reports / Papers Published

7.1 A performance test of the generalized beamforming method applied to a data base of regional events

Introduction

In the real time processing of seismic network data, one of the most important aspects is to properly associate phases detected at individual stations. For a network of regional arrays, the current state-of-the-art is represented by the IAS system, where the Assess procedure is used for phase association and location estimation (Bache, 1987).

The generalized beamforming method introduced by Ringdal and Kværna (1989) is a different approach that has shown considerable promise as an efficient way to obtain phase grouping and initial epicenter estimates. In this paper, the method is applied to a data base of 77 regional and local events and compared to IAS results. It is found that the generalized beamforming is able to match the good results by Assess as far as phase grouping is concerned, and that the epicenter determinations are also quite accurate.

It is concluded from this study that the new method could be useful as a supplement to the expert systems techniques in future extensions of the IAS system. While some further testing would be required, it would appear that the method could be particularly valuable as a pre-processor in this regard. In this way, the results from the generalized beamforming could be taken as input to a procedure where the rule-based and script-based algorithms implemented in the IAS could be used to further refine the solutions.

Data analysis

The data set of event recordings from NORESS and ARCESS were first processed by the IAS detector program, called Sigpro, to generate detection lists for each array. The detection list was then processed by the IAS rule-based expert system, called Assess, to define event groups and event locations.

Subsequently the automatic Assess solutions were reviewed by an analyst, and if necessary, phases were retimed or new phases were picked to get more precise locations. When false events occurred, these were invalidated by the analyst.

As we consider the analyst-reviewed event definitions and locations to be correct, we will use those as a basis for evaluating the performance of the gen-

eralized beamforming method. For reference, we will also present the results produced by Assess.

1) Identification of event groups

After analyst review of the Assess solutions, 76 events were observed. Phase detections belonging to a common event, will be called an event group. 72 of the 76 event groups were validated or relocated after analyst review. The remaining 4 events can be divided into the following classes:

a) One multiple event that was observed as a separate event group, but with wrong phase id's. This event was not relocated by the analyst.
b) One triple event that was observed as one separate event group, but with wrong phase id's. These events were not relocated by the analyst.
c) One multiple event that was observed by analyst, but was not given any separate event group by Assess.

Both the generalized beamforming method and Assess in a few cases gave automatic locations that deviated considerably from the locations found after analyst review. But as long as a real event candidate is identified, the analyst can later make the necessary adjustments of phase id's and arrival times. We will therefore consider the event in 1a) as identified by Assess, one of the two events in 1b) as identified, whereas the second event in 1b) and the event in 1c) is missed.

The generalized beamforming method found 71 of the 72 events that were validated or relocated after analyst replacement. The events in 1a) and 1b) were missed, whereas the event in 1c) was identified. One new event was identified, so we set the number of events observed by analyst to 77.

If we discard the multiple events in 1a)-1c) from the statistics, the generalized beamforming method and Assess remain with one missing event each, both of these being small interfering events observed on one array only.

	Analyst	Generalized	Assess
Events identified	77	73	74
Excluding multiples	73	72	72

2) False events

An important factor in real-time operation of seismic networks is the number of false event groups created by the automatic system. If an analyst is going to review the automatic output, he will want the number of false events to be at a reasonable level. By split two-array events we mean that a single event was detected on two arrays, but the automatic algorithm created an extra event that was false. By split one-array event we mean that the event was detected on one array only, but the automatic algorithm created an extra event that was false. Implausible associations were decided on the basis of detection list information like amplitudes and frequency content of the different phases, knowledge of propagation characteristics and/or by inspecting the actual data.

	Generalized	Assess
Split two-array events	1	7
Split one-array events	0	4
Implausible associations	7	4
Number of false events	8	15

3) Phase identification

The generalized beamforming method takes advantage of the travel-time pattern of the detected phases when event groups and phase identifications are defined. For events with detections on one array only, we know that these patterns in many cases do not contain sufficient information for defining the individual phase identifications. In those situations a rule-based approach has to be invoked.

For 39 events in the sample data base with detections on two arrays, we have made some statistics for both the generalized beamforming method and Assess that reflect the ability to assign correct phase id's to the different detections. The reference will be the phase id's selected by analyst.

The columns of the following tables need some explanation.

correct - gives the number of correctly identified detections.
early - gives the number of cases where a detection preceding the correct one is selected.
late - gives the number of cases where a detection following the correct one is selected.

missed - gives the number of cases were a detection is identified by the analyst, but missed by the automatic method.

phases - means number of detections identified as defining phases by the analyst. # phases=correct+early+late+missed
The number of events analyzed is 39, as indicated earlier.

false - gives number of cases where the automatic method picked a defining phase that was not identified by the analyst.

For both the generalized beamforming method and Assess, we give tables for the phase identification performance on Noress and Arcess detections. By adding the two tables, we also indicate the overall performance.

Generalized beamforming

NORESS

	correct	early	late	missed	# phases	false
nrs-pn	31	0	5	1	37	0
nrs-pg	0	0	0	0	0	1
nrs-sn	23	0	6	0	29	0
nrs-lg	24	1	4	1	30	2
sum	78	1	15	2	96	3

ARCESS

	correct	early	late	missed	# phases	false
arc-pn	34	0	4	1	39	0
arc-pg	3	0	0	0	3	11
arc-sn	15	1	12	2	30	3
arc-lg	13	2	10	1	26	3
sum	65	3	26	4	98	17

NORESS and ARCESS

	correct	early	late	missed	# phases	false
sum-pn	65	0	9	2	76	0
sum-pg	3	0	0	0	3	12
sum-sn	38	1	18	2	59	3
sum-lg	37	3	14	2	56	5
sum	143	4	41	6	194	20

Assess

NORESS

	correct	early	late	missed	# phases	false
nrs-pn	30	0	1	6	37	0
nrs-pg	0	0	0	0	0	0
nrs-sn	21	0	0	8	29	1
nrs-lg	20	1	2	7	30	2
sum	71	1	3	21	96	3

ARCESS

	correct	early	late	missed	# phases	false
arc-pn	34	0	3	2	39	0
arc-pg	1	0	0	2	3	0
arc-sn	12	1	3	14	30	1
arc-lg	14	2	4	6	26	4
sum	61	3	10	24	98	5

NORESS and ARCESS

	correct	early	late	missed	# phases	false
sum-pn	64	0	4	8	76	0
sum-pg	1	0	0	2	3	0
sum-sn	33	1	3	22	59	2
sum-lg	34	3	6	13	56	6
sum	132	4	13	45	194	8

Within the data base there were 9 one-array events with three or more defining phases. That all of these events were observed on ARCESS, reflect the fact that very few events within the data base had epicenters close to NORESS. In cases with one-array events defined by three or more phases, there is a possibility that the generalized beamforming method can utilize the travel-time pattern to come up with correct phase id's.

The following two tables indicate the performance of the two methods on this data set.

Generalized beamforming

	correct	early	late	missed	# phases	false
arc-pn	6	0	3	0	9	0
arc-pg	2	0	1	0	3	5
arc-sn	7	0	1	0	8	1
arc-lg	5	0	0	1	6	1
sum	20	0	5	1	26	7

Assess

	correct	early	late	missed	# phases	false
arc-pn	8	1	0	0	9	0
arc-pg	1	0	0	2	3	0
arc-sn	5	0	0	3	8	0
arc-lg	1	1	2	2	6	1
sum	15	2	2	7	26	1

4) Initial location estimates

Although the generalized beamforming method gave reasonable phase id's for the 9 one-array events considered above, we can not give very much confidence to the initial event locations. Within the predefined azimuth acceptance limits, all points with the same radius from the observation point will be equally good location candidates. As we have not run any location program on the phases identified by the generalized beamforming method, the location estimates for these events will not be very accurate. But for completeness, we present the results.

For the epicenter estimates obtained by the generalized beamforming method and Assess, we calculated the deviations from the epicenters computed after analyst review. These deviations were grouped into different intervals, as shown below.

Deviation from analyst reviewed epicenter solutions for all one-array events with three or more defining phases.

Deviation in km	Number of events within distance interval	
	Generalized	Assess
d≤10	0	3
10<d≤25	0	2
25<d≤50	4	1
50<d≤100	2	2
100<d≤200	3	1
200<d	0	0
events	9	9

In the following table we consider the 39 events that were detected on two arrays.

Deviation from analyst-reviewed epicenter solutions for all two-array events

Deviation in km	Number of events within distance interval	
	Generalized	Assess
d≤10	3	8
10<d≤25	8	5
25<d≤50	15	12
50<d≤100	7	7
100<d≤200	4	2
200<d	2	5
events	39	39

Discussion

We have in the preceding section shown that when processing data from two arrays, the generalized beamforming method identified 73 out of 77 event groups. When discarding multiple events from the same location, only one small interfering one-array event was missed.

Some false event groups were created, and this requires some attention. In the cases were two phases from two arrays are erroneously associated together, a check on the amplitude (magnitude) of the two phases would remove some of the event candidates.

One of the main problems in automatic identification of seismic phases, is the relatively large number of detections in the coda of the seismic signals. If the travel-time functions of the different phases do not fit with what we acually observe, there is a possibility that the generalized beamforming method will

assign a phase id to one of the coda detections. For the 39 two-array events, we find that this happened in 41 cases.

As an additional test, we wanted to check if we could improve the performance by introducing some simple rules to the procedure. They were as follows:

a) If a phase is assigned the id Pn, and the event group contains a preceding Pn candidate (within some given time interval), the preceding phase is given the id Pn.
b) If a phase is assigned the id Sn, and the event group contains a preceding Sn candidate (within some given time interval), the preceding phase is given the id Sn.
c) If a phase is assigned the id Lg, and the event group contains an Lg candidate with a larger STA value (within some given time interval), that phase is given the id Lg.

The time intervals were for all 3 phases set to 10 seconds, and we did of course also check how these rules affected the previously correct phase assignments. The results are shown in the tables below.

Generalized beamforming

NORESS

	correct	early	late	missed	# phases	false
nrs-pn	36	0	0	1	37	0
nrs-pg	0	0	0	0	0	1
nrs-sn	27	0	2	0	29	0
nrs-lg	26	0	3	1	30	2
sum	89	0	5	2	96	3

ARCESS

	correct	early	late	missed	# phases	false
arc-pn	36	0	2	1	39	0
arc-pg	3	0	0	0	3	11
arc-sn	23	1	4	2	30	3
arc-lg	14	2	9	1	26	3
sum	76	3	15	4	98	17

NORESS and ARCESS

	correct	early	late	missed	# phases	false
sum-pn	72	0	2	2	76	0
sum-pg	3	0	0	0	3	12
sum-sn	50	1	6	2	59	3
sum-lg	40	2	12	2	56	5
sum	165	3	20	6	194	20

What we found was that these simple rules improved the performance on Pn and Sn considerably, but the Lg-rule did not provide almost any improvement. Another approach that could possibly be used to better identify Lg is to compute an event location based on the identified phases and thereafter reselect Lg from the detection that best fitted the predicted Lg arrival time.

But the fundamental problem is that for many regions, we do not have the correct travel-time functions, so to further improve the performance of the generalized beamforming method, we need to introduce regionalized travel-time functions that reflect the automatic picks.

For the 9 one-array events with three or more defining phases, 5 out of 26 phase id's were assigned to coda detections. By introducing the same rules as outlined for the two-array events, this number was reduced to 2, as shown in the table below.

Generalized beamforming

	correct	early	late	missed	# phases	false
arc-pn	9	0	0	0	9	0
arc-pg	2	0	1	0	3	5
arc-sn	8	0	0	0	8	1
arc-lg	4	0	1	1	6	1
sum	23	0	2	1	26	7

For the two-array data set, the analyst only identified 3 Pg phases, all on ARCESS. The generalized beamforming method correctly identified these phases, but in addition, 12 Pn coda detections were assigned the id Pg. Some of these false Pg identifications may be removed by giving this phase some stronger constraints on apparent velocity and/or polarization attributes.

The generalized beamforming produced initial locations that were consistent with the relatively good performance on phase identification. The natural next step would be to run a location program on the identified phases, and then compare to the location obtained after analyst review.

In this study we have presented results on the performance of the generalized beamforming method on a network of two arrays. The next step will be to get detection data (real or synthetic) for a larger network of arrays and single stations, and test the method on this data set. Since the computer programs for this method is almost fully parameterized, only minor modifications are needed for such an experiment.

References

Bache, T.C. (1987): A knowledge-based system for analyzing data from a network of NORESS-type arrays. Papers presented at 9th DARPA/AFGL Research Symposium, 15-18 June, 167-172.

Ringdal, F. and T. Kværna (1989): A multichannel processing approach to real time network detection, phase association and threshold monitoring. Bull. Seism. Soc. Am., 79, 1927-1940.

T. Kværna

7.2 NORSAR P-wave detection and yield estimation of selected Semipalatinsk explosions

In the most recent NORSAR Semiannual Technical Summary (NORSAR Scientific Report No. 2-88/89) results are presented showing that the Lg phase provides very stable measurements of magnitudes of Semipalatinsk underground nuclear explosions, thereby showing considerable promise with regard to explosion yield estimation (Ringdal and Marshall, 1989). A possibility to compare Lg and P magnitudes to published yields for Semipalatinsk explosions has now emerged with the recent publication by Soviet scientists quoting yield estimates for a number of such explosions (Bocharov *et al.* 1989, Vergino, 1989). This paper presents preliminary results from a study comparing NORSAR measurements to these yield data.

Yield estimation based on NORSAR Lg data

We have made an effort to conduct detailed analysis of available NORSAR Lg data for the largest explosions in the data set given by Bocharov *et al* (1989) (Table 7.2.1). The results are as follows:

The Shagan River event of 11/02/72: This event was included in the data base of Ringdal and Marshall (1989), with an M(Lg) value of 6.118.

The Shagan River event of 12/10/72: This event was likewise in the above data base, with M(Lg) = 6.116. However, a factor not compensated for in this estimate was the occurrence of a smaller (m_b = 5.6) explosion at Degelen Mountains with origin time a few seconds before the Shagan River event (Fig. 7.2.1). The quoted M(Lg) value includes a contribution from Lg waves from this smaller event, and is therefore slightly high. Making the reasonable assumption that the Lg signals from the two events add up incoherently, i.e., that the signal power adds up, it is possible to compensate for this interference in the same way as the noise compensation is performed. To do this, we need an estimate of M(Lg) for the smaller event, and a range of 5.5–5.7 seems reasonable. The corresponding bias values are found to range from 0.013 to 0.030 units, with a mean of 0.021. Thus a revised M(Lg) estimate of 6.116-0.021 = 6.095 is obtained, with an uncertainty of about ± 0.01 units resulting from this compensation procedure.

The Shagan River event of 11/30/69: We have been able to recover initial NORSAR data from this explosion. At the time, only 13 NORSAR SP channels (out of 132) were in operation, and 5 of these were among the 42 channels used in the previous analysis. Based on these 5 channels, we have estimated M(Lg) = 6.043 ± 0.021 for this event.

The Degelen Mountains event of 4/25/71: We have processed this event, using exactly the same procedure as for the Shagan River explosions, with the same

time windows, filter setting and channel corrections. The resulting estimate is M(Lg) = 5.862 ± 0.013, based on 42 NORSAR channels.

Fig. 7.2.2 shows a plot of M(Lg) versus published yields (Bocharov *et al*, 1989) for these four explosions. We note that the correspondence is excellent, although there are of course far too few data points to draw any firm conclusion. Nevertheless, it is interesting to note that the Degelen event appears to give consistent observations with the Shagan River explosions, which also would be expected from the earlier observed stability of the M(Lg) estimates.

For comparison, Fig. 7.2.3 shows a plot of world-wide m_b versus these yield values for the same four events. The scatter is far greater than for the Lg data. Looking at the differences m_b-log Y, it is interesting to note that the two explosions in the SW and NE Shagan River area show a relative bias of 0.13 units, which is very close to the m_b-M(Lg) anomaly of 0.15 magnitude units found by Ringdal and Marshall (1989) between these two subregions.

Detection of low-yield explosions

The cited Soviet publication also lists a number of low-yield nuclear explosions conducted at Semipalatinsk. We have analyzed available NORSAR data for these explosions, for the purpose of assessing the detection thresholds of the NORSAR/NORESS system in terms of explosion yields. Fig. 7.2.4 shows NORSAR single instrument P-wave recordings of the three smallest explosions with NORSAR data available: 2 Sep 72 (2 kt), 28 Mar 72 (6 kt) and 16 Aug 72 (8 kt). We have chosen to display the instrument 06C02, which is co-located with the center seismometer of the NORESS array (Note that NORESS data have only been available since 1984). The traces have been filtered in the band 2.0-4.0 Hz, and the signal-to-noise ratios (STA/LTA) are given for each trace. Note that an STA/LTA treshold of 4.0 is generally sufficient to confidently declare a signal detection.

It is clear from this figure that the NORSAR detection threshold, at the single seismometer level, is well below the yields of the three events shown. By a reasonable extrapolation, it can be inferred that, given similar coupling conditions and noise levels as in these three examples, Semipalatinsk explosions of yields as low as 0.5 kt would be expected to produce detectable signals at NORSAR, even at the single sensor level.

While the available data are not sufficient to draw any firm conclusions regarding the NORSAR/NORESS array thresholds, some preliminary observations may nevertheless be made. Thus, it has been established in earlier studies that the SNR gains of NORESS in the filter band shown are at least 14 dB (Kværna, 1989), which corresponds to a factor of 5 in signal amplitude. This indicates a detection threshold of 0.1 kt or lower for the NORESS array for fully coupled Semipalatinsk explosions, assuming normal noise con-

ditions. Such an assertion is also consistent with earlier studies indicating that NORESS has a detection threshold, in terms of m_b, of about 3.0 or lower for the Semipalatinsk region.

Conclusions

Studies of NORSAR recordings of Semipalatinsk explosions for which Soviet yield estimates are available confirm that NORSAR Lg magnitudes have a potential for providing very accurate yield estimates in the magnitude range where there is sufficient signal-to-noise ratio. Notably, the P-Lg bias earlier observed between the NE and SW parts of the Shagan River test site is reflected in a similar bias between m_b and log (Yield).

Furthermore, the excellent signal detectability of the NORSAR/NORESS system has been confirmed. The detection threshold for fully coupled Semipalatinsk explosions, assuming normal noise conditions, appears to be below 1 kt, even at the single sensor level. Additional significant improvement would be obtainable through array processing. Clearly, this detection level will not be achieved in cases where the noise level is abnormally high (e.g., in the coda of a large earthquake) or if coupling conditions are not optimal (e.g., in case of full or partial cavity decoupling). It must also be noted that the event identification threshold is necessarily higher than the signal detection threshold, and that there are currently no seismic methods available to distinguish reliably between small underground nuclear explosions and chemical explosions of similar yields.

F. Ringdal

References

Bocharov, V.S., S.A. Zelentsov and V.I. Mikhailov (1989): Characteristics of 96 underground nuclear explosions at the Semipalatinsk test facility, *Atomic Energy*, 67, 3, 210-214 (in Russian).

Kværna, T. (1989): On exploitation of small-aperture NORESS type arrays for enhanced P-wave detectability, *Bull. Seism. Soc. Am.*, 79, 888-900.

Ringdal, F., and P.D. Marshall (1989): Yield determination of Soviet underground nuclear explosions at the Shagan River Test Site. *NORSAR Semiannual Technical Summary, 1 Oct 1988 - 31 Mar 1989*, NORSAR Sci. Rep. 2-88/89.

Vergino, E.S. (1989): Soviet Test Yields, EOS, Nov [illegible] 1989, 1511-1525.

Date	Region	m_b	NORSAR M(Lg)	Yield kt
11/30/69	Shagan (TZ)	6.02	6.043	125
04/25/71	Degelen	5.94	5.862	90
11/02/72	Shagan (SW)	6.16	6.118	165
12/10/72	Shagan (NE)	5.96	6.095*)	140

*) Adjusted for interfering explosion

Table 7.2.1 Parameters of four explosions analyzed in this study. Yield estimates are from Bocharov *et al* (1989).

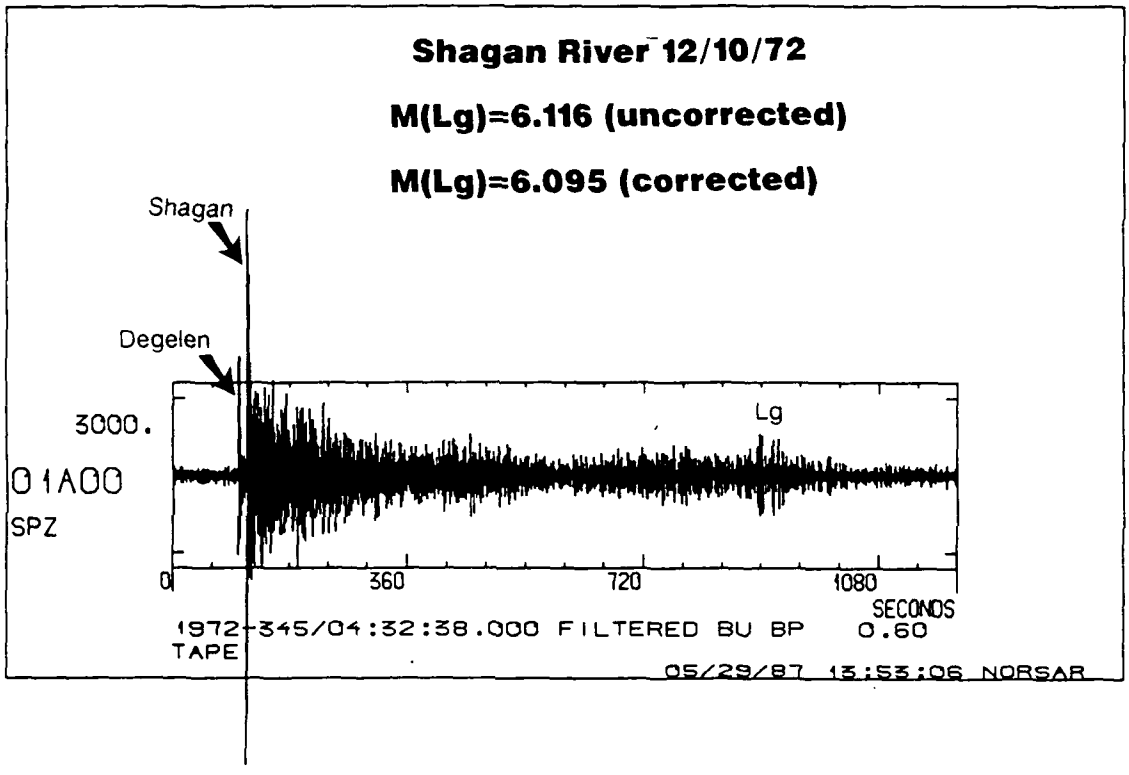

Fig. 7.2.1 NORSAR recordings (instrument 01A00) of the double explosion on Dec 12, 1972. Note that the Lg phase is a superposition of signals from both sources, although the contribution from the smaller explosion (Degelen) is relatively modest. By estimating a confidence interval of the M(Lg) for the Degelen event, it is possible to compensate for the effects on the M(Lg) for the Shagan River event, as described in the text.

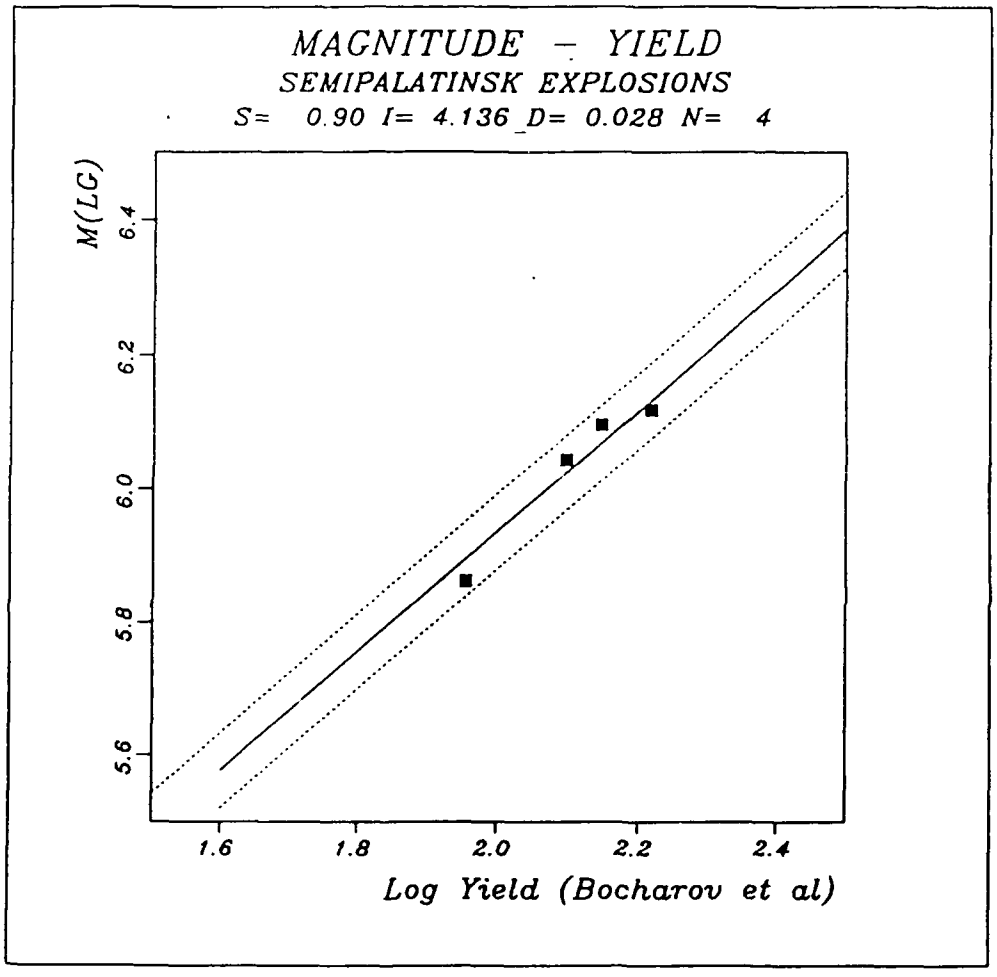

Fig. 7.2.2 Comparison of M(Lg) and log(yield), of the four explosions in Table 7.2.1, with the yield values taken from Bocharov *et al* (1989). The slope of the straight lines has been restricted to 0.9. Note the excellent correspondence.

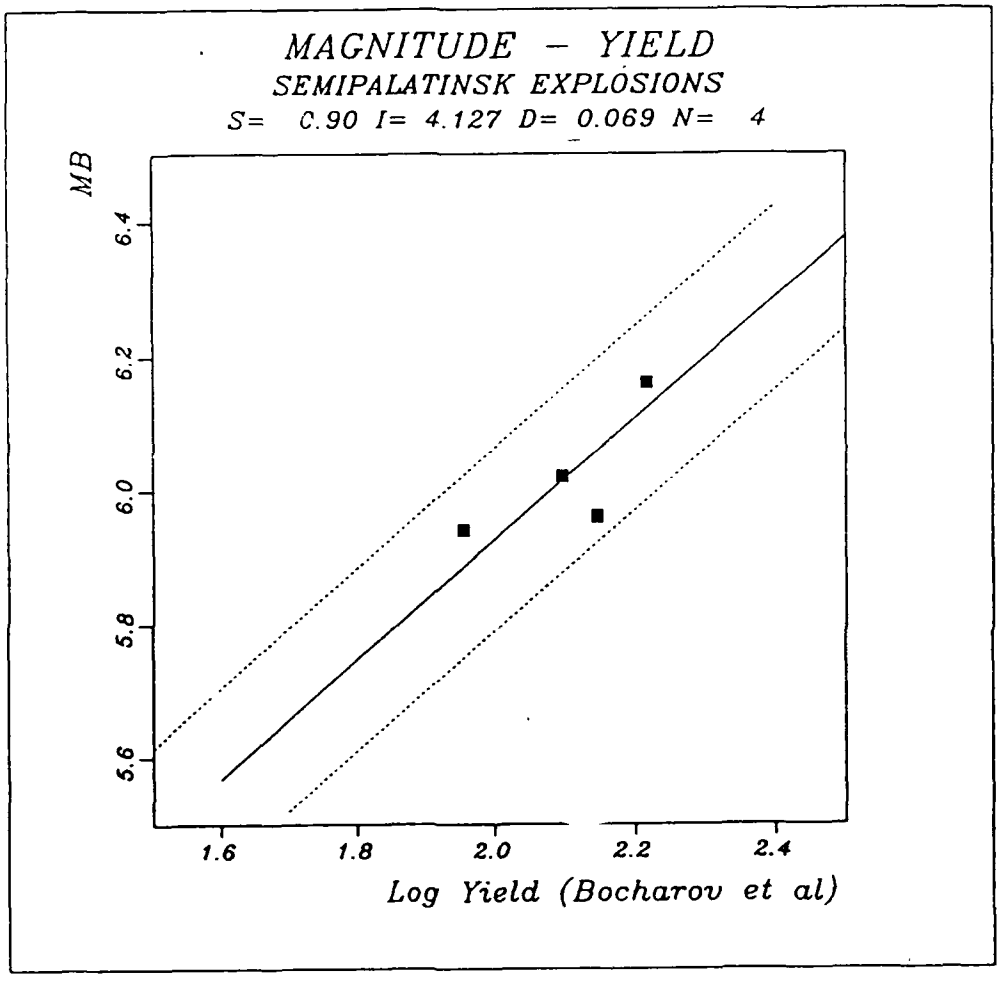

Fig. 7.2.3 Same as Fig. 7.2.2, but using m_b instead of M(Lg). Note the much greater scatter in this plot.

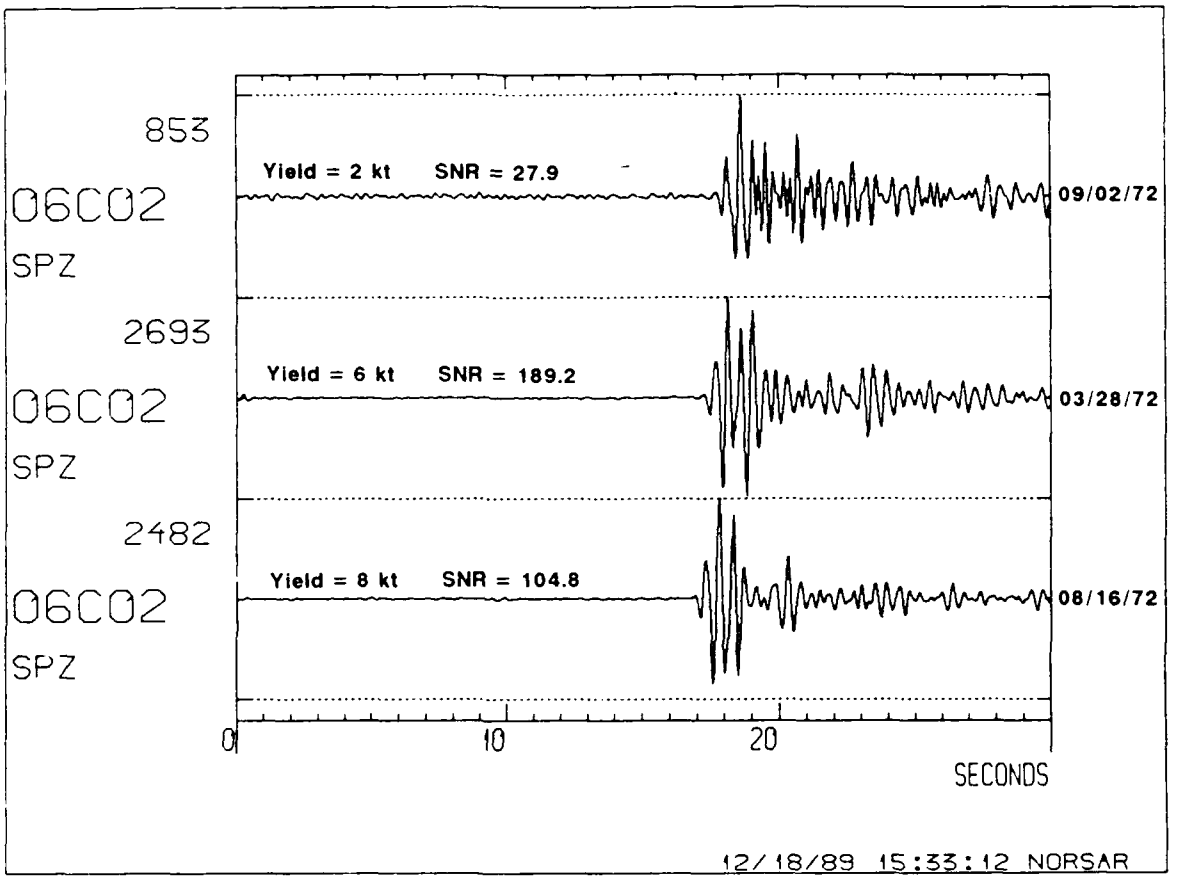

Fig. 7.2.4 NORSAR single seismometer recordings (instrument 06C02) of three low-yield Semipalatinsk nuclear explosions. The traces have been filtered in the band 2.0-4.0 Hz, and the signal-to-noise ratio is shown for each trace. Note the very high SNR observed even at the single sensor level. Significant additional SNR gain would be obtained through array processing of the NORSAR data.

7.3 Analysis of data from the China Digital Seismograph Network (CDSN) for Soviet nuclear explosions

This paper is a follow-up to earlier work (Ringdal and Marshall, 1989; Hansen *et al*, 1989) aimed at evaluating the stability of seismic Lg magnitudes for yield estimation purposes. In particular, these efforts have involved analyzing available Lg data from Soviet nuclear explosions at the Shagan River, Semipalatinsk test site, and conducting comparative analyses of Lg and P recordings at various seismograph stations.

Hansen *et al* (1989) analyzed data recorded at four digital stations installed by IRIS in the Soviet Union, and found an excellent correspondence between Lg measurements at these stations and the NORSAR M(Lg) estimates published by Ringdal and Marshall (1989). Furthermore, they noted the very high Lg signal-to-noise ratio observed at the IRIS stations, in particular ARU and GAR, and concluded that reliable Lg measurements at these stations would be possible for explosions as small as $m_b = 4.0$, assuming normal noise conditions.

In this paper, we extend the analysis to data from the China Digital Seismograph Network (CDSN), which is operated by the USGS in cooperation with the State Seismological Bureau, Beijing. Two of the CDSN stations, WMQ in Urumqi and HIA in Hailar, have particularly good Lg propagation paths from Semipalatinsk, and we have based our analysis on data from these two stations.

Fig. 7.3.1 shows the locations of the two stations in relation to the test site, as well as locations of the NORSAR and the IRIS stations. WMQ has an epicentral distance to Shagan River of 960 km, whereas HIA is at a distance of about 3000 km. Both stations show excellent Lg recordings of Semipalatinsk explosions, as illustrated by the examples in Figs. 7.3.2 and 7.3.3.

In our analysis of WMQ and HIA Lg recordings, we have employed the exact same procedure as described for IRIS data by Hansen *et al* (1989), and the details will not be repeated here. Data from a total of 12 Shagan River explosions, dating back to 1987, were provided to us for this analysis by the Center for Seismic Studies. Table 7.3.1 lists these events along with the estimated parameters.

Fig. 7.3.4 shows a comparison of WMQ and NORSAR log RMS (Lg) estimates for these 12 events. The slope of the plot has been restricted to 1.00, and the standard deviation of the differences between the two stations is only 0.034 units. This is essentially the same scatter found earlier by Hansen *et al* (1989) when comparing data from NORSAR and the Soviet station ARU, and confirms the excellent stability of the RMS Lg estimates.

Fig. 7.3.5 shows a comparison of HIA and NORSAR log RMS (Lg) esti-

mates. In this case, the slope of the least squares linear relationship (1.48) is significantly different from unity, and we note that a similar observation was also made by Ringdal and Marshall (1989) when comparing NORSAR and Gräfenberg Lg. We will not go into any detail discussing possible underlying physical reasons for this variability in slopes. For our purpose, the important point is to note that the scatter of the relationship is still very small: the standard deviation in the y-axis direction being 0.041 units. The "orthogonal" standard deviation relative to the straight line fit is 0.023, which in fact compares very closely to the orthogonal standard deviation of 0.024 which can be inferred from the WMQ-NORSAR data shown in Fig. 7.3.4.

In Fig. 7.3.6 we plot the HIA versus WMQ log RMS (Lg) values, and again observed that the least-squares slope (1.36) is significantly different from unity. Once more, the scatter is very small, with an orthogonal standard deviation of 0.028 units.

Fig. 7.3.7 is a plot comparing WMQ Lg data with maximum likelihood ISC m_b estimates. Compared to the previous figures, this plot shows a somewhat greater standard deviation of 0.060 measured in the y-axis direction. This scatter is still quite small, but it must be noted that only one event from the northeast part of Shagan is in the data base. Thus, we cannot assess whether the M(Lg) versus m_b bias earlier found for this subregion (Ringdal and Marshall, 1989) is also present when measuring Lg at WMQ.

Finally, Fig. 7.3.8 compares the signal-to-noise ratios (defined as Lg signal to pre-P noise) for stations at various distances, using 5 large explosions. It is noteworthy that WMQ shows the best SNR for all the events. The figure suggests that WMQ would be able to give Lg measurements for events two magnitude units smaller than the NORSAR threshold of approximately 5.5. Unfortunately, there were no low magnitude events in our data base, so we have not been able to confirm this hypothesis.

In conclusion, our studies confirm that Lg magnitude estimates of Semipalatinsk explosions are remarkably consistent between stations widely distributed in epicentral distance and azimuth. It thus appears that a single station with good signal-to-noise ratio can provide M(Lg) measurements with an accuracy (one standard deviation) of about 0.03–0.04 magnitude units. Thus, the Lg phase shows considerable promise for use in yield determination, although more data will be needed before the accuracy of Lg-estimated yields can be firmly established.

R.A. Hansen
F. Ringdal

References

Hansen, R.A., F. Ringdal and P.G. Richards (1989): Analysis of IRIS data for Soviet nuclear explosions, *NORSAR Semiannual Tech. Summary, 1 Oct 1988 - 31 Mar 1989*, NORSAR Sci. Rep. 2-88/89.

Ringdal, F. and P.D. Marshall (1989): Yield determination of Soviet underground nuclear explosions at the Shagan River Test Site, *NORSAR Semiannual Tech. Summary, 1 Oct 1988 - 31 Mar 1989*, NORSAR Sci. Rep. 2-88/89.

No.	Date	m_b	NAO Lg	WMQ Lg	HIA Lg
1	87171	6.03	3.012	3.851	2.189
2	87214	5.83	2.911	3.693	2.072
3	87319	5.98	3.014	3.870	2.298
4	87347	6.06	3.133	3.907	2.352
5	87361	6.00	3.086	3.851	2.339
6	88044	5.97	3.082	3.911	-
7	88094	5.99	3.103	3.925	2.307
8	88125	6.09	3.084	3.958	-
9	88258	6.03	3.014	3.827	2.224
10	88317	5.20	2.307	3.104	-
11	88352	5.80	2.846	3.636	1.947
12	89043	5.90	2.836	3.619	1.921

Table 7.3.1 Magnitudes (m_b) and log RMS Lg values at NORSAR, WMQ and HIA for 12 explosions analyzed in this study.

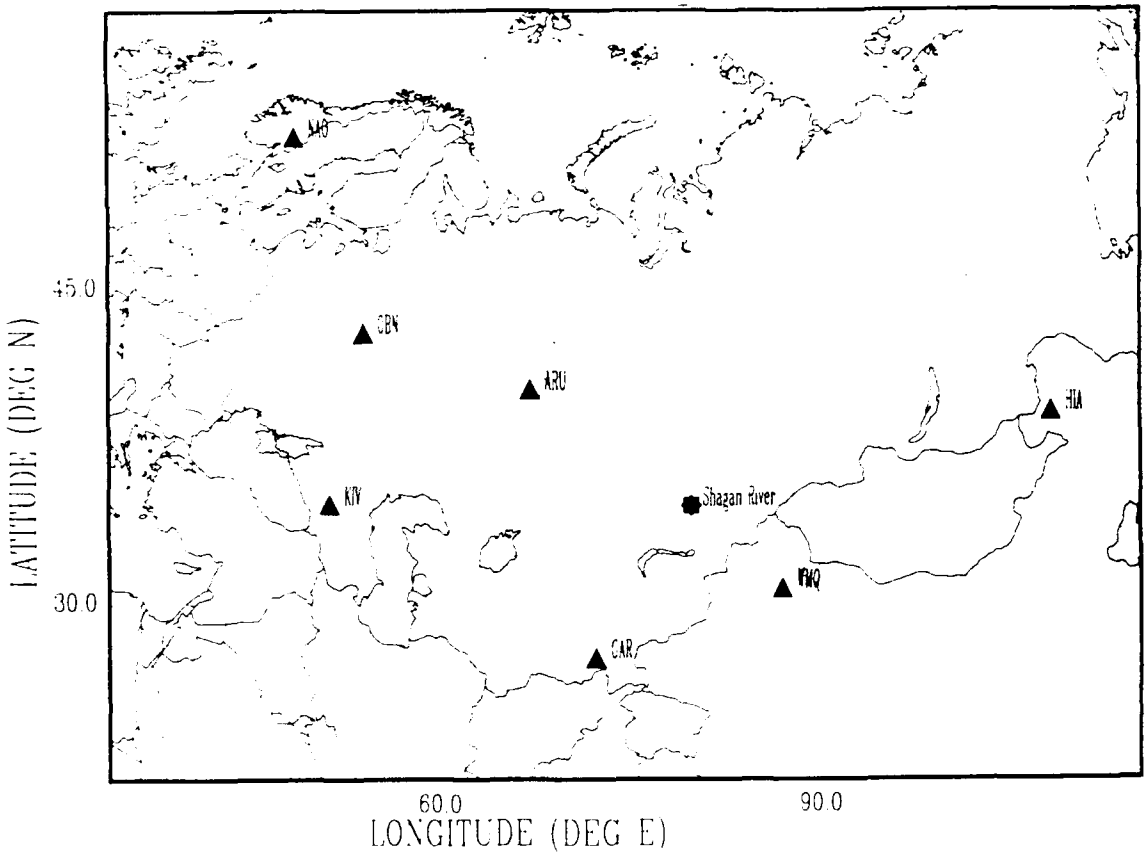

Fig. 7.3.1 Map indicating the locations of the Shagan River Test Site, the IRIS stations in the USSR, the NORSAR array in Norway and the stations WMQ and HIA in China.

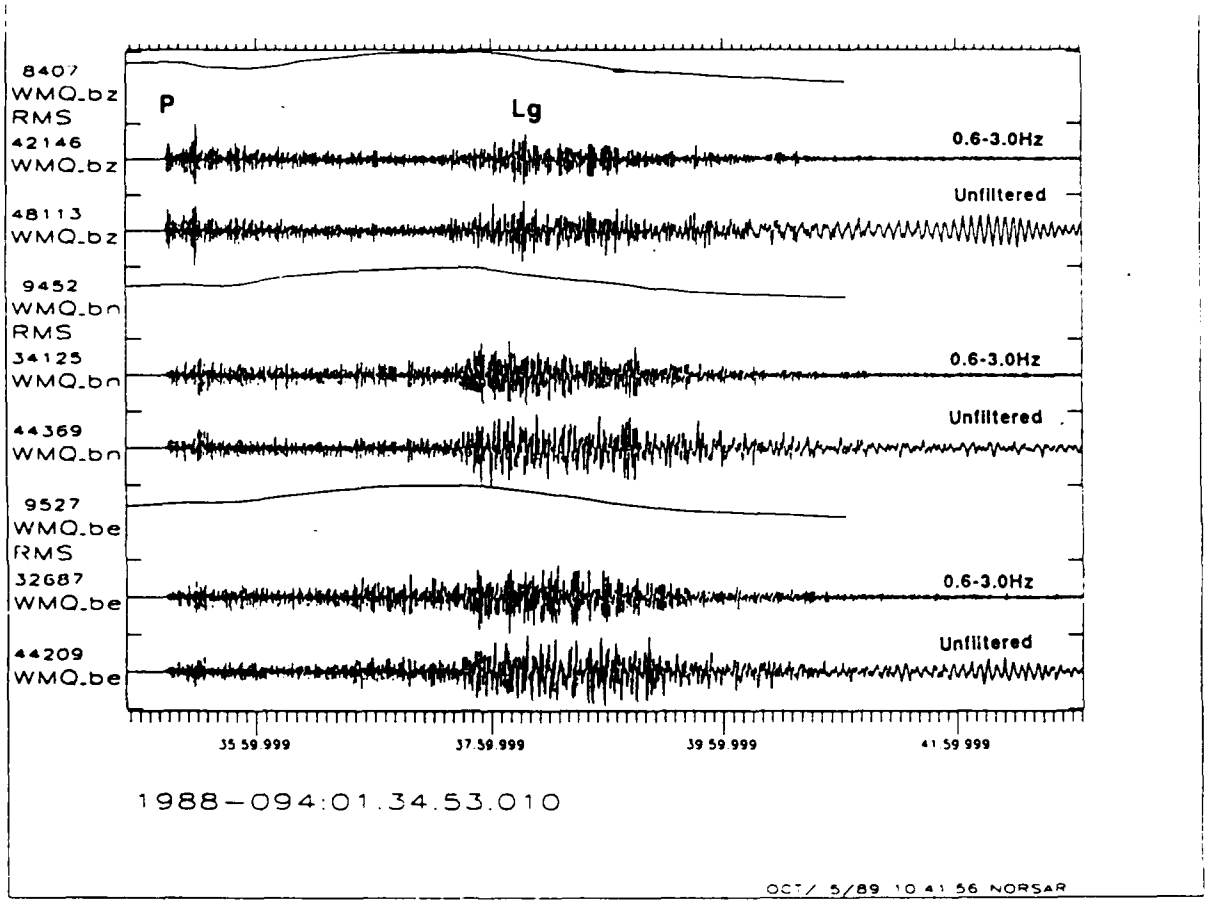

Fig. 7.3.2 Example of recordings from a Soviet nuclear explosion (3 April 1988) at the station WMQ. For each of the three components we show the unfiltered trace (bottom), the filtered trace (0.6-3.0 Hz) and the 120-second window RMS measure (top) as a function of time.

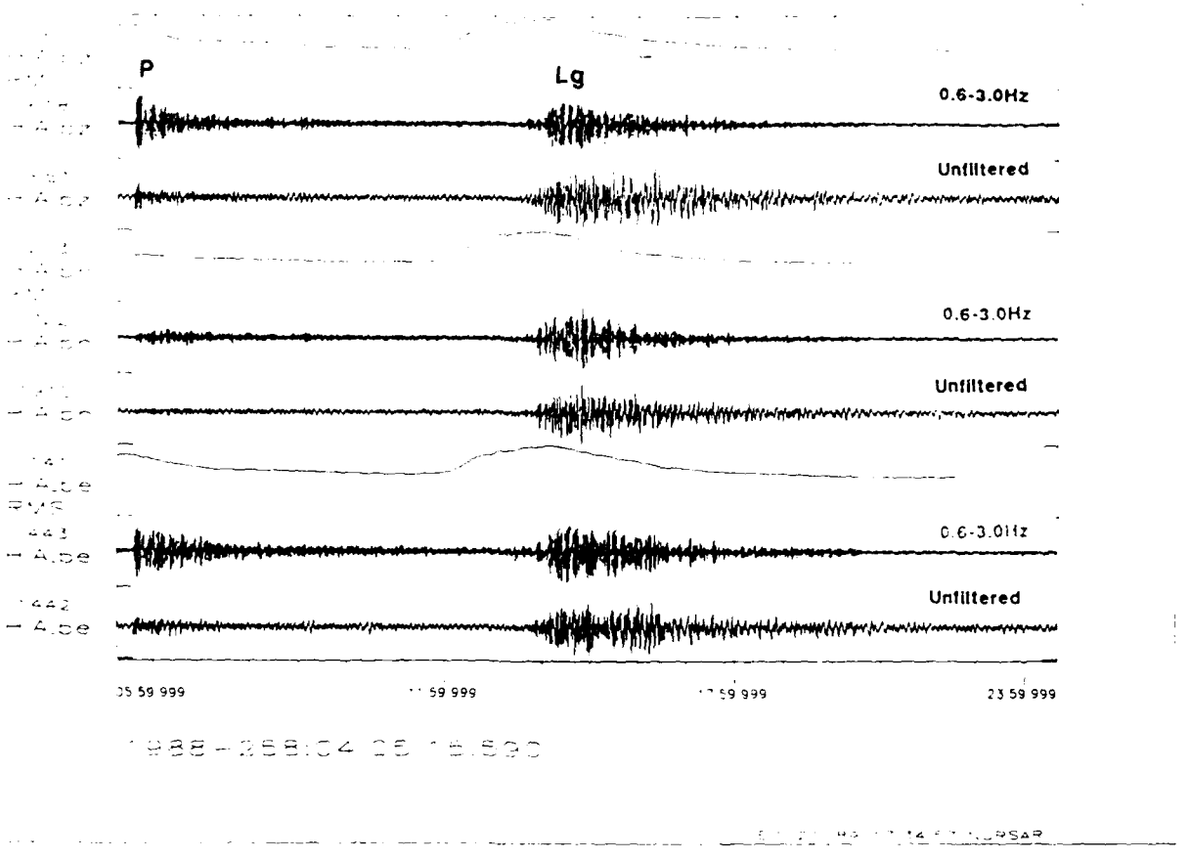

Fig. 7.3.3 Example of recordings from the Soviet JVE explosion (14 Sep 1988) at the station HIA. The three traces for each component are as on Fig. 7.3.2.

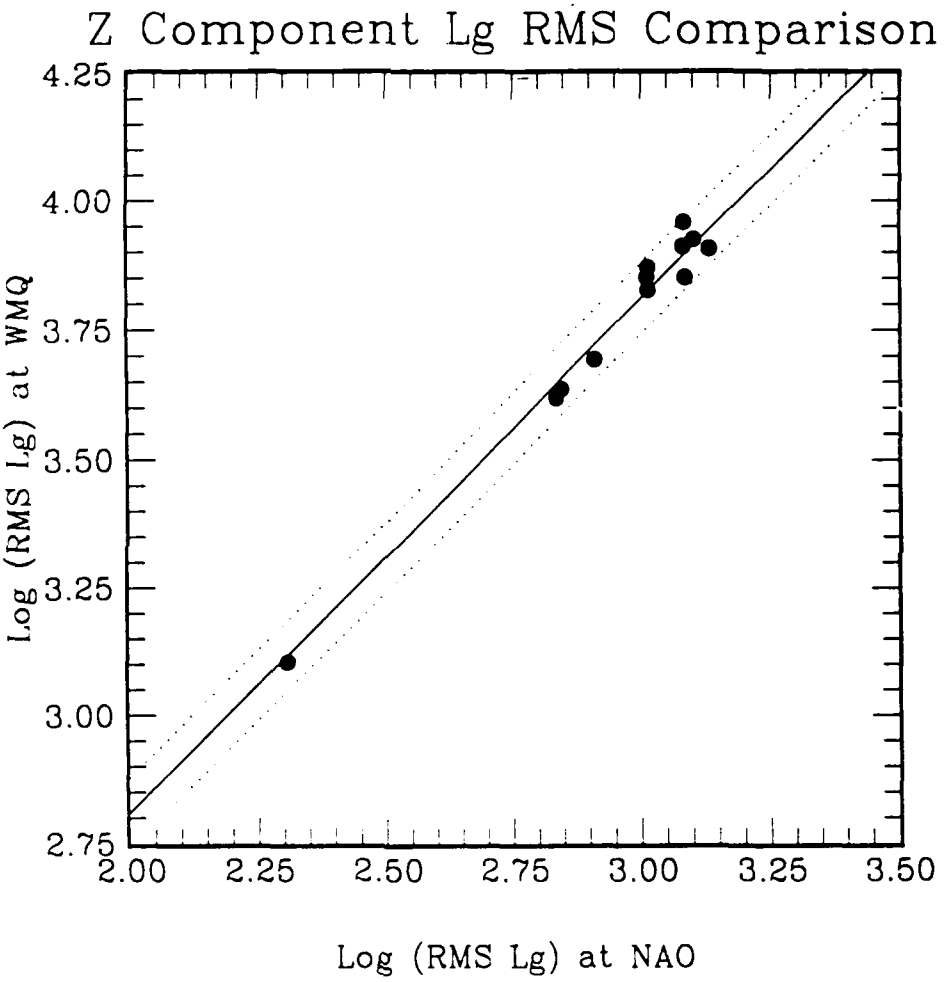

Fig. 7.3.4 Comparison of log RMS Lg measurements obtained at WMQ and NORSAR. The standard deviation of the differences is 0.034 in the y-direction and 0.024 orthogonal to the line. The dotted lines correspond to plus or minus two standard deviations.

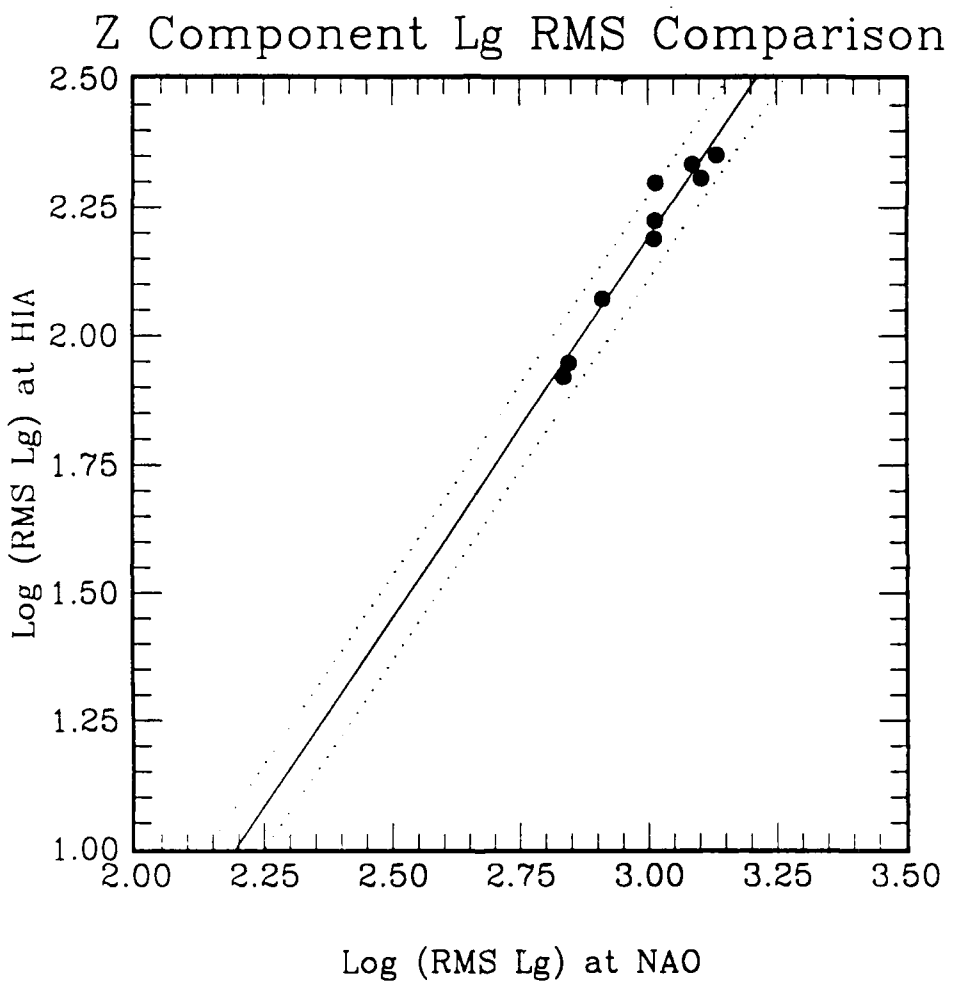

Fig. 7.3.5 Comparison of log RMS Lg measurements at HIA and NORSAR. The slope of the line is 1.48 and the standard deviation of the misfit of the line to the data is 0.04 in the y-direction and 0.023 orthogonal to the line. The dotted lines correspond to plus or minus two standard deviations.

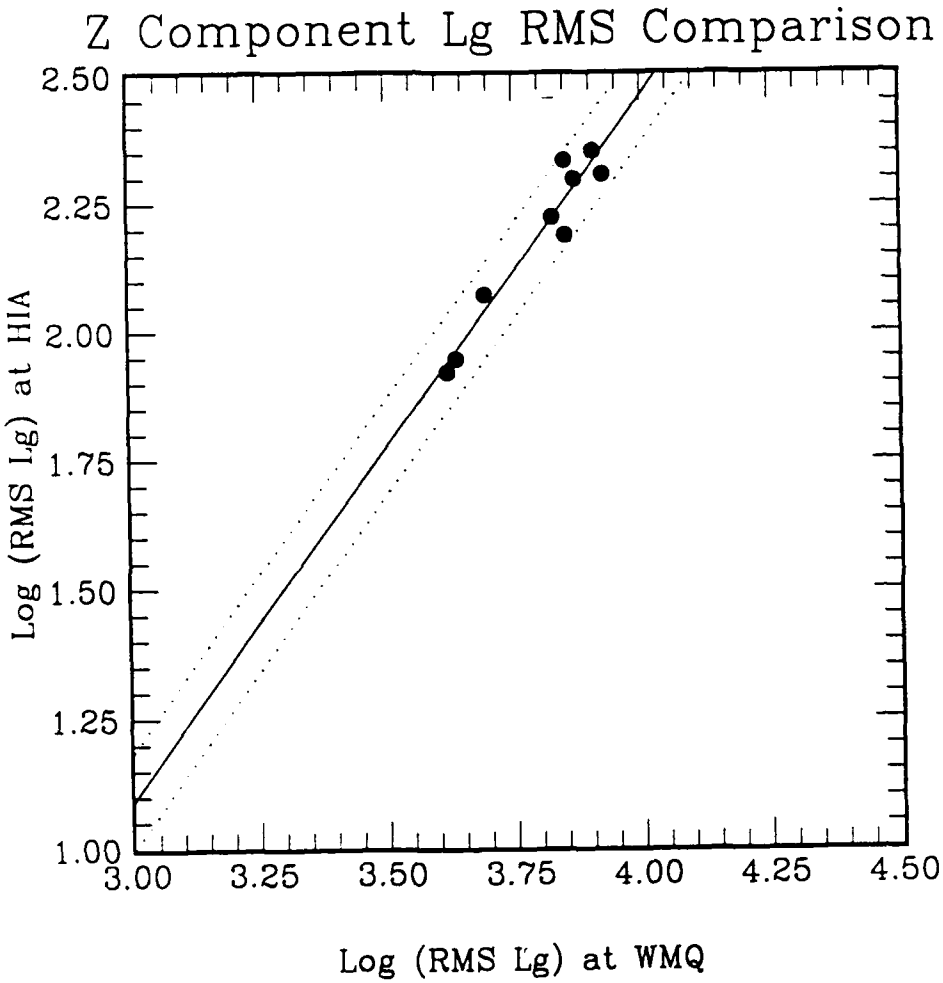

Fig. 7.3.6 Comparison of log RMS Lg measurements at HIA and WMQ. The slope of the line is 1.36 and the standard deviation of the misfit of the line to the data is 0.047 in the y-direction and 0.028 orthogonal to the line. The dotted lines correspond to plus or minus two standard deviations.

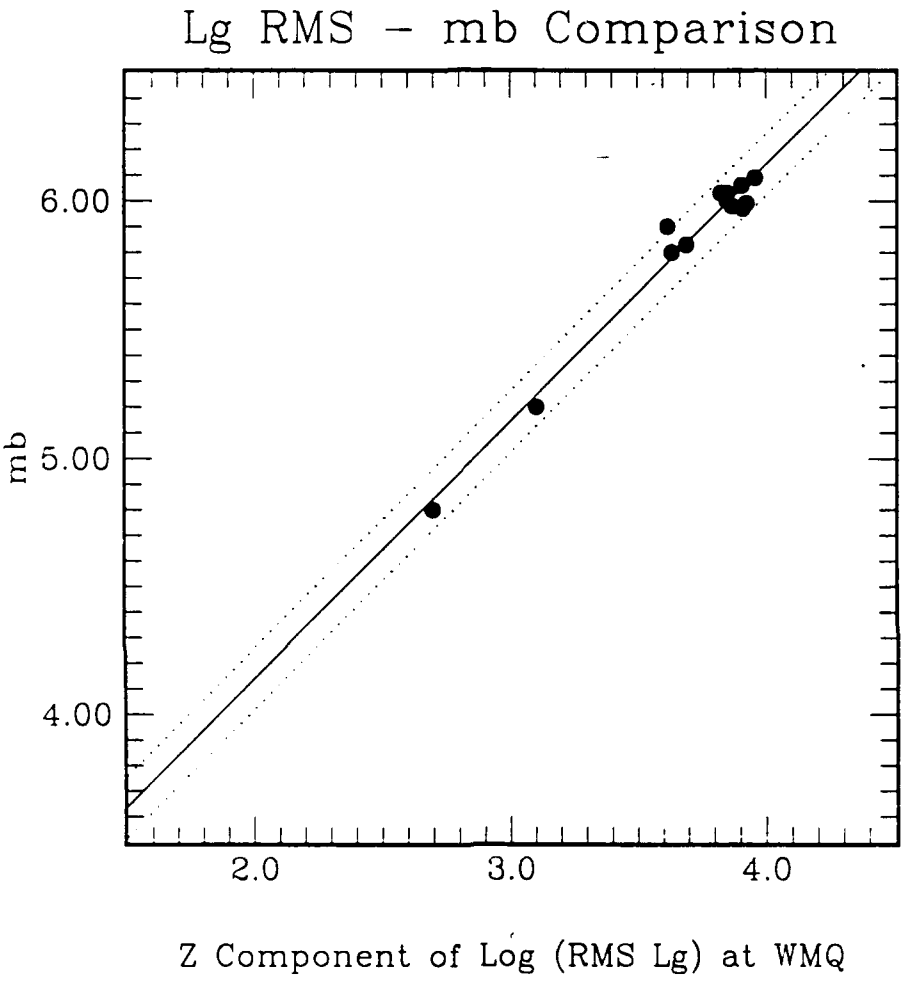

Fig. 7.3.7 Comparison of log RMS Lg at WMQ to world-wide m_b magnitude. Standard deviation is 0.060 units in the y-direction and 0.042 orthogonal to the line. The dotted lines correspond to plus or minus two standard deviations.

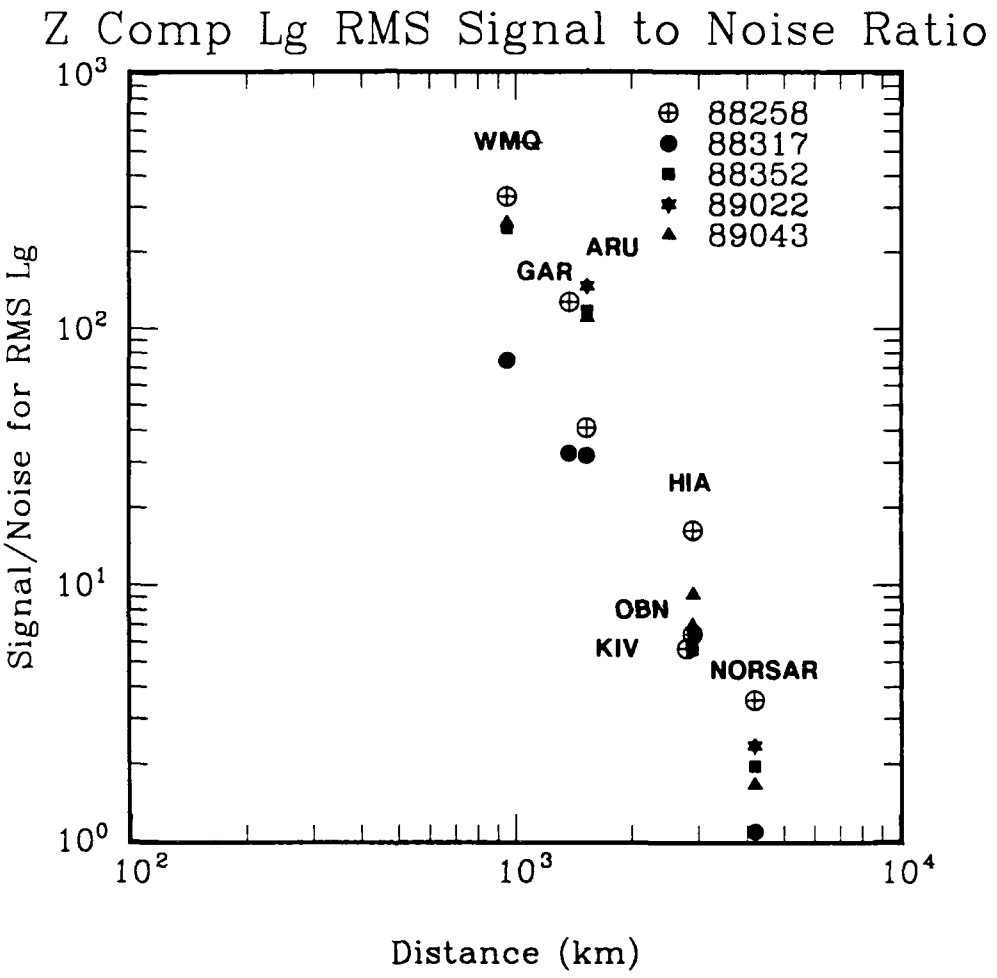

Fig. 7.3.8 Graph showing the variation of the signal-to-noise ratios (log RMS minus log RMS noise) from the four IRIS stations, the NORSAR array and the CDSN stations WMQ and HIA. Epicentral distance to the test site is plotted along the horizontal axis.

7.4 A new data acquisition system for FINESA

The FINESA array was installed in Finland in 1985 and comprised in its original version 10 SPZ seismometers. Results from data analysis using the FINESA array in its initial configuration are given in Ringdal *et al* (1987). In 1988, the geometry of the array was expanded by the addition of five elements, and the FINESA array geometry currently comprises 15 vertical only seismometers within an aperture of 2 km, as shown in Fig. 7.4.1. An evaluation of the performance of the expanded array is offered by Mykkeltveit *et al* (1988).

Until this year (1989), the only way of acquiring FINESA data has been by on-site recording on magnetic tapes, and all analysis of FINESA data has been strictly off-line. With the development of the Intelligent Array processing System (IAS), it has become an objective, however, to provide the capability of transmitting data from FINESA in real time to the NORSAR data processing center. At the same time, it has been an objective to enable real time transmission of FINESA data to Helsinki, for the independent analysis of this data by the staff of the Institute of Seismology at the University of Helsinki. A new data acquisition system, meeting the above objectives, has been developed at NORSAR and put into operation. Short descriptions of the field system, the communications interface used, the data transmission lines that have been established, and the SUN-based data acquisition and processing systems installed at NORSAR and Helsinki, are the subjects of this contribution.

The field system

The field unit is a VME-based system manufactured by Force Computers. The software was developed in Norway by the company Data Respons A/S, under the guidance and supervision of NORSAR personnel. A detailed description of this field system is provided in a manual prepared by Data Respons A/S, entitled NORSAR Field System Description Manual. This manual is available upon request.

The main functions of the field unit are:

- A/D conversion at a sampling rate of 40 Hz of up to 32 channels (15 channels currently in use)
- Synchronized sampling using a Kinemetrics clock feeding the system with GMT time
- Data buffering, reformatting and adding of header information
- SDLC communication.

The entire FINESA acquisition system is shown schematically in Fig. 7.4.2. The units located at the FINESA array site in Sysmä are shown in the upper left corner: The field unit (Force Computer with A/D cards), Kinemetrics clock, an RS232 to V.35 converter, and a modem.

Communications interface and data transmission lines

NORSAR has recently developed a communications system named BUSC-VME (*BU*ffered *S*DLC *C*ommunications system for SUN VME-based systems). Our major requirements for a new communications interface were:

- Low cost
- VME-based
- SDLC communication
- No hardware developments
- Easy and low cost maintenance.

The BUSC-VME system meets these requirements and is easily interfaced with a SUN VME-based system. The BUSC-VME system is based on commercially available cards for installation directly into a SUN system.

The BUSC-VME system is based on two VME cards (CPU and memory) installed in the SUN VME bus. There is no requirement for outside units. The SDLC stream is plugged directly into the CPU board. The CPU board is MC68020-based and handles two high speed SDLC links (array and HF-data in case of NORESS; array data only in the current FINESA implementation). Data received by the CPU card are stored in a cyclic buffer on a memory board. A 2 Mb board has buffer capacity for 10 minutes of array data. The buffer size may easily be changed. The transfer speed between SUN and the BUSC-VME system is only limited by the SUN VME bus and the activity on the SUN.

The software driver is very simple since the BUSC-VME memory is mapped into the SUN VME bus and there is no need for interrupt routines to communicate with the memory board. The driver simply reads data out of the buffer like a program fetches data from the regular SUN memory space. All handshaking is controlled on a VME hardware level and has no influence on the SUN itself.

Two spare cards are the only requirements for backup and an acceptable maintenance scheme for the communications system.

The BUSC-VME interface has been installed in the SUN computers at NORSAR and Helsinki to enable reception of FINESA data at these locations.

High speed (64 Kbit/s) digital land lines have been installed between the FINESA array site and Helsinki and between Helsinki and NORSAR. As shown in Fig. 7.4.2, the data stream is split in Helsinki, and forwarded to both NORSAR and the Seismological Institute of the University of Helsinki.

Data acquisition and processing

Data from FINESA are received continuously in real time both at NORSAR and in Helsinki, as shown in Fig. 7.4.2. The data acquisition and processing systems are based on SUN 3/2xx computers. Both systems are equipped with local disk, and the SUN system at NORSAR also has an Exabyte tape drive for data archiving.

The data received are written on to a cyclic diskloop, and only available disk space limits the size of this loop. For the NORSAR installation, the disk drive installed permits a loop containing approximately 70 hours of data, which matches the length of the disk loops implemented for the NORESS and ARCESS data acquisition systems.

The detection processing (DP) and event processor (EP) program packages described by Fyen (1989) have been installed on the acquisition computers both at NORSAR and in Helsinki. The beam deployment chosen was designed from the NORESS/ARCESS experience and adapted to the FINESA array geometry. An example of an event automatically detected and located (after an association of a P and an Lg phase) by the DP/EP packages is shown in Figs. 7.4.3–7.4.5. The event is a small mining explosion in Estonia. The format of the plots and the information contained therein are as explained in Fyen (1989).

In the future, data from FINESA will be processed jointly with NORESS and ARCESS data (as well as GERESS data, when available) in the IAS.

R. Paulsen
J. Fyen
P.W. Larsen
S. Mykkeltveit

References

Fyen, J. (1989): Event processor program package, *Semiann. Tech. Summ., 1 October 1988 - 31 March 1989*, NORSAR Sci. Rep. No. 2-88/89, Kjeller, Norway.

Mykkeltveit, S., J. Fyen, T. Kværna and M. Uski (1988): Analysis of regional seismic events using the NORESS/ARCESS/FINESA arrays, *Semiann. Tech. Summ., 1 April - 30 September 1988*, NORSAR Sci. Rep. No. 1-88/89, Kjeller, Norway.

Ringdal, F., S. Mykkeltveit, T. Kværna, R. Paulsen, H. Korhonen, S. Pirhonen (1987): Initial results from data analysis using the FINESA experimental small aperture array, *Semiann. Tech. Summ., 1 October 1986 - 31 March 1987*, NORSAR Sci. Rep. No. 2-86/87, Kjeller, Norway.

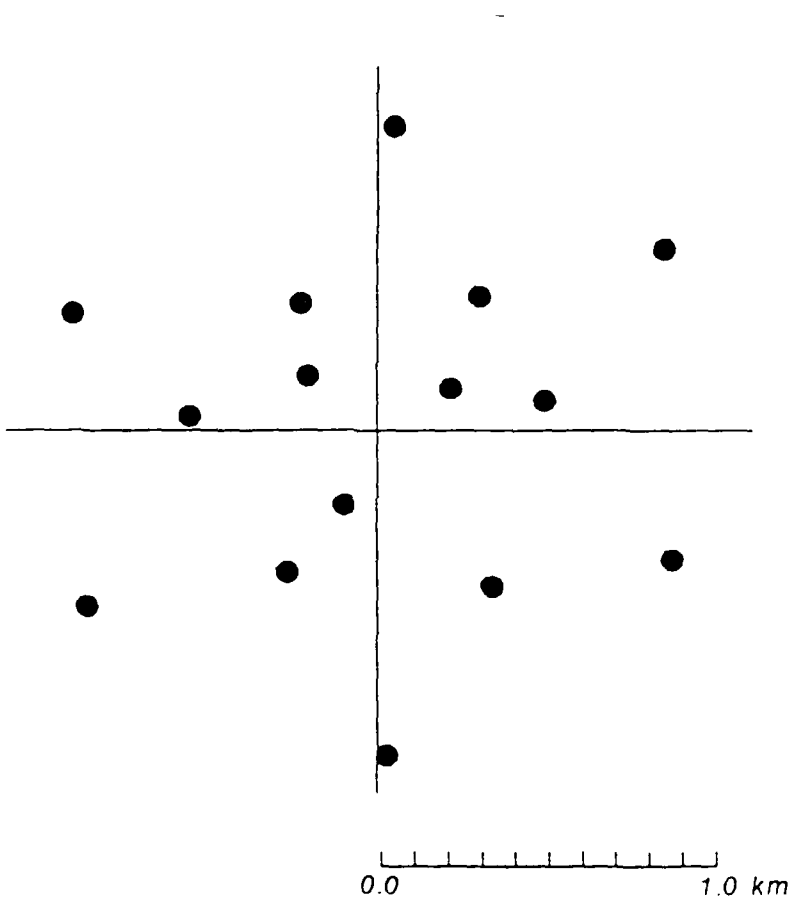

Fig. 7.4.1 Configuration of the FINESA array in Sysmä, Finland, after the expansion of the array geometry in 1988.

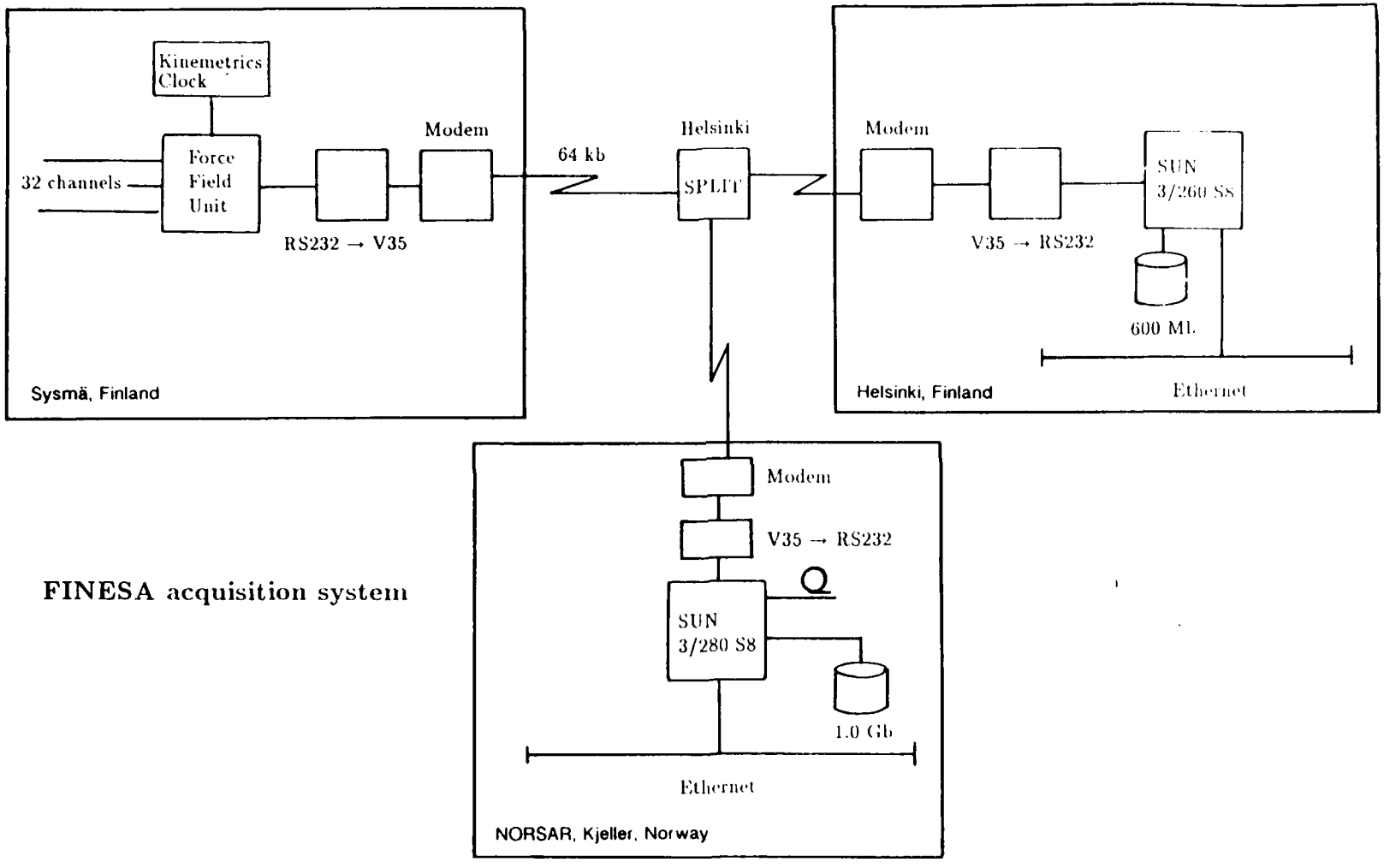

FINESA acquisition system

Fig. 7.4.2 The new FINESA data acquisition system, comprising the field unit with clock, RS232-V.35 converter and modem (upper left), data transmission lines, and data acquisition and processing systems in Helsinki (upper right) and NORSAR (lower middle).

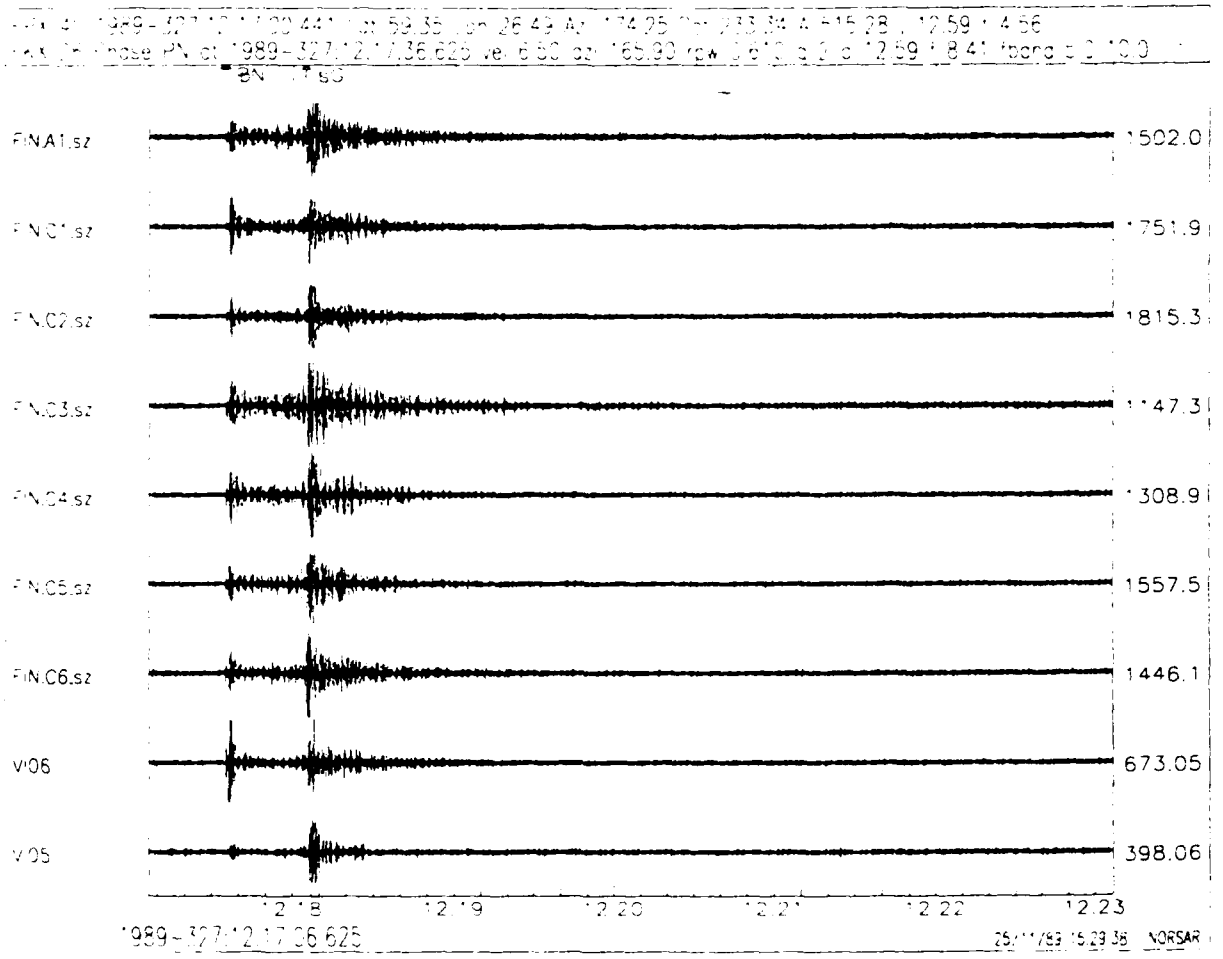

Fig. 7.4.3 Six-minute plot of a regional event located by FINESA. "Best" P and S beams (VI06 and VI05, respectively; for explanation, see the caption of Fig. 7.4.4) are displayed as the two bottom traces.

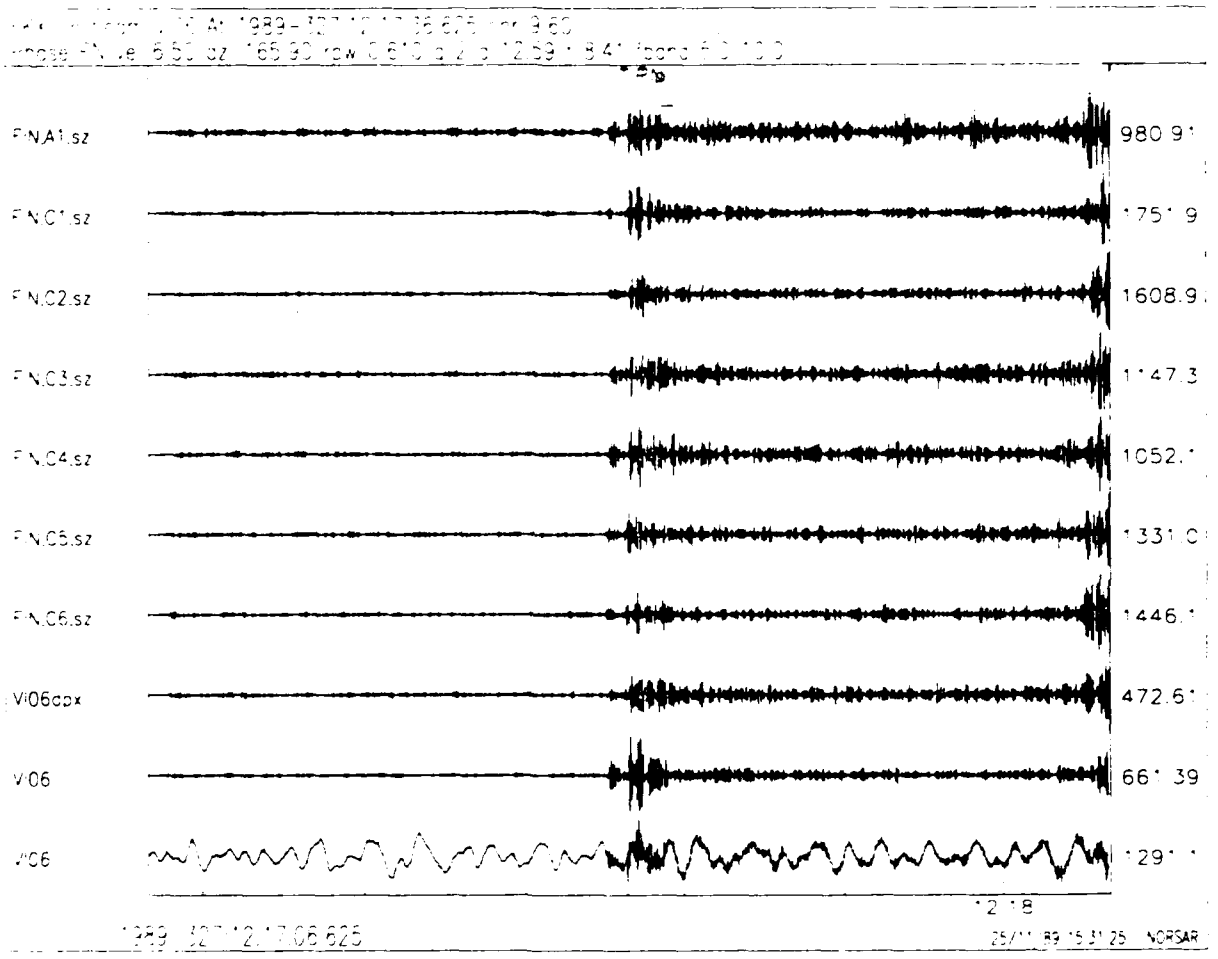

Fig. 7.4.4 Expanded display of the P-phase for the event of Fig. 7.4.3. VI06dpx is the detecting beam that gives the best SNR for this phase. This is an incoherent beam with infinite velocity, but plotted here as a coherent beam, using the same steering parameters. VI06 (shown both filtered and unfiltered) is the coherent beam using the same configuration, and steered according to the f-k estimate (here: phase velocity 6.50 km/s; azimuth 165.90°).

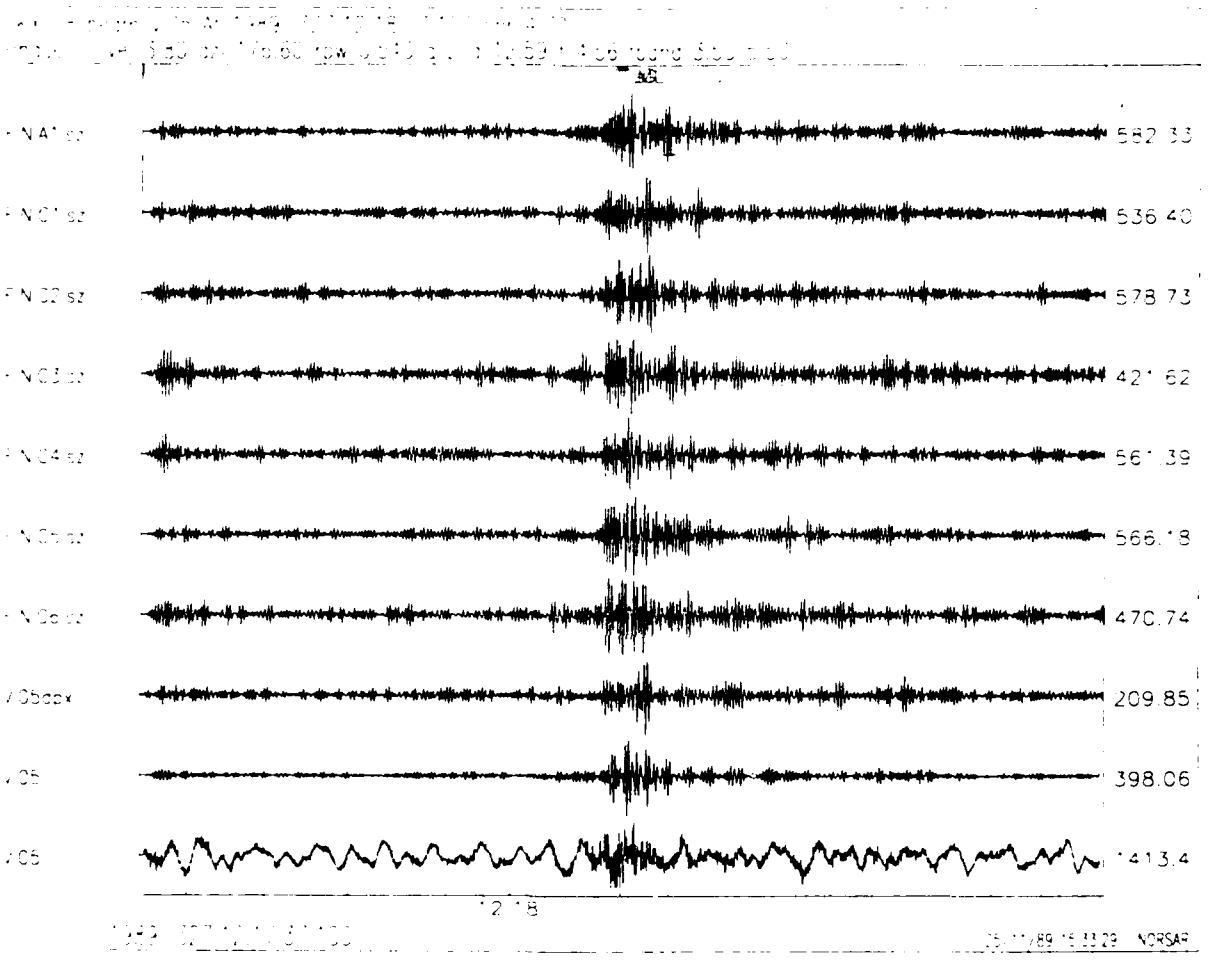

Fig. 7.4.5 Same as Fig. 7.4.4, but corresponding to the Lg phase.

7.5 Establishment of a mining explosion data base

On a daily basis, numerous local and regional events are detected and located by the signal analysis procedures applied to the high-frequency arrays NORESS and ARCESS. The majority of these events are related to mining activity in the area monitored by these arrays. Specific knowledge pertaining to mining explosions such as mine locations, charge sizes, firing practices, etc., will aid in the regular analysis of the array data. In addition, such information will be the basis for adequately addressing a range of interesting and important topics within seismological verification research.

With the purpose of obtaining such information, a survey of mining activity in the areas monitored by NORESS and ARCESS was initiated during the reporting period. The work consists of four steps including gathering of back ground material, acquiring information from the mines, defining relational tables and selecting time series from our data archives.

Collection of background information

The authorization of mining activity in Scandinavia is decentralized to local police; however, there is no official regulation requiring recording of blasting parameters, etc. The initial work towards establishing a mining explosion data base therefore was aimed at obtaining an overview of activities from branch organizations and companies relating to mining activity. The survey of activity resulted in a list of 24 Swedish and 43 Norwegian companies some of which may operate at several locations. These companies represent presumably continuous operation of mining activity underground or at the surface, or simply rock quarries for the purpose of producing building materials. At present, no effort has beer made to map temporary mining activity relating to various construction projects or military activity. However, data regarding larger naval detonations are available via a reporting schedule to the University of Bergen. A list of explosions from the largest open pit mine in southern Norway (Titania) was also obtained as a part of a reporting program to the University of Bergen.

Submission of a questionnaire to actual mines and quarries

Common practice regarding filing of information about past explosions varies considerably from one mine to another, as the mining companies are not required to provide reports on their explosions. A questionnaire was submitted to the 67 companies identified, asking for a number of details about blasting practice and explosions detonated since 1984. Out of the 67 companies approached, answers were obtained from 16, corresponding to an answering per cent of about 25. The quality of the responses varied greatly, apparently due to the lack of details in their files. The sparse response may also be at-

tributed to the fact that the workload on the part of the companies was not associated with any compensation by NORSAR. A map showing the location of mines presently contributing to the explosion data base is given in Fig. 7.5.1. The mines from which data are acquired include four of the main open pit mining sites in Norway, located in southern Norway, western Norway, mid Norway and northern Norway, respectively.

Details of explosion locations at the mine in mid-Norway (Rana Gruber) are shown in Fig 7.5.2, and for the mine in northern Norway (Sydvaranger) located close to the Russian border in Fig. 7.5.3. The latter mine performs blasting at five different locations within an area of about 10 km across. The distances to ARCESS and NORESS from these four mines are shown in Fig. 7.5.4. The amounts of explosives detonated vary from less than 10,000 kg to more than 200,000 kg, thus providing a good range of charge sizes and distances for consideration in future research.

Establishing mining explosion relations according to CSS data base structure

The mines responding to the questionnaire do provide a basis for defining elements of a mining explosion data base for future research and master event selections. Two relations are proposed in conformance with the 2.8 CSS data base structure for the mining explosions. The relational table MINFO contains information specific for one particular mine location, but common to many explosions in that mine. The description of individual explosions is contained in the relation MINEX. Details of the proposed relations are provided in Appendix A.

The information contained in the returned questionnaires has been edited to a computer file and subsequently processed and rewritten to a file in conformance with CSS external file format. The processing includes conversion from local time to EPOC-time and conversion from local coordinates provided by the Norwegian Mapping Authority (NGO) to geodetic latitude and longitude. Subroutines needed for this transformation were acquired and implemented at NORSAR as part of this project.

Examples of the external files of the relational tables MINFO and MINEX are presented in Tables 7.5.1 and 7.5.2. The description of ripple firing is given in terms of one tuple for each individual detonation in the ripple. For many ripple-fired explosions reported by the mines, detailed descriptions of the cap delay times and charge distribution were not provided. In cases where the charge configuration parameter 'chacon' is set to 'obtainable', details of ripples may be obtained upon specific request and entered into the tables at a later time.

Selection of master recordings of mine explosions

The work towards entering typical mine explosion recordings at our a rays into master files is at a preliminary stage, and must await the consideration of a large number of recordings supported by data processing results in terms of energy distribution in time, frequency and space. Crucial issues for further consideration ar the attenuation of the seismic waves from various types of mining explosions and the characteristics of ripple firing in time-frequency estimates (spectograms) of such recordings; see, e.g., Baumgardt and Ziegler (1988), Hedlin *et al* (1989), Richards *et al* (1989). Some examples of mine recordings are shown in Figs. 7.5.5 to 7.5.7.

Plans for further work

From the information gathered from the mining industry so far, we are in a good position to judge which of the mines that have not yet returned the questionnaire are of interest to us. We will make an effort to contact these mines again. Many of the mines in this category are located in Sweden, and we expect to obtain some help and advice from Swedish seismologists in establishing contact with the mines in question. After this second round of information gathering, we hope to be able to compile a fairly comprehensive data base of mining explosions in Norway and Sweden.

The network of regional arrays providing real time data to the NORSAR Data Processing Center is currently being expanded. Very soon, data from the FINESA array in Finland and the GERESS array in the Federal Republic of Germany will become available. It will then be necessary to expand the survey of mining activity described in this report to new regions, in particular Finland, the western USSR, Poland, Czechoslovakia and the FRG. Again, we expect to be able to obtain help and information from colleagues in these countries.

A. Dahle
A. Alsaker
S. Mykkeltveit

References

Baumgardt, D.R., and K.A. Ziegler, Spectral evidence for source multiplicity in explosions: application to regional discrimination of earthquakes and explosions, *Bull. Seis. Soc. Am.*, 78, 1773-1795, 1988

Hedlin, M.A.H., J.B. Minster, and J.A. Orcutt (1989): The time-frequency characteristics of quarry blasts and calibration explosions recorded in Kazakhstan U.S.S.R., *Geophys. J. Int.*, 99, 109-121, 1989.

Richards, P.G., A. Lerner-Lam, R. Such and D. Simpson (1989): Chemical explosions and the discrimination problem, Contract No F19628-8-K-0041.

Mine No.	Name	Lat, deg	Lon, deg	Mine Type
1	Olivin	62.04000	5.52333	open pit
3	Rana Gruber	66.42063	4.67853	open pit
4	Sydvaranger	69.65189	30.02533	open pit
5	Sulitjelma	67.14769	16.07007	shaft
6	Fz.f.Bryggja	61.93000	5.45000	shaft
7	Grong	64.87000	13.88000	shaft
8	Bleikvassli	65.93000	13.88000	shaft
9	Fosdalen	64.07000	11.20000	shaft
13	Steens Kalkverk	60.74000	11.02000	open pit
14	Fz.f.Sandvika	59.90000	10.50000	shaft/pit
15	Titania	58.30000	6.40000	open pit
16	Fz.f.Vinterbro	59.75000	10.77000	open pit
101	Vammala	61.33000	23.03000	
102	Enonkoski	62.04000	28.77000	
103	Taipalsaari	61.18000	28.04000	
104	Pyhaesalmi	63.66000	26.05000	
105	Hitura	63.85000	25.05000	
106	Vihanti	64.41000	25.15000	
107	Elijaervi	65.78000	24.70000	
108	Saattopora	67.78999	24.43000	
109	Faarby	60.10000	22.88000	
110	Mustio	60.17000	23.84000	
111	Sipoo	60.25000	25.39000	
112	Tytyri	60.27000	24.07000	
113	Parainen	60.30000	22.29000	
114	Ihalainen	61.03000	28.18000	
115	Vampula	61.05000	22.64000	
116	Otama	61.81000	21.74000	
117	Ruokojaervi	61.94000	29.03000	
118	Ankele	62.07000	27.41000	
119	Ryytimaa	63.15000	24.02000	
120	Kalkkimaa	65.90000	24.47000	
121	Kemiaa	60.14000	22.59000	
122	Horsmanaho	62.82000	29.25000	
123	Lipasvaara	63.02000	29.23000	
124	Siilinjaervi	63.12000	27.74000	
125	Nilsiae	63.16000	27.99000	
126	Lahnaslampi	64.12000	28.06000	

Mine No.	Name	Lat, deg	Lon, deg	Mine Type
201	Dala Kalk AB	60.62000	15.10000	open pit
202	Dannemora	60.12000	17.52000	
203	Garpenberg Nord	60.20000	16.13000	
204	Garpenberg	60.18500	16:11500	
205	Zinkgruvan	58.80000	15.10000	
206	Glanshammar	59.30000	15.40000	
207	Grängesberg	60.10000	15.00000	
208	Yxsjöberg	60.00000	14.80000	
209	Gåsgruvan	59.70000	14.10000	
210	Svärdsjö	60.70000	15.90000	

Table 7.5.1 Example of attributes contained in the MINFO relation. Mines 1–100 are Norwegian, mines 101–200 Finnish, and mines 201–300 are Swedish.

Epoch	Mine No.	Charges	Charge No.	Delay,ms	Configur.
610812300.000	1	9	1	0.000	ripple
610812300.000	1	9	2	45.000	ripple
610812300.000	1	9	3	90.000	ripple
610812300.000	1	9	4	135.000	ripple
610812300.000	1	9	5	180.000	ripple
610812300.000	1	9	6	225.000	ripple
610812300.000	1	9	7	270.000	ripple
610812300.000	1	9	8	315.000	ripple
610812300.000	1	9	9	360.000	ripple
612021900.000	1	8	1	0.000	ripple
612021900.000	1	8	2	45.000	ripple
612021900.000	1	8	3	90.000	ripple
612021900.000	1	8	4	135.000	ripple
612021900.000	1	8	5	180.000	ripple
612021900.000	1	8	6	225.000	ripple
612021900.000	1	8	7	270.000	ripple
612021900.000	1	8	8	315.000	ripple
507291300.000	3	22	0	0.000	obtainable
508768800.000	3	24	0	0.000	obtainable
509991000.000	3	21	0	0.000	obtainable
516042900.000	3	26	0	0.000	obtainable
518026200.000	3	27	0	0.000	obtainable
526588200.000	3	21	0	0.000	obtainable
578831400.000	3	14	0	0.000	obtainable
581738400.000	3	20	0	0.000	obtainable
584957700.000	3	34	0	0.000	obtainable
592677600.000	3	10	0	0.000	obtainable
595688100.000	3	16	0	0.000	obtainable
604710000.000	3	17	0	0.000	obtainable
609668100.000	3	26	0	0.000	obtainable
532384500.000	4	103	0	0.000	obtainable
613826100.000	5	0	0	0.000	obtainable
602370000.000	6	17	1	0.000	ripple
602370000.000	6	17	2	100.000	ripple
602370000.000	6	17	3	200.000	ripple
602370000.000	6	17	4	300.000	ripple
602370000.000	6	17	5	400.000	ripple
602370000.000	6	17	6	450.000	ripple
602370000.000	6	17	7	950.000	ripple
602370000.000	6	17	8	1450.000	ripple

Epoch	Mine No.	Charges	Charge No.	Delay,ms	Configur.
602370000.000	6	17	9	1950.000	ripple
602370000.000	6	17	10	2450.000	ripple
602370000.000	6	17	11	2950.000	ripple
602370000.000	6	17	12	3450.000	ripple
602370000.000	6	17	13	3950.000	ripple
602370000.000	6	17	14	4450.000	ripple
602370000.000	6	17	15	4950.000	ripple
602370000.000	6	17	16	5450.000	ripple
602370000.000	6	17	17	5950.000	ripple
599612400.000	9	1	1	0.000	single

Table 7.5.2 Example showing some of the attributes of the MINEX relation. The middle section of the table contains data of ripple fired charges where the details of ripple firing is not specified, however, the data may be obtainable from the mining company.

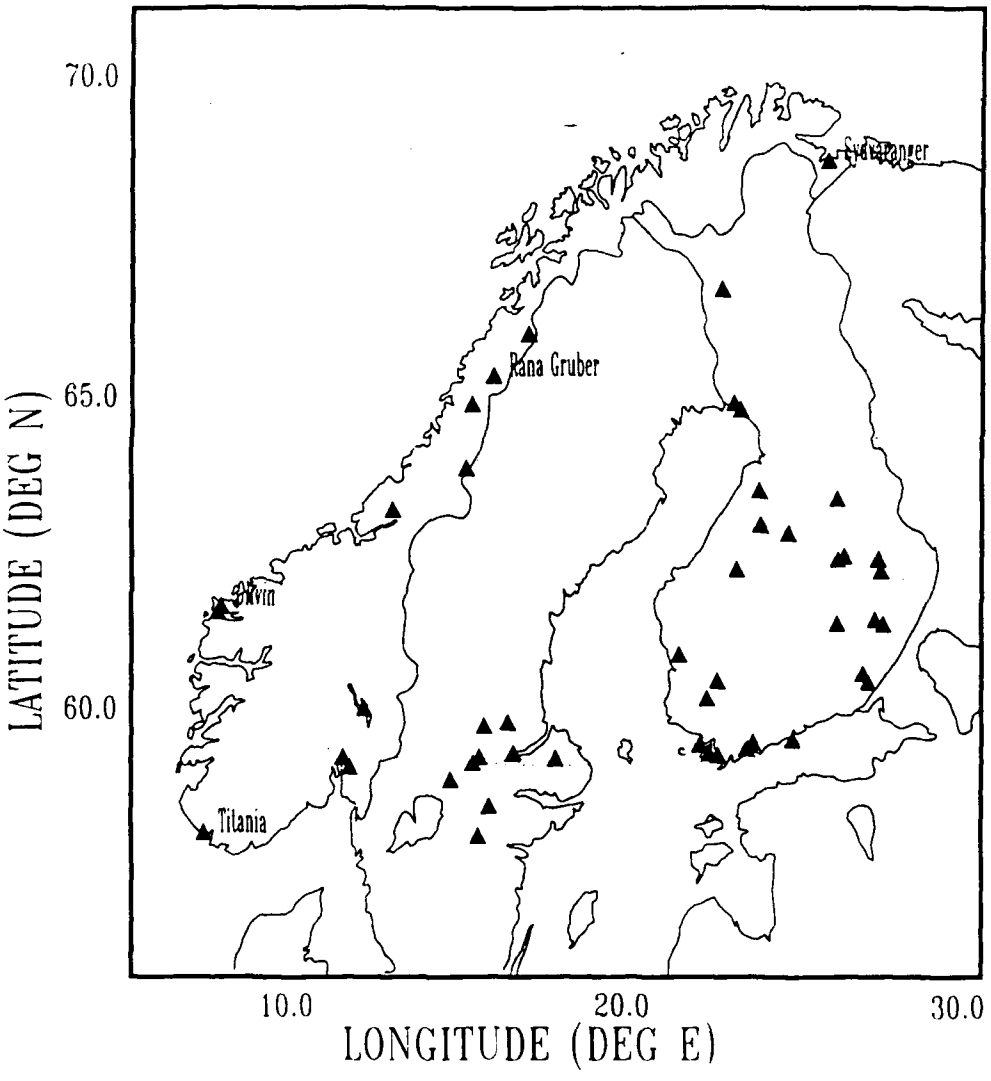

Fig. 7.5.1 Mines and quarries in Scandinavia presently registered in the mining explosion data base. The most important mines in Norway are shown as Titania, Olivin, Rana Gruber and Sydvaranger.

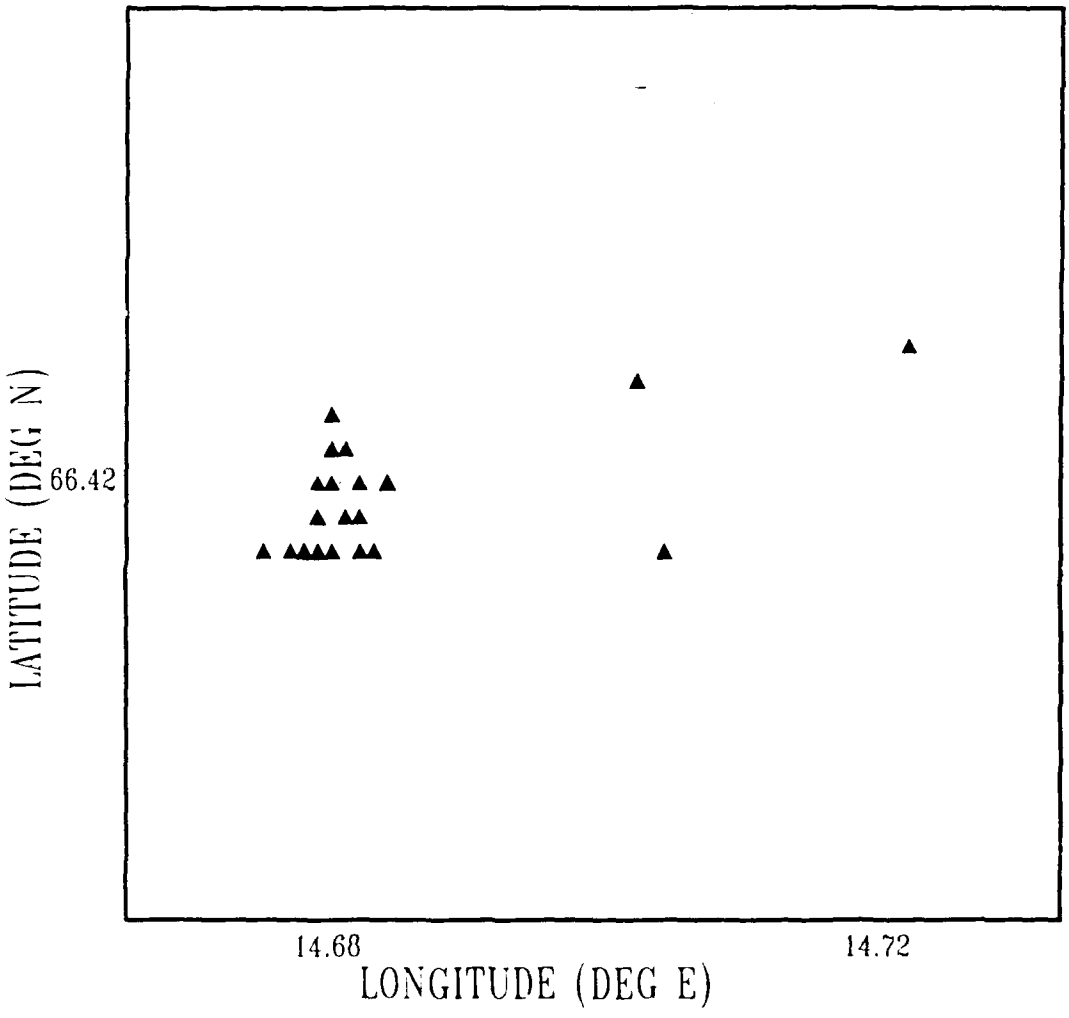

Fig. 7.5.2 Location of explosions in the open pit mine Rana Gruber, mid-Norway.

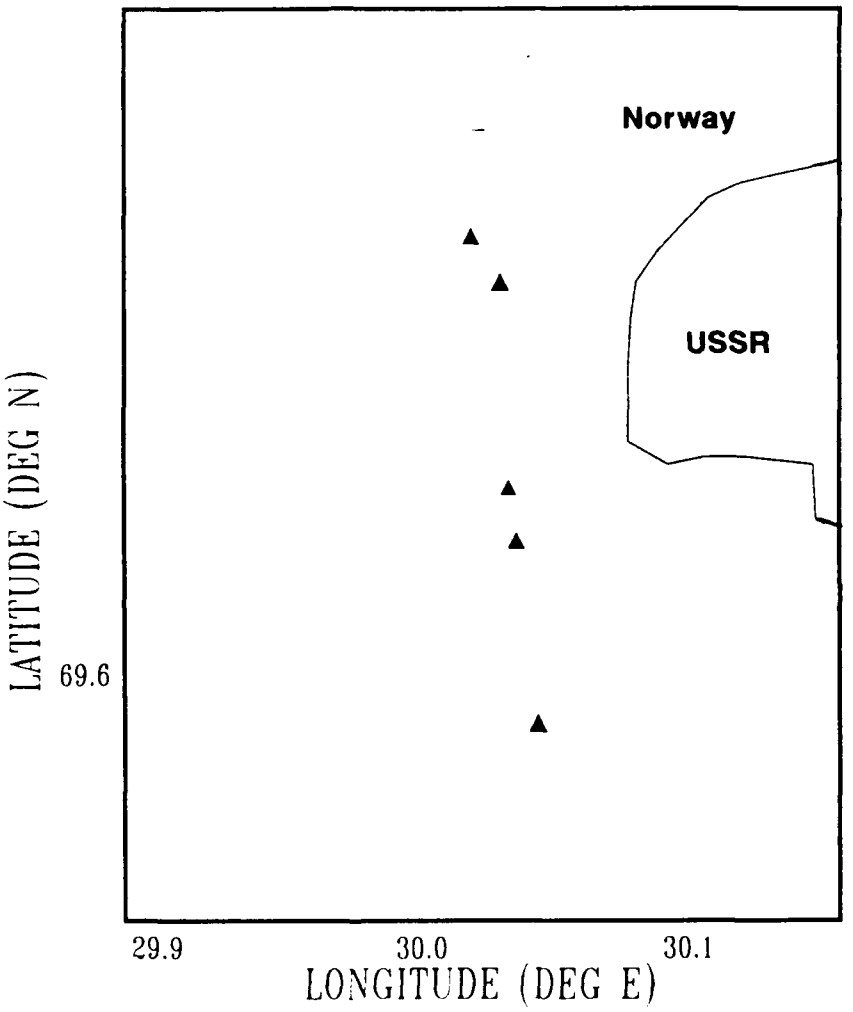

Fig. 7.5.3 Main explosion sites of the open pit mine Sydvaranger close to the Russian border in northern Norway.

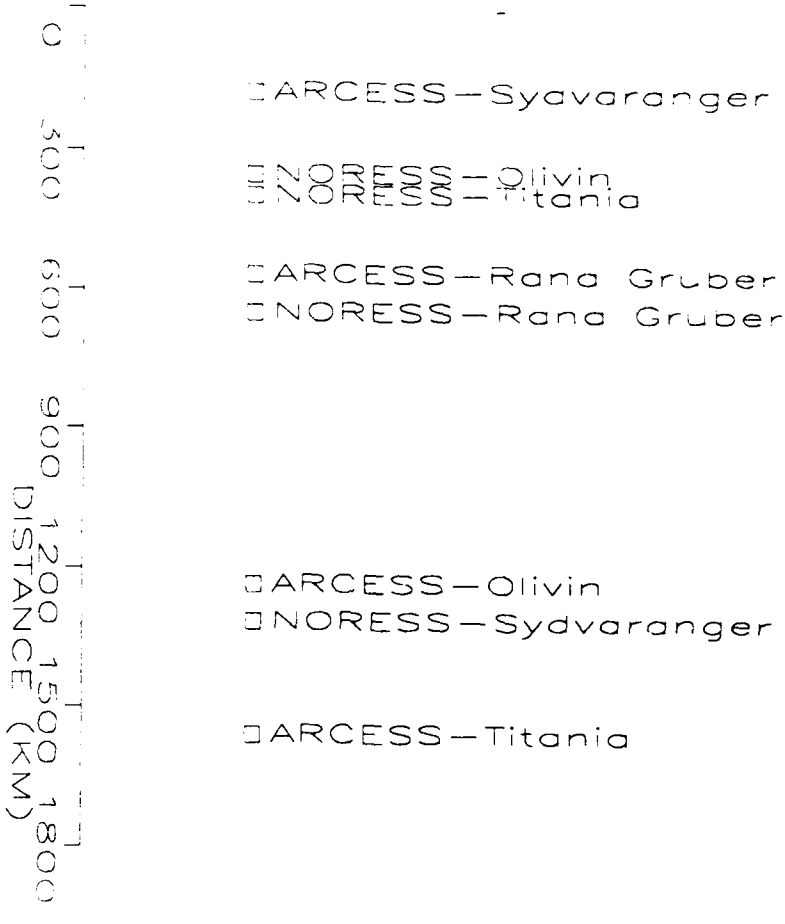

Fig. 7.5.4 Distance from ARCESS/NORESS to four of the main mines in Norway. Location of the mines is shown in Fig. 7.5.1

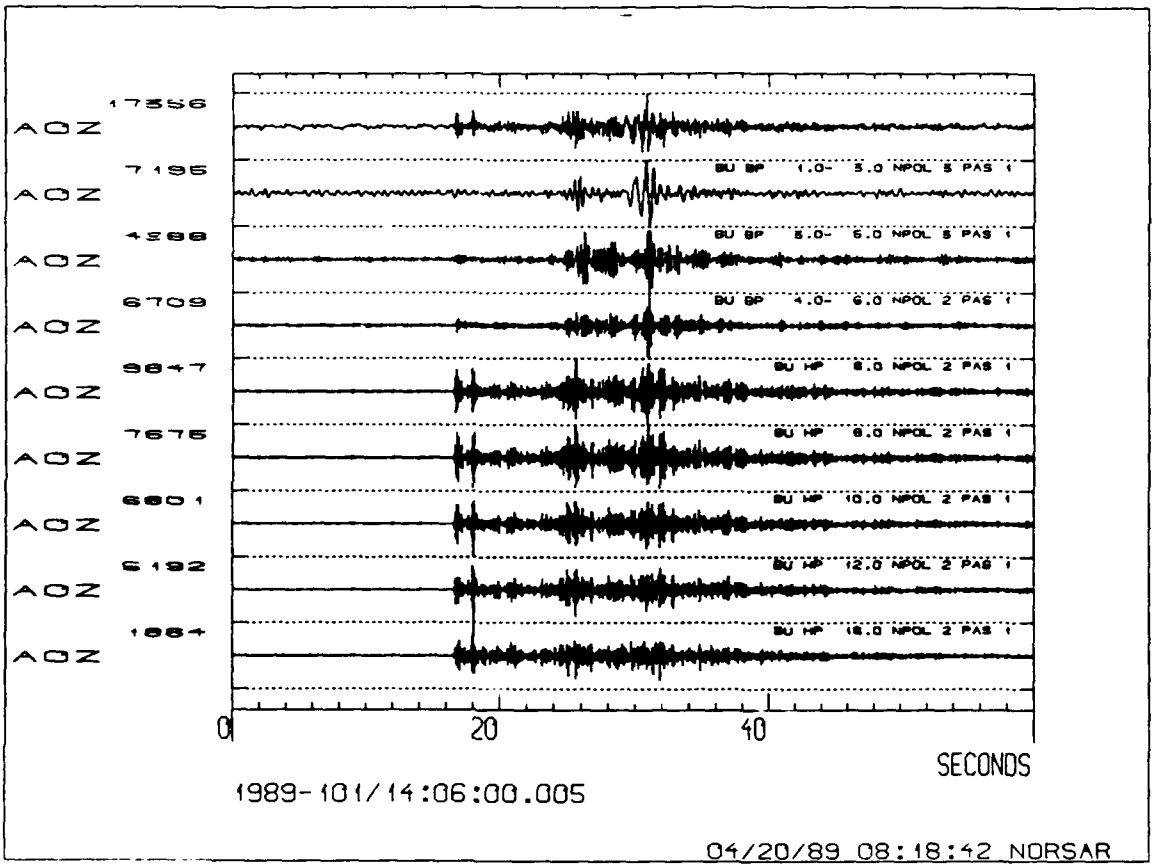

Fig. 7.5.5 NORESS single channel recording of ripple fired explosion at Sandvika (near Oslo), shown in nine filter bands. Charge was 1.615 tons over 68 delays in the time interval 0–578 ms.

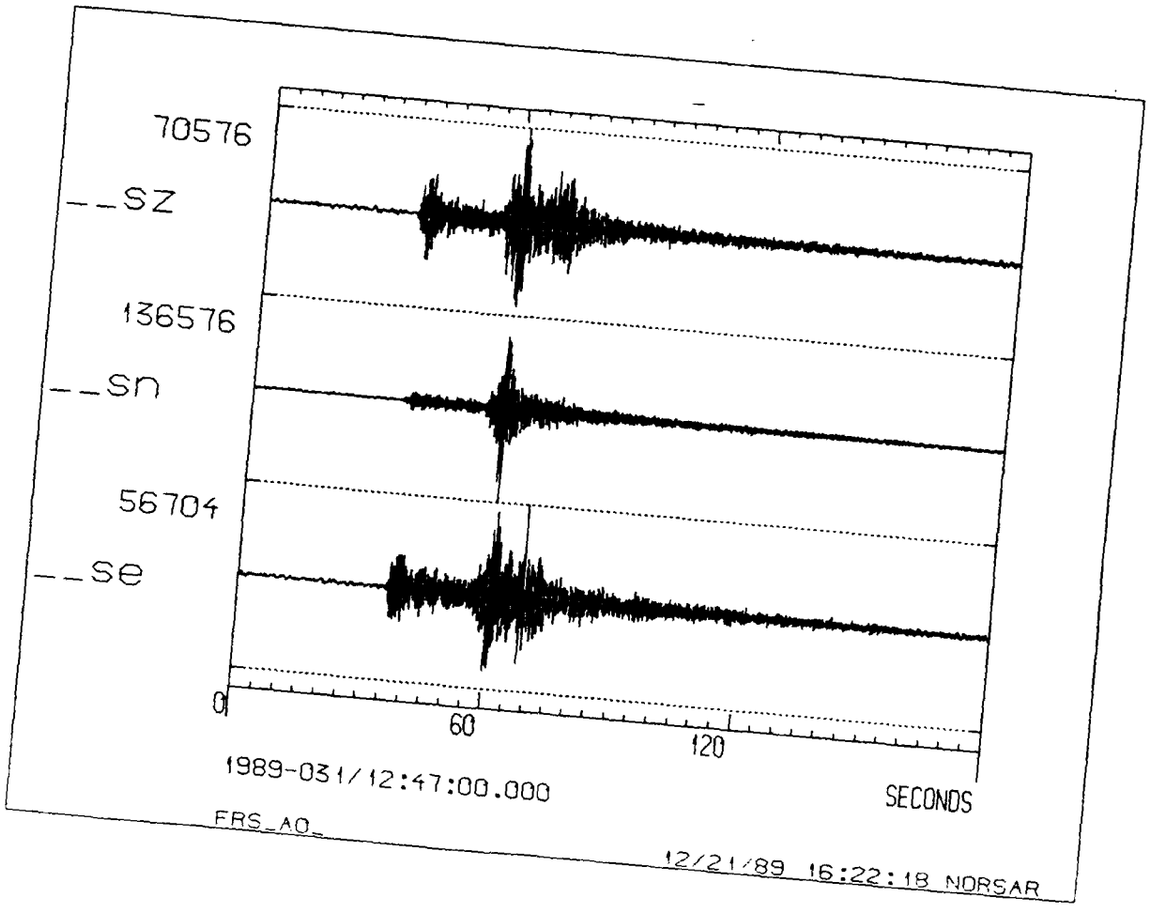

Fig. 7.5.6 ARCESS recording of ripple fired explosion at Sydvaranger, shown for a three-component station. Charge size over 200 tons.

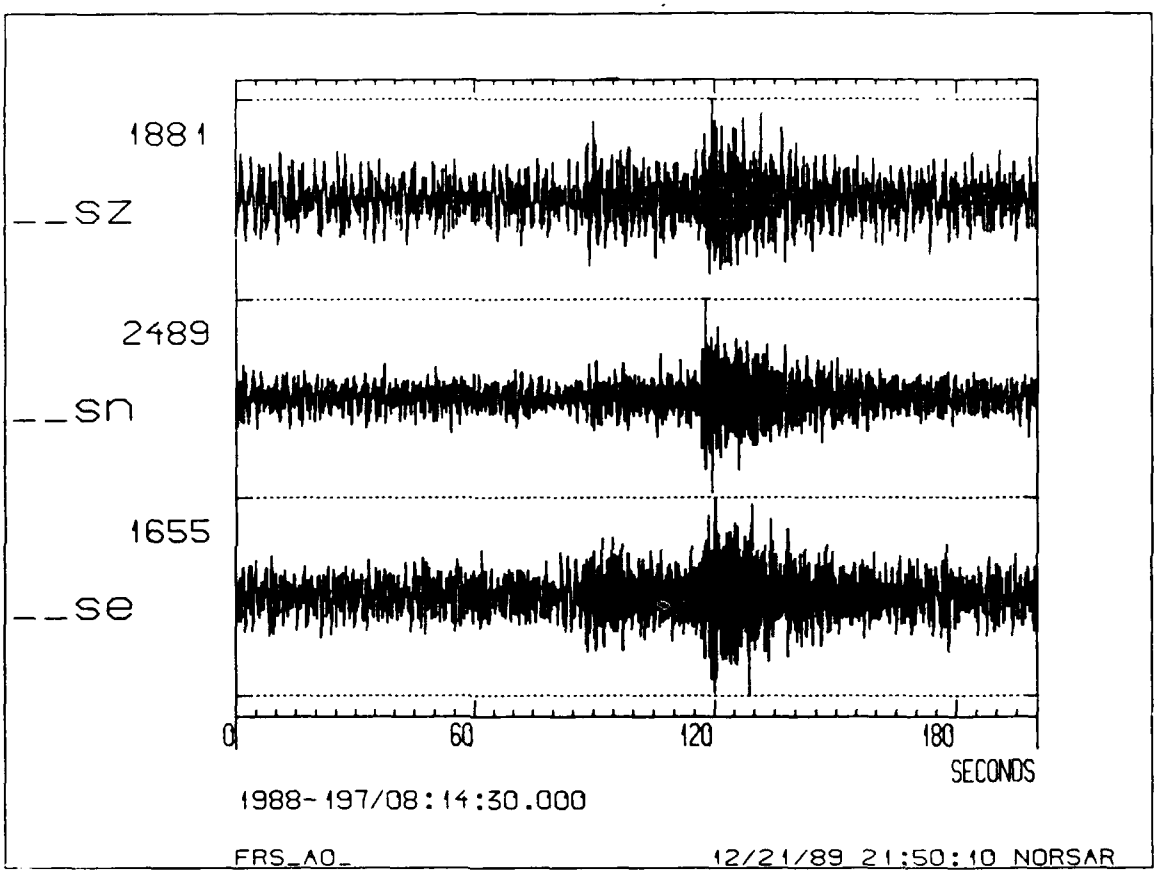

Fig. 7.5.7 ARCESS recording of ripple fired explosion at Rana Gruber. Charge was 180 tons over 34 delays in the time interval 0–1530 ms.

APPENDIX A

Note on Data Base Structure
Proposal for Mine Explosion Relations

The present note proposes two relations in conformance with CSS Database Structure, Version 2.8. The relations and attributes are those proposed by NORSAR based on a sparse return of questionnaires submitted to 67 mines and quarries. The answering per cent is around 25, and it may prove necessary to include more attributes during future research and contact with the mining companies.

The relations proposed are denoted minex and minfo. Minfo contains the basic information about each mine not pertaining to specific explosions. The relation with minex is secured via the relational key minid, the unique identification number of each mine. Further attributes contained in minfo are defined below.

The minex relation contains the relational evid key and other attributes proposed for mine explosions (see below). The minex relation describes each detonated charge in ripple firing by one tuple. The number of tuples pertaining to a ripple fired explosion thus equals the number of charges in the ripple. The charge configuration attribute chacon characterizes the charge as being 'single', 'ripple', 'unknown' or 'obtainable'. In the case of 'unknown', and rdur given, the charge is a ripple but the details of the ripple configuration is only known as the time from first to last subcharge in the ripple. In the case of 'obtainable', the ripple description may be requested from the mining company.

minex

attribute name	field no.	storage type	external format	character positions	attribute description
evid	1	i4	i8	1-8	event id
time	2	f8	f15.3	10-24	epoch time of explosion
date	3	i4	i8	26-33	shot date (julian)
minid	4	i4	i8	35-42	mine id
depth	5	f4	f9.4	44-52	shot depth (km)
elev	6	f4	f9.4	54-62	surface elevation (km)
lat	7	f4	f10.5	64-73	latitude (geodetic)
lon	8	f4	f10.5	75-84	longitude (geodetic)
extyp	9	c15	a15	86-100	type of explosive
grade	10	f4	f9.4	102-110	strength relative tnt
nex	11	i4	i8	112-119	tot no. charges in ripple
subnex	12	i4	i8	121-128	actual charge number
delt	13	f4	f9.3	130-138	delay rel. first charge (ms)
rdur	14	f4	f9.3	140-148	ripple duration (ms)
totcha	15	f4	f9.1	150-158	total charge (kg)
charge	16	f4	f9.1	160-168	indiv. ripple charge (kg)
chacon	17	c10	a10	170-179	charge config. description
auth	18	c15	a15	181-195	author

minfo

attribute name	field no.	storage type	external format	character positions	attribute description
minid	1	i4	i8	1-8	mine id
minam	2	c15	a15	10-24	name of mine
lat	3	f4	f10.5	26-35	latitude (geodetic)
lon	4	f4	f10.5	37-46	longitude(geodetic)
elev	5	f4	f9.5	48-56	surface elev. (km)
prodpt	6	f4	f9.5	58-66	production depth (km)
mintyp	7	c15	a15	68-82	mine type
prodct	8	c20	a20	84-103	product
geolog	9	c30	a30	105-134	bedrock geology
firprc	10	c40	a40	136-145	firing practice
auth	11	c15	a15	177-191	author

Glossary of attributes

minid Relations : minex minfo
Mine id; each mine is assigned a positive unique number which identifies it in the data base. (i4) No null.

extyp Relation : minex
Explosive type; type of explosive used in a charge.(c15) Mixed case.

grade Relation : minex
Explosive strength; messured relative to TNT=1. Slurry may be of grade 0.9, the unit weight of slurry is equivalent to 0.4 units of TNT. used to normalize charge strength to common reference strength. (f4) Null = -1.

nex Relation : minex
Total number of charges in a ripple firing. (i4) Null = -1.

subnex Relation : minex
Charge number in ripple firing; sequencial unique number identifying the acctual charge for the current entry. values 1 - nex. subnex=0 means obtainable charge distribution in a ripple firing. (i4) Null = -1.

delt Relation : minex
Delay time in ripple firing; delay for current charge (entry) relative to first charge measured in miliseconds. (f4) Null = -1.

rdur Relation : minex
Duration of ripple firing when chacon is 'unqnown';
relative to first charge measured in miliseconds. (f4) Null = -1.

totcha Relation : minex
Total charge; sum of nex individual charges (charge) measured in kg. For single charges totcha=charge. (f4) Null = -1.

charge Relation : minex
Individual charge size in a ripple firing measured in kg. (f4) Null = -1.

chacon Relation : minex
Charge configuration attaining values 'single', 'ripple', 'unknown', 'obtainable' (c10) lower case

minam Relation : minfo
Name of mine; (c15) Mixed case

prodpt Relation : minfo
Production depth below surface in km. (f4) Null = -1.

mintyp Relation : minfo
Type of mine ; Pit or shaft (c15) Case = lower

prodct Relation : minfo
Type of product of the mine; Ore (type), rock etc. (c20)

geolog Relation : minfo
Type of geological environment; sedimentary, crystalline, metamorphic, specific rock types etc. (c30)

firprc Relation : minfo
Firing practice information; Time of day, regularity, etc. (c40)

7.6 Transverse components of explosion-induced Lg waves and upper crustal anisotropy

Introduction

Vertical components of Lg waves have been successfully modelled by many authors (e.g., Bouchon, 1982; Herrmann & Kijko, 1983), but specific problems occur when one attempts to model also their horizontal components. Synthesis of Lg waves produced by explosions and propagating in an isotropic vertically layered crust predicts displacement on the vertical and radial components only. Lg waves produced by explosions, however, commonly show transverse components as large or even larger than the vertical and radial ones both in Eurasia (Mykkeltveit & Husebye, 1981) and in the United States (Blandford, 1981). Examples of Lg recordings at NORSAR 3-component short period station 01A are given in Fig. 7.6.1 for 3 explosions fired at sea during the CANOBE and FENNOLORA refraction experiments (Cassell *et al*, 1983; Ansorge, 1981). The data have been band-pass filtered between 0.5 and 2 Hz. Note in particular that the Lg waves arrive on the transverse components as early as on the vertical or radial ones and cannot therefore be considered only as coda waves. These recordings are representative of a larger collection of NORSAR explosion recordings where Lg wave transverse components are systematically present and large. In the present case, the explosions were fired close to the sea-bed, 73 km from the coast for the CANOBE example, and close to the coast for the FENNOLORA recordings. The near-source structure certainly generates SV waves, but less likely large SH waves. Propagation in a complex structure is required to produce these transverse components.

The heterogeneous nature of the crust is more commonly invoked than anisotropy in order to explain complex polarization of short period waves, though anisotropy has been observed in various regions of the world, and its effect on polarization of body waves and surface waves is well-documented (see Crampin, 1977, for a review). We plan here to contribute to a better understanding of Lg wave propagation by presenting synthetic seismograms of explosion-induced 3-component Lg waves propagating in models with apparent upper crustal anisotropy.

Anisotropy in the upper crust

Shear-wave splitting, the most typical signature of anisotropy, is observed in an increasing number of regional and local studies. Of special interest to us is the analysis of Brooks *et al* (1987) who show evidence of crustal anisotropy in Scandinavia. Anderson *et al* (1974) and Hudson (1981) showed how a uniform distribution of aligned cracks in an otherwise isotropic matrix can be viewed in the long wavelength approximation as a homogeneous anisotropic material. Crampin *et al* (1984) proposed that widespread crustal anisotropy

coherent over large areas proceeds from opening of microcracks in preferred directions related to the regional stress field. The polarization directions of observed split S-waves always support this hypothesis, which has become the most commonly accepted one to explain upper crustal anisotropy.

The nature and depth of the anisotropy are very seldom and poorly constrained by S-wave splitting data. Anisotropy confined to the first 10 km of the crust is the best model for Japan after Kaneshima *et al* (1988), and anisotropy to at least 6 km depth has been found in the crystalline basement of the Urals by Koshubin *et al* (1984). When the depth is not directly constrained, an anisotropy in the first few kilometers of the crust is usually consistent with the observations. Observed shear wave delays are often around 0.2 s (Kaneshima *et al*, 1988: Zollo & Bernard, 1989: Brooks *et al*, 1987) and suggest an open crack density of 0.1 over 5 km depth (or any combination giving the same delay such as 0.05 crack density over 10 km). More directly constrained velocities support a crack density averaging 0.05 (Babuska & Pros, 1984; Koshubin *et al*, 1984).

Model and modelling method

In accordance with the foregoing, we assume that the upper crust in Scandinavia has an apparent anisotropy due to a uniform distribution of circular vertical cracks with small aspect ratio and preferred orientation related to the regional stress field, as indicated schematically in Fig. 7.6.1. The formula for calculating the effective elastic coefficients of a medium containing dry og liquid-filled cracks are given in Crampin (1984) after Hudson (1981). We retain only the purely elastic perturbation due to the cracks, and neglect the anelastic part since one can estimate from Crampin (1984) that metric cracks with a 0.1 crack density lead to an attenuation factor Q^{-1} of the order 10^{-11} for the 1 Hz Lg wave. The attenuation depends on the crack radius in the power of 3 and is therefore even smaller for microcracks.

Our basic model for the Scandinavian crust is taken from Cassell *et al* (1983) who interpreted P-wave arrival times and amplitudes from the CANOBE refraction experiment along a profile which exactly fits the propagation path of the Lg wave from CANOBE shot H2 to NORSAR (Fig. 7.6.1). We have replaced the upper 5 km of their model, unconstrained by their data, by a layer having P-wave velocities increasing from 6 to 6.25 km/s. This is similar to what was found by Gundem (1984) in southern Norway, and accounts better for the group velocity and short duration of the observed Lg wavetrains in this area. We derive the S-wave velocity model from the P-wave velocity model assuming a Poisson ratio equal to 0.25. Quality factors are introduced in the model with frequency dependence of $\sqrt{f}$ after Campillo *et al* (1985). The model is displayed in Fig. 7.6.2.

The Lg modes in the frequency band 0.5 to 2 Hz are calculated in the anisotropic models at first order in deviation from isotropy using the quasi-degenerate perturbation method (Luh, 1973; Maupin, 1989). This method is capable of accounting for the full 3-D polarization of the Lg wave generalized modes, though retaining the advantages of treating anisotropy as a small perturbation of an isotropic model. The source for the explosions is taken as a unit pressure dirac at a depth of 150 m, chosen to mimic the refraction shots of the CANOBE profile, though very imperfectly since we cannot account for the water layer in which the explosions were fired or the sedimentary layer underneath. No absolute amplitude is tied to the source, and amplitudes of the synthetic seismograms are reported relative to the maximum amplitude of the synthetic seismogram in the isotropic reference structure. The ground displacement is convolved with the NORSAR short-period instrument response.

Explosion Lg waves and upper crustal anisotropy

Synthetic Lg waves calculated in models having various crack densities at various depths are presented in Fig. 7.6.3. These cases all correspond to a wave propagation direction at 15° from the crack normal preferred orientation, similar to the angle which can be inferred from Brooks *et al* (1987) between crack orientation in Scandinavia and propagation path to NORSAR of the Lg wave from the CANOBE shot H2 and FENNOLORA shot E2 (Fig. 7.6.1). The source-station distance is 450 km. The reference synthetic Lg wave calculated in the isotropic structure has of course no transverse component (Fig. 7.6.3a). For liquid-filled cracks between 0 and 10 km depth and a crack density of 0.02, a small transverse component appears (Fig. 7.6.3b). Increasing the crack density to 0.05 (Fig. 7.6.3c), the transverse component grows larger than the radial one. Note that this anisotropy, the amplitude and depth extension of which are compatible with observations of split shear wave delays (Brooks *et al*, 1987), yields relative amplitudes of the three Lg components that closely resemble the observations (Fig. 7.6.1). In Fig. 7.6.3d is shown the synthetic Lg wave when the cracks are confined to the upper 5 km of the crust with 0.1 crack density. The Lg wavetrain is lengthened on the three components. This lengthening appears also for other propagation directions. The last example (Fig. 7.6.3e) is for a uniform distribution of dry cracks in the upper 10 km of the crust with 0.05 crack density. The transverse components are not strongly developed in that case.

Synthetic Lg waves for wave propagation at other angles from the crack normal direction have also been calculated. For propagation in the crack orientation symmetry planes at 0 and 90°, no transverse component of course appears. For angles ranging from 0 to 45°, the Lg waves are like those for a 15° angle and displayed in Fig. 7.6.3. For angles approaching 90°, the amplitude of the transverse component decreases gradually and its maximum is shifted towards later arrival times. However, the onset time of the Lg wave or group

velocity of its first wave packet does not depend on azimuth. The effect of upper crustal anisotropy on the Lg wave is basically a polarization effect and not a velocity effect.

Assuming a uniform anisotropy along the whole propagation path, we have calculated Lg synthetic seismograms for different epicentral distances. Besides fluctuations due to variations in modal interferences, which occur also in isotropic structures, it appears that the ratio between different components is stable with epicentral distance. For an epicentral distance of 150 km, at which the Lg wavetrain becomes an "individualized" wavetrain, the ratio between the transverse and vertical components in our synthetic data is already the ratio which is measured at 750 km, whether large or small. This is in agreement with observations made by Blandford (1981).

The extensive dilatancy anisotropy hypothesis of Crampin *et al* (1984) on which we have based our models, and the widespread character of transverse component observations, rather suggest a regional crustal anisotropy than a local one. We can, however, test the minimum lateral extension of an anisotropic zone necessary to explain the data. As for body waves, if anisotropy along only part of the wavepath introduces polarization anomalies, they are propagated to the station even if the remainder of the propagation path is isotropic. The analysis of Lg wave character as a function of epicentral distance implies that anisotropy over 150 km is sufficient to produce the observed polarization anomalies.

Conclusion

We have shown that an upper crust with a uniform distribution of microcracks aligned in the regional stress field can account for transverse components of Lg waves induced by explosions. Our preferred model to explain with upper crustal anisotropy the observations in Scandinavia is a distribution of liquid-filled cracks in the upper 10 km of the crust with a crack density larger than 0.02 and most favorably around 0.05. This model is consistent with observations of shear wave splitting by Brooks *et al* (1987) in northern Scandinavia.

Valerie Maupin, Inst. de Physique du Globe, Strasbourg

References

Anderson, D.L., B. Minster and D. Cole (1974): The effect of oriented cracks on seismic velocities, *J. Geophys. Res.*, 79, 4011-4015.

Ansorge, J. (1981): Fennoscandia long-range project 1979 (FENNOLORA), first results, *Working Group of European Seismological Commission.* Presented at the 21st General Assembly of IASPEI, London, Ontario, July 1981.

Babuska, V. and Z. Pros. (1984): Velocity anisotropy in granodiorite and quartzite due to the distribution of microcracks, *Geophys. J. R. astr. Soc.*, 76, 121-127.

Blandford, R.R. (1981): Seismic discrimination problems at regional distances, in *Identification of Seismic Sources — Earthquake or Underground Explosion*, E.S. Husebye and S. Mykkeltveit (eds.), D. Reidel Publ., Dordrecht.

Bouchon, M. (1982): The complete synthesis of seismic crustal phases at regional distances, *J. Geophys. Res.*, 87, 1735-1741.

Brooks, S.G., P.N. Chroston and D.C. Booth (1987): Extensive dilatancy anisotropy (EDA) inferred from observations of crustal shear waves generated by a refraction experiment in northern Scandinavia, *Geophys. J. R. astr. Soc.*, 90, 225-232.

Campillo, M., J.-L. Plantet and M. Bouchon (1985): Frequency-dependent attenuation in the crust beneath Central France from Lg waves: data analysis and numerical modelling, *Bull. Seism. Soc. Am.*, 75, 1395-1411.

Cassell, B.R., S. Mykkeltveit, R. Kanestrøm and E.S. Husebye (1983): A North Sea-southern Norway seismic crustal profile, *Geophys. J. R. astr. Soc.*, 72, 733-753.

Crampin, S. (1977): A review of the effects of anisotropic layering on the propagation of seismic waves, *Geophys. J. R. astr. Soc.*, 49, 9-27.

Crampin, S. (1984): Effective elastic constants for wave propagation through cracked solids, *Geophys. J. R. astr. Soc.*, 76, 135-145.

Crampin, S., R. Evans and B.K. Atkinson (1984): Earthquake prediction: a new physical basis, *Geophys. J. R. astr. Soc.*, 76, 147-156.

Gundem, M.B. (1984): 2-D seismic synthesis of the Oslo Graben, M.Sc. thesis, Univ. of Oslo.

Herrmann, R.B. and A. Kijko (1983): Modeling some empirical vertical component Lg relations, *Bull. Seism. Soc. Am.*, 73, 157-171.

Hudson, J.A. (1981): Wave speeds and attenuation of elastic waves in material containing cracks, *Geophys. J. R. astr. Soc.*, 64, 133-150.

Kaneshima, S., M. Ando and S. Kimura (1988): Evidence from shear-wave splitting for the restriction of seismic anisotropy to the upper crust, *Nature*, 335, 627-629.

Koshubin, S.I, N.I. Pavlenkova and A.V. Yegorkin (1984): Crustal heterogeneity and velocity anisotropy from seismic studies in the USSR, *Geophys. J. R. astr. Soc.*, 76, 221-226.

Luh, P. (1973): Free oscillations of the laterally inhomogeneous earth: quasi-degenerate multiplet coupling, *Geophys. J. R. astr. Soc.*, 32, 197-202.

Maupin, V. (1989): Surface waves in weakly anisotropic structures; on the use of ordinary or quasi-degenerate perturbation methods, *Geophys. J.*, 98, 553-563.

Mykkeltveit, S. and E.S. Husebye (1981): Lg wave propagation in Eurasia, in *Identification of Seismic Sources — Earthquake or Underground Explosion*, E.S. Husebye and S. Mykkeltveit (eds.), D. Reidel Publ., Dordrecht.

Zollo, A. and P. Bernard (1989): S-wave polarization inversion of the 15th October 1979, 23:19, Imperial Valley Shock: Evidence for anisotropy and a simple source mechanism, *Geophys. Res. Lett.*, 16, 1047-1050.

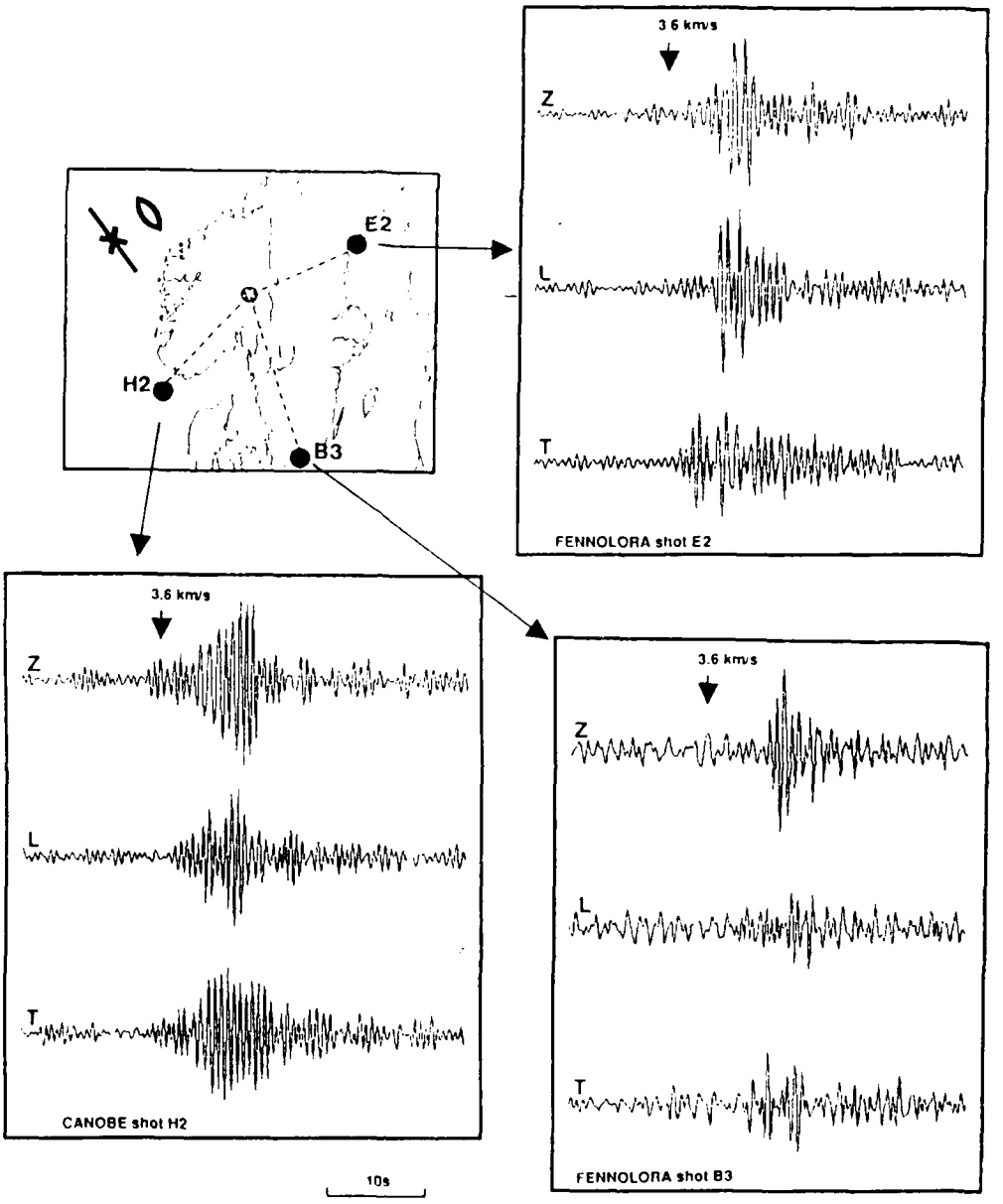

Fig. 7.6.1 3-component Lg recordings at NORSAR short-period station 01A of CANOBE shot H2 and FENNOLORA shots B3 and E2, band-pass filtered between 0.5 and 2 Hz. The arrival time of the wave with group velocity 3.6 km/s is indicated. The amplitude scale is identical on the three components for each recording. The direction of regional maximum horizontal compression and a schematic vertical crack opened by the regional stress field are indicated in the upper left corner of the map of southern Scandinavia.

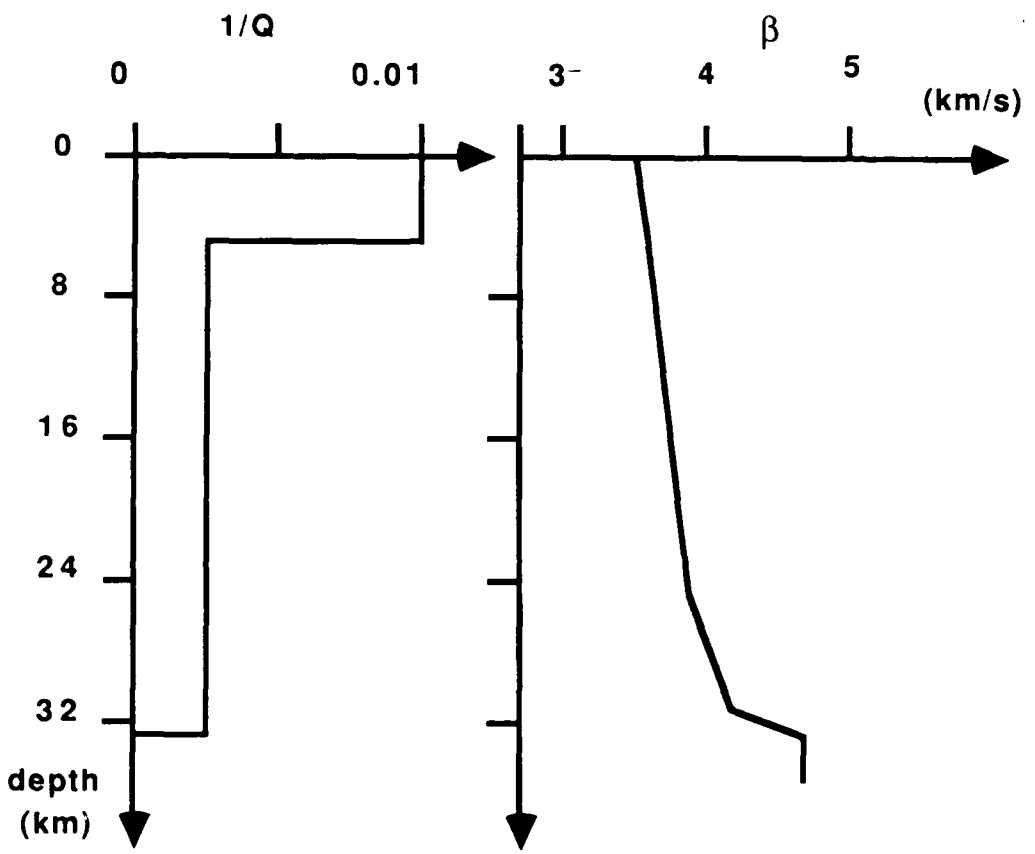

Fig. 7.6.2 Models of inverse quality factor at 1 Hz and shear wave velocity with depth used in the synthesis of the Lg waves.

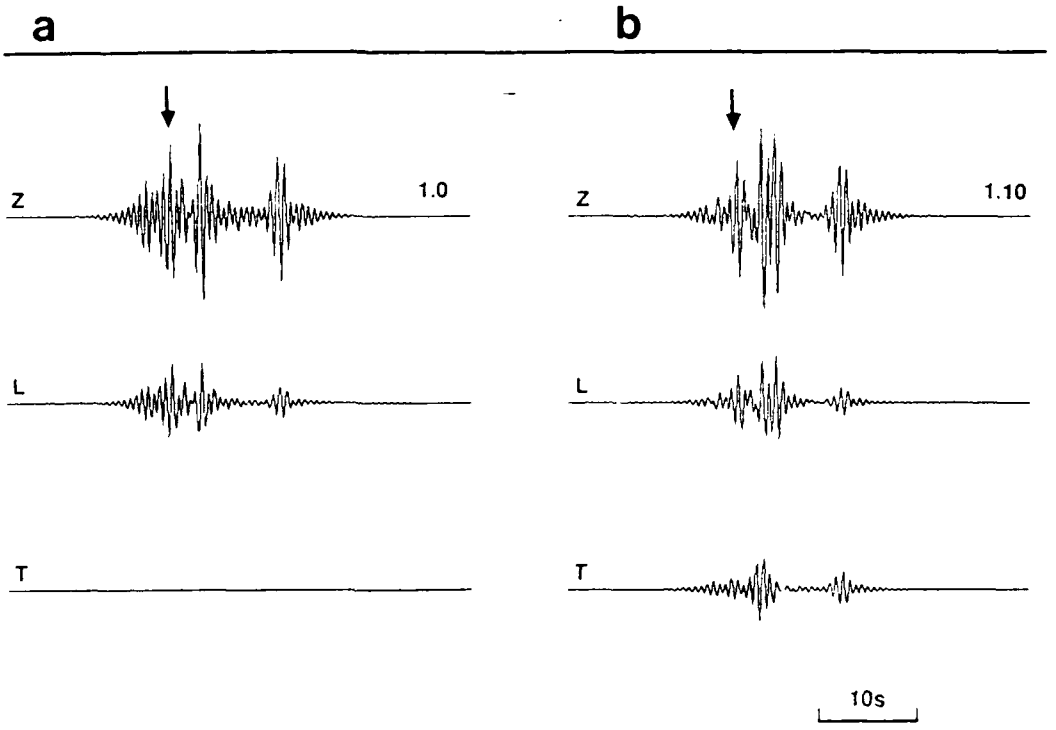

Fig. 7.6.3 3-component synthetic Lg waves produced by an explosion at 150 m depth and 450 km epicentral distance in different models of southern Scandinavia. **(a)** Isotropic model; **(b)** model with liquid-filled circular vertical cracks between 0 and 10 km depth, 0.02 crack density and orientation of the crack normal at 15° from the wave propagation direction; **(c)** the same as for case (b) for 0.05 crack density; **(d)** the same as for case (b) for 0.1 crack density and cracks between 0 and 5 km depth; **(e)** the same as case (c) for dry cracks. The arrow on the vertical traces indicates the arrival time of the 3.6 km/s group velocity wave. The three components of each plot have the same amplitude scale. The ratio between the maximum amplitude of the largest component and the maximum amplitude of the vertical component in the isotropic case is indicated in each 3-component plot at the end of the vertical trace.

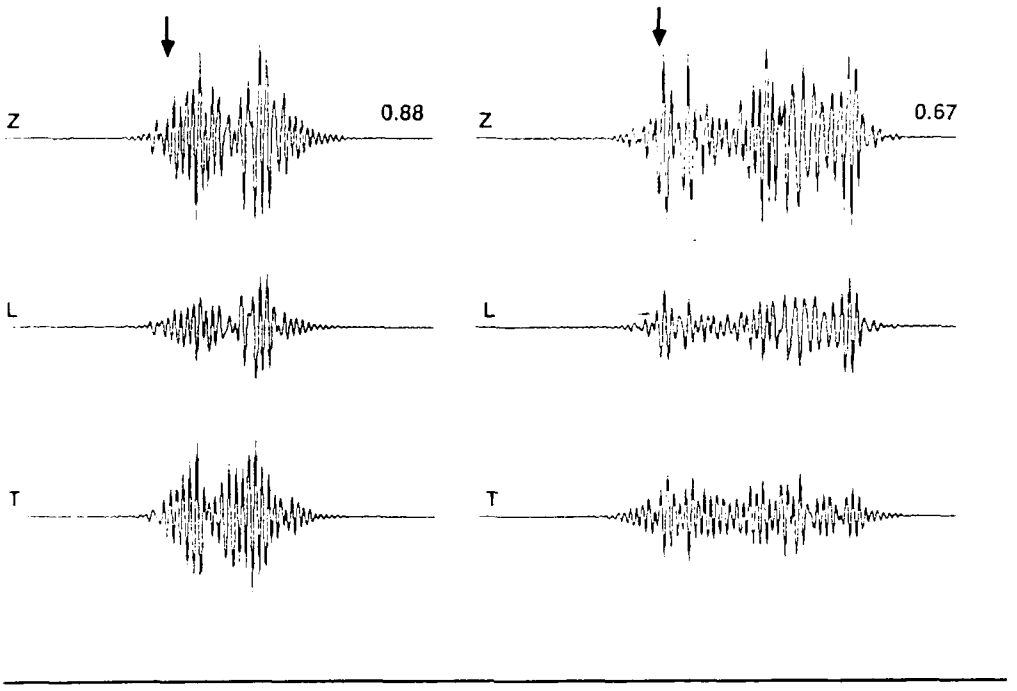

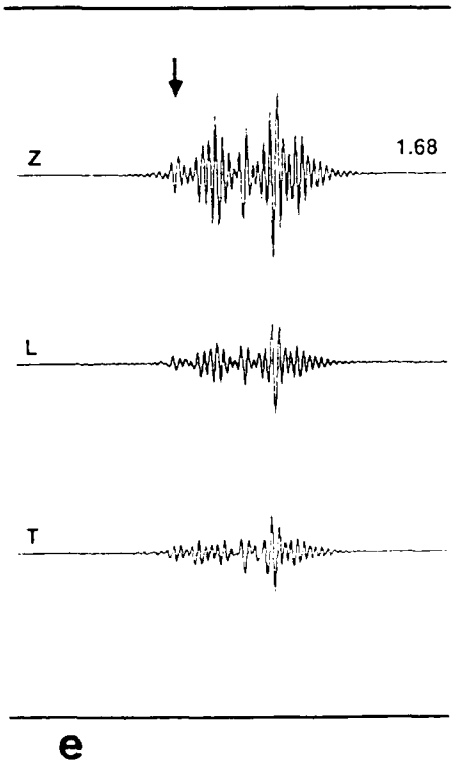

Fig. 7.6.3 (cont.)

7.7 Statistically optimal event detection using small array data

A generalization of Capon's maximum likelihood technique for detection and estimation of seismic signals is introduced. By using a multidimensional autoregressive approximation of seismic array noise, we have developed a technique to use Capon's group filter for on-line processing. Such autoregressive adaptation to the current noise matrix power spectrum yields good suppression of mutually correlated array noise processes. An example is shown of this technique as applied to detection of the a small Semipalatinsk underground explosion recorded at the ARCESS array.

Nuclear explosion monitoring using seismic data is faced with the problem that signals of small explosions are masked by noise, and thus have to be extracted using features of both the noise and the signal. Small arrays appear to be especially suited for that purpose. This is due to the strong correlation of noise between different closely located receivers which gives us an opportunity to obtain significant noise suppression. To realize this opportunity, special software is needed.

We have to solve two main problems: (1) to detect event signals, and (2) to classify detected signals as originating from either an explosion or an earthquake. The second task is very complex. The proper identification needs first of all estimation of signal waveform and then estimation of signal parameters such as onset times of different phases, power and spectral features, and so on. While the detection of a signal can be done in a relatively narrow frequency band (for example using a high frequency band only) the classification must in principle be based on wide band methods. This is so because bandpass filtering distorts not only the noise but also the signal, thus possibly eliminating useful classification features.

The problems mentioned can be formulated in terms of mathematical statistics, and optimal decision rules for these mathematical problems have to be found. The first task is to detect the signal. The time series received by the array has the following structure: $X_t = S_t + \xi_t, t \in \ldots -1, 0, 1, \ldots$, where S_t is signal and ξ_t is noise, X_t is a vector of different receiver outputs. These outputs are observed through a moving window. Using data in the window we must make a decision: does it contain a signal or not. This problem can be solved in terms of statistical hypothesis testing theory. It is necessary to test hypothesis H_0: observations in the moving window are pure noise, versus hypothesis H_1: they comprise signal plus noise. We consider hypothesis H_0 to be simple, but hypothesis H_1 to be complex. This is because the statistical characteristics of noise can be measured before the signal arrival in a stage of adaptation, but the statistical features of seismic signals are almost completely unknown.

The problem is now to choose a decision function which would provide the smallest average error probability for all possible signals. This problem can be solved using a Bayesian approach and finite dimensional parameterization of the signal (Kushnir and Lapshin, 1984) (see Appendix). The decision has the form of an algorithm as shown in Fig. 7.7.1. It consists of a group filter followed by autocorrelators, calculation of a quadratic form and a trigger which compares the quadratic form with a threshold. The transfer function of the group filter is a vector described as a product of the inverse matrix power spectrum F^{-1} of the noise ξ_t and a vector G of phase shift factors due to signal delays τ_1. The algorithm shown has a form which can be easily realized as an on-line procedure. This is mostly due to the use of multidimensional autoregressive (AR) estimation of the matrix power spectrum density F of the noise. This allows us to avoid direct inversion of spectral power matrices and is very convenient in an adaptive procedure (Haykin, 1979; Kushnir *et al.* 1980).

The second problem mentioned above is to estimate properly the signal waveform. The main purpose of this estimation is to make a correct decision of whether we have an explosion or an earthquake. We must do it as precisely as possible. The model of observation here has the following form: $X_t = G_t * u_t + \xi_t$, where $*$ is a sign of convolution, u_t is a signal waveform to be estimated — (the particle motion along the seismic ray), G_t is the transfer function on the path from the seismic source to the receiver. For plane waves, this vector is defined by time delays only. For solving the estimation problem, a conditional Wiener filter can be constructed. This filter minimizes the variance of the estimate $E\{(\hat{u}_t - u_t)^2\}$ under the condition that the mathematical expectation of the estimate coincides with the real signal: $E\{\hat{u}_t\} = u_t$.

It so happens that the Wiener filter we are looking for consists of the same group filter which is used for the detection followed by a restitution filter (which makes it possible to obtain the signal undistorted). Capon was the first to propose this filter for seismic signal extraction from array data (Capon, 1970). The complete array procedure for detection and classification is shown in Fig.7.7.2. We adapt to the noise matrix power spectrum by estimating its AR parameters and computing vector coefficients of the group filter. Then we perform group filtration in the moving window and detect the signal. The first two operations are made periodically according to the interval of noise stationarity. The third — group filtration — can be devised as an on-line procedure. After the signal is detected it must be filtered by the restitution filter, which refines its shape. And finally classification may be done using the estimates of signal parameters.

The software designed was tested using simulated data with the aim of comparing its actual efficiency with the theoretical one. The results of these tests are shown in Fig. 7.7.3. The depicted curves are the gains in power signal-

to-noise ratio of undisturbed optimal group filtration relative to a conventional beam versus the coherence coefficient of the noise. The latter is defined as the ratio between the largest and the smallest eigenvalues of the noise power spectrum matrix. We see that the mentioned gain may be very significant if the array noise is coherent enough. This happens in practice at small aperture arrays. The calculations were made for the central subarray of the NORSAR array.

Highly promising results were obtained by the use of ARCESS data for signals from one of the smallest nuclear tests known to have been conducted at the Semipalatinsk test site. In Fig. 7.7.4 we display the records for four ARCESS channels and note that the signal is obscured by the noise. For the conventional beam trace (Fig. 7.7.5) the signal is likewise not seen, but inspecting the output of the undisturbed group filter we can see the signal clearly. The power signal-to-noise ratio gain relative to the beam is approximately a factor of 70–80 and it is 140–160 when compared with a single channel. The trace shown is calculated using 6 matrix AR parameters of noise. We also used other numbers of AR parameters and the results seemed to be stable. Such high suppression of noise is achieved mainly due to the high correlation of noise records in the inner ARCESS stations (see Fig. 7.7.4, traces A0,A3).

Fig. 7.7.6 shows that the group filter used does in fact retain the shape of the original waveform. The first trace is a wide frequency band waveform used for simulating the plane wave arriving at ARCESS. These simulated data were processed by the group filter used for the previously shown signal extraction. The resulting (second) trace practically coincides with the first. So, if the real signal is plane wave, it will be undisturbed by the group filter in the frequency band from 0.5 to 5 Hz.

The conventional method used for the detection of weak signals is the filtration of the array beam in a band of optimum signal-to-noise ratio (Kværna, 1989). The two traces at the bottom of Fig. 7.7.5 show the signal filtered in the frequency band 2.5–4 Hz after beamforming and after undisturbed group filtration. The gain here is not as large as in broad band, but still exceeds a factor of 5 in power SNR. Fig. 7.7.7 (at the top) shows the same signals, but in another time scale. The chosen frequency band seems to be the best for filtering the signal after beamforming. For comparison we have plotted two traces at the bottom of Fig. 7.7.7 presenting the same signals filtered in the frequency band 3–5 Hz.

For the detection of signals in our experiments, 4 different variants of the optimal detector previously described were used. All of these detectors are sensitive not only to the increase in trace power due to signal arrival, but also to changes of the trace spectrum (Kushnir *et al*, 1983). The first is optimal in a statistical sense, the second is a modification of STA/LTA using prewhitening

of the noise, and the last two are components of the first. Fig. 7.7.8 shows how the detectors work when applied to the beam and group filter outputs. The gain due to optimal group filtration is evident.

The final picture (Fig. 7.7.9) shows the results of the signal onset time estimation. Estimation is performed by an algorithm based on the maximum likelihood method applied to the problem of estimating the moment in time when parameters of the AR process are abruptly changed (Pisarenko *et al*, 1987). One can see that the likelihood function maximum coincides exactly with the beginning of the signal.

Conclusions

1. Application of an adaptive optimal group filtration technique to small aperture arrays can provide large gains in SNR in comparison with conventional beamforming due to high mutual correlation of array noise.

2. By using AR estimation of the power noise spectrum for group filter adaptation, we greatly reduce time and memory needed for the adaptation procedure while providing high quality of noise suppression.

3. Optimal group filtration does not distort the signal. Thus, when seen in connection with 1. and 2. above, it is clear that optimum filtration has great advantages as a preprocessor to be applied prior to subsequent broad band operations such as source classification.

In future work, it is recommended that the following studies be undertaken:

1. To perform a large-scale experiment concerning detection and classification capability of optimal group filtration applied to seismic signals recorded at NORESS and ARCESS. Comparison of false alarm rates of the optimum detector versus conventional beam detectors should form part of this investigation.

2. To develop algorithms for the compensation of signal frequency dependent waveform distortions due to propagation in real media under the array. This will give us an opportunity to equalize signal waveforms in different array receivers and improve signal extraction at high frequencies.

3. To implement these algorithms in an operational environment at the NORSAR data center.

4. To develop algorithms for designing optimal array geometry on the basis of the optimal group filtration features.

5. To use optimal group filtration for holographic investigations of the earth's interior using NORSAR data.

We plan to continue further work along these lines in future co-operative projects between NORSAR and the Institute of Physics of the Earth, Moscow.

A.F. Kushnir, Inst. of Physics of the Earth, Moscow
V.I. Pinsky, Inst. of Physics of the Earth, Moscow
J. Fyen, NORSAR

References

Capon, J. (1970): Application of signal detection and estimation theory to the large-array seismology, *Proc. IEEE*, 58.

Haykin, S. (ed.) (1979): *Nonlinear methods of spectral analysis.* Topics in Applied Physics, 34, Springer-Verlag, 234 pp.

Kushnir, A.F., and V.M. Lapshin (1984): Optimal processing of the signals received by a group of spatially distributed sensors. *Computational Seismology*, 17, Allerton Press, Inc., 163-174.

Kushnir, A.F., V.F. Pisarenko and T.A. Rukavishnikova (1980): Noise compensation in multidimensional geophysical observations. I. Theory and method of data processing. *Computational Seismology*, 13, Allerton Press, Inc., 146-151.

Kushnir, A.F., I.V. Nikiforov and I.V. Savin (1983): Statistical adaptive algorithms for seismic signals automatic detection. *Computational Seismology*, 15, Allerton Press, Inc., 145-162.

Kværna, T. (1989): On exploitation of small-aperture NORESS type arrays for enhanced P-wave detectability. *Bull. Seism. Soc. Am.* 79, 888-900.

Pisarenko, V.F., A.F. Kushnir and I.V. Savin (1987): Statistical adaptive algorithms for estimations of onset moments of seismic phases. *Phys. Earth Planet. Inter.*, 47, 4-10.

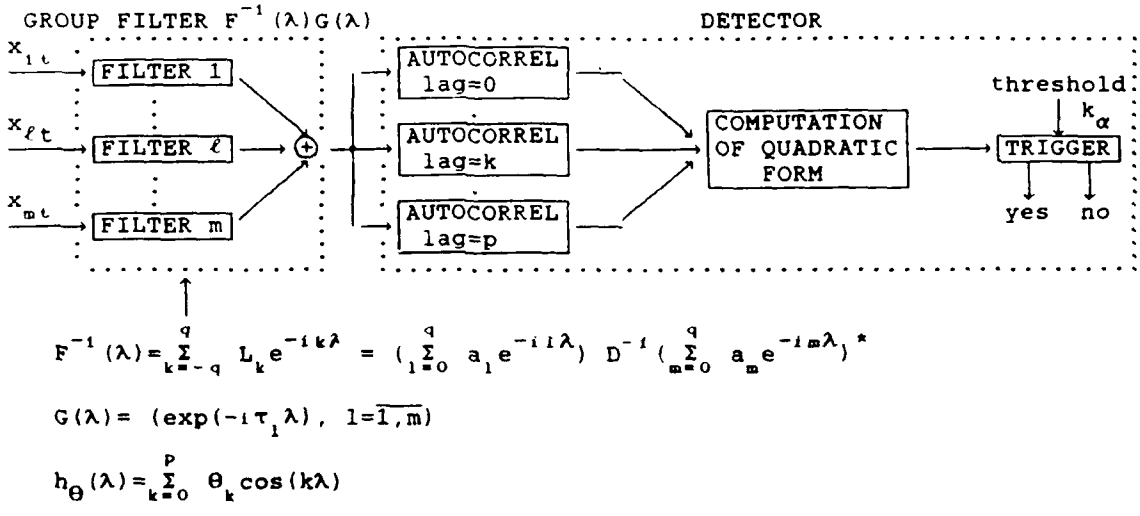

Fig. 7.7.1 Optimal group detector flowchart.

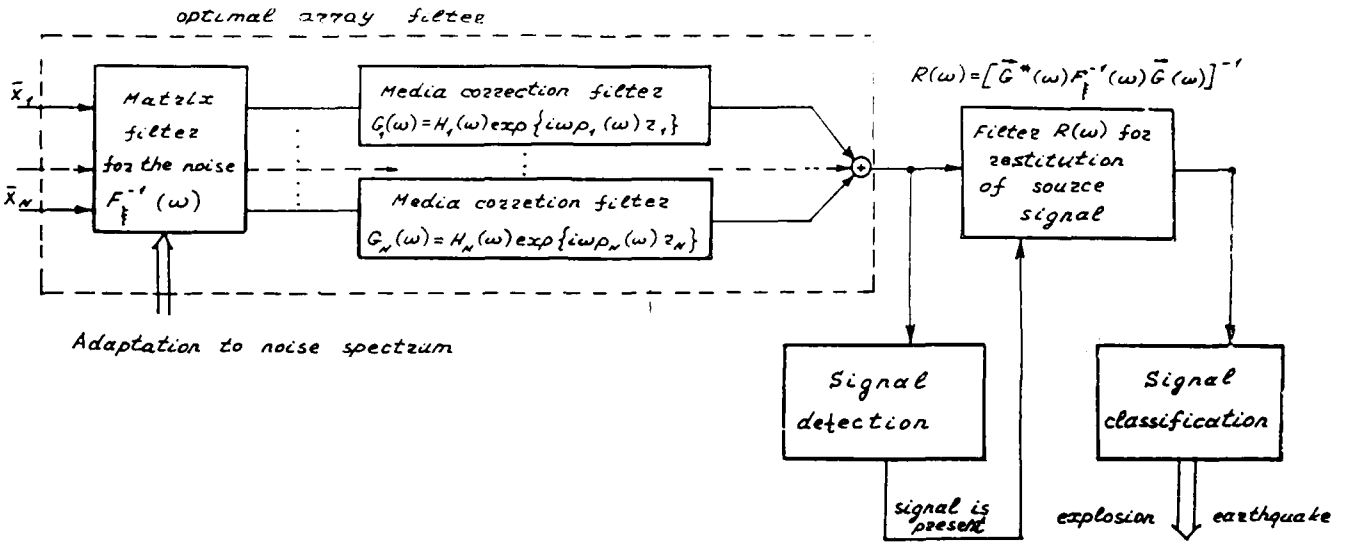
optimal array filter
Matrix filter for the noise $F_f^{-1}(\omega)$
Media correction filter $G_1(\omega) = H_1(\omega)\exp\{i\omega\rho_1(\omega)z_1\}$
Media correction filter $G_N(\omega) = H_N(\omega)\exp\{i\omega\rho_N(\omega)z_N\}$
$R(\omega) = [\bar{G}^*(\omega)F_f^{-1}(\omega)\bar{G}(\omega)]^{-1}$
Filter $R(\omega)$ for restitution of source signal
Adaptation to noise spectrum
Signal detection
Signal classification
signal is present
explosion
earthquake

Fig. 7.7.2

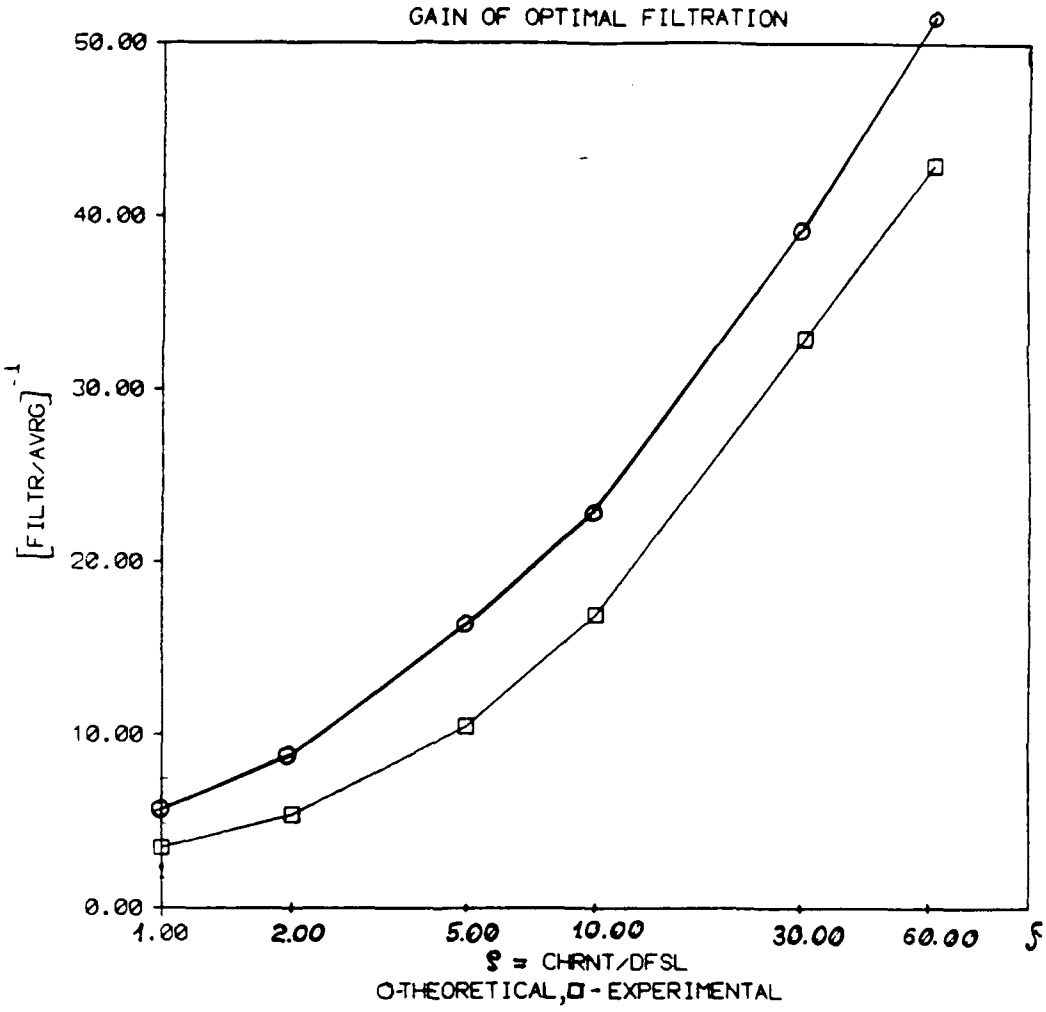
GAIN OF OPTIMAL FILTRATION
50.00
40.00
30.00
20.00
10.00
0.00
[FILTR/AVRG]^-1
1.00
2.00
5.00
10.00
30.00
60.00
ξ
ξ = CHRNT/DFSL
O-THEORETICAL, □ - EXPERIMENTAL

Fig. 7.7.3

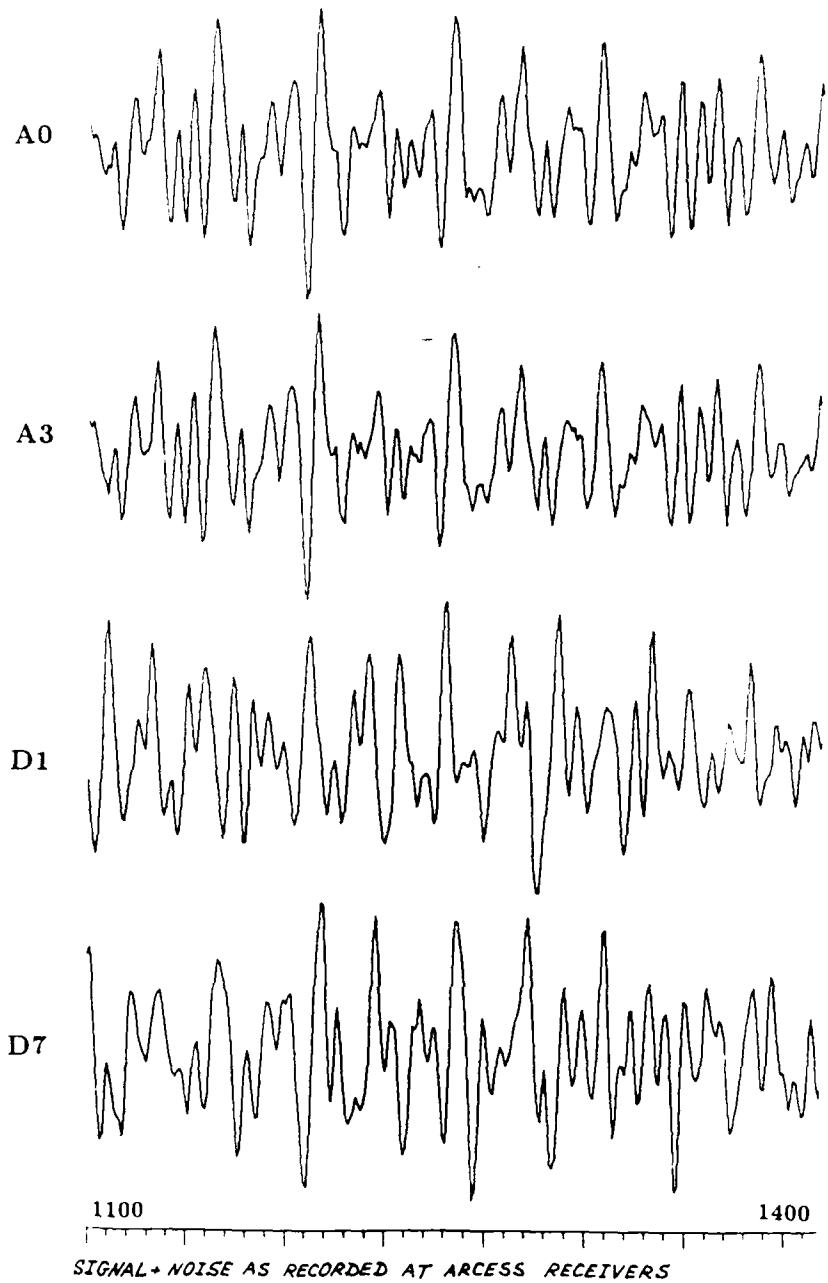
A0
A3
D1
D7
1100
1400
SIGNAL + NOISE AS RECORDED AT ARCESS RECEIVERS

Fig. 7.7.4

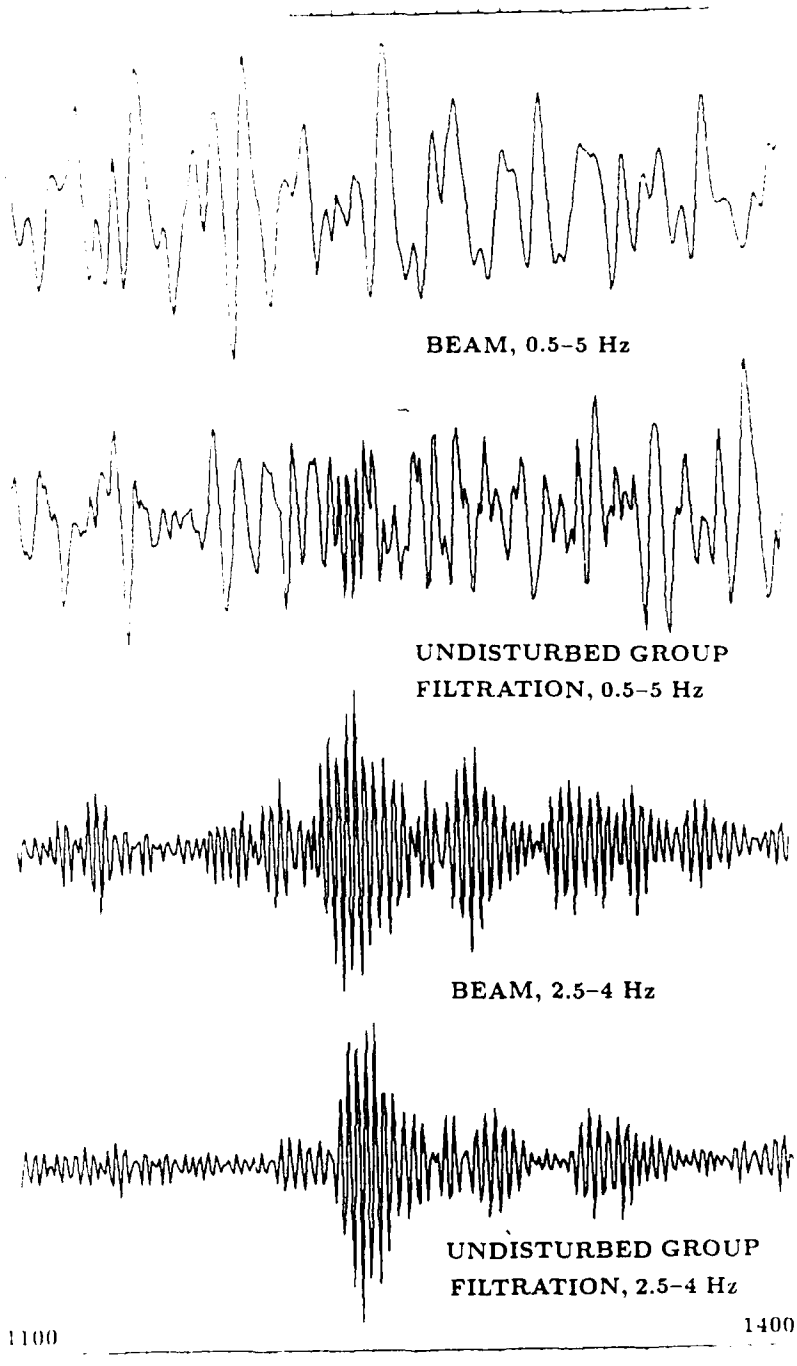
BEAM, 0.5–5 Hz
UNDISTURBED GROUP
FILTRATION, 0.5–5 Hz
BEAM, 2.5–4 Hz
UNDISTURBED GROUP
FILTRATION, 2.5–4 Hz
1100
1400

Fig. 7.7.5

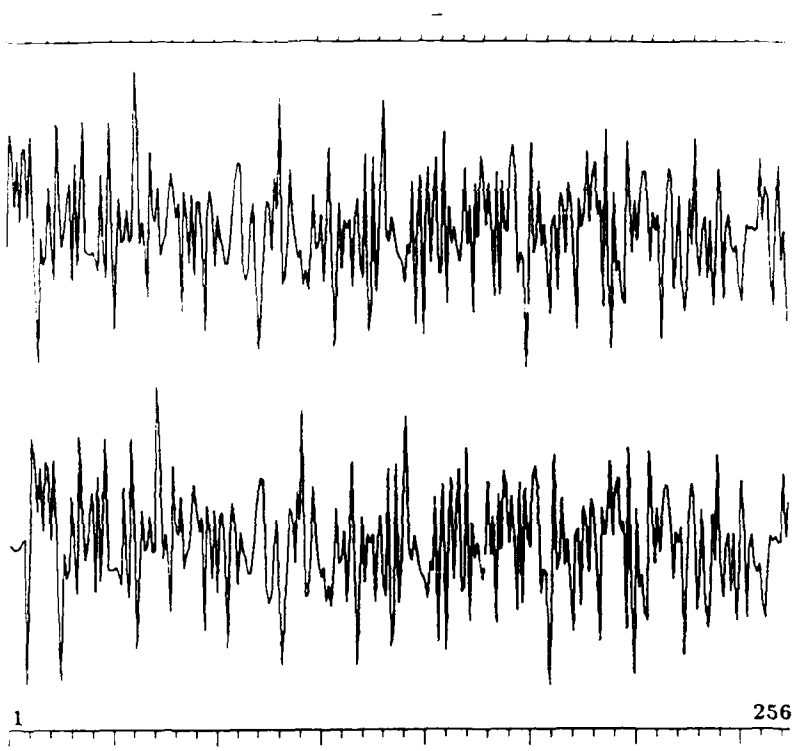

Fig. 7.7.6

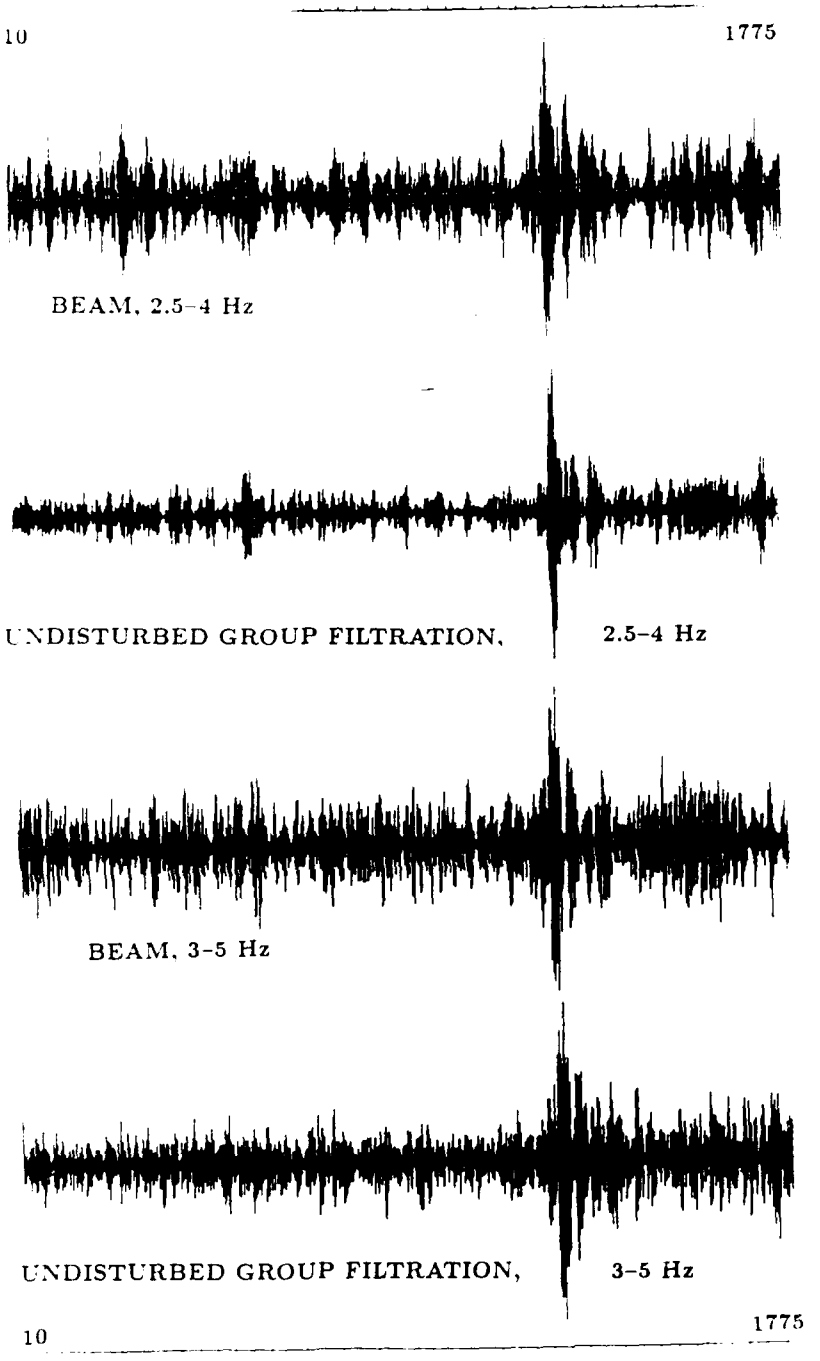
10
1775
BEAM, 2.5–4 Hz
UNDISTURBED GROUP FILTRATION, 2.5–4 Hz
BEAM, 3–5 Hz
UNDISTURBED GROUP FILTRATION, 3–5 Hz
10
1775

Fig. 7.7.7

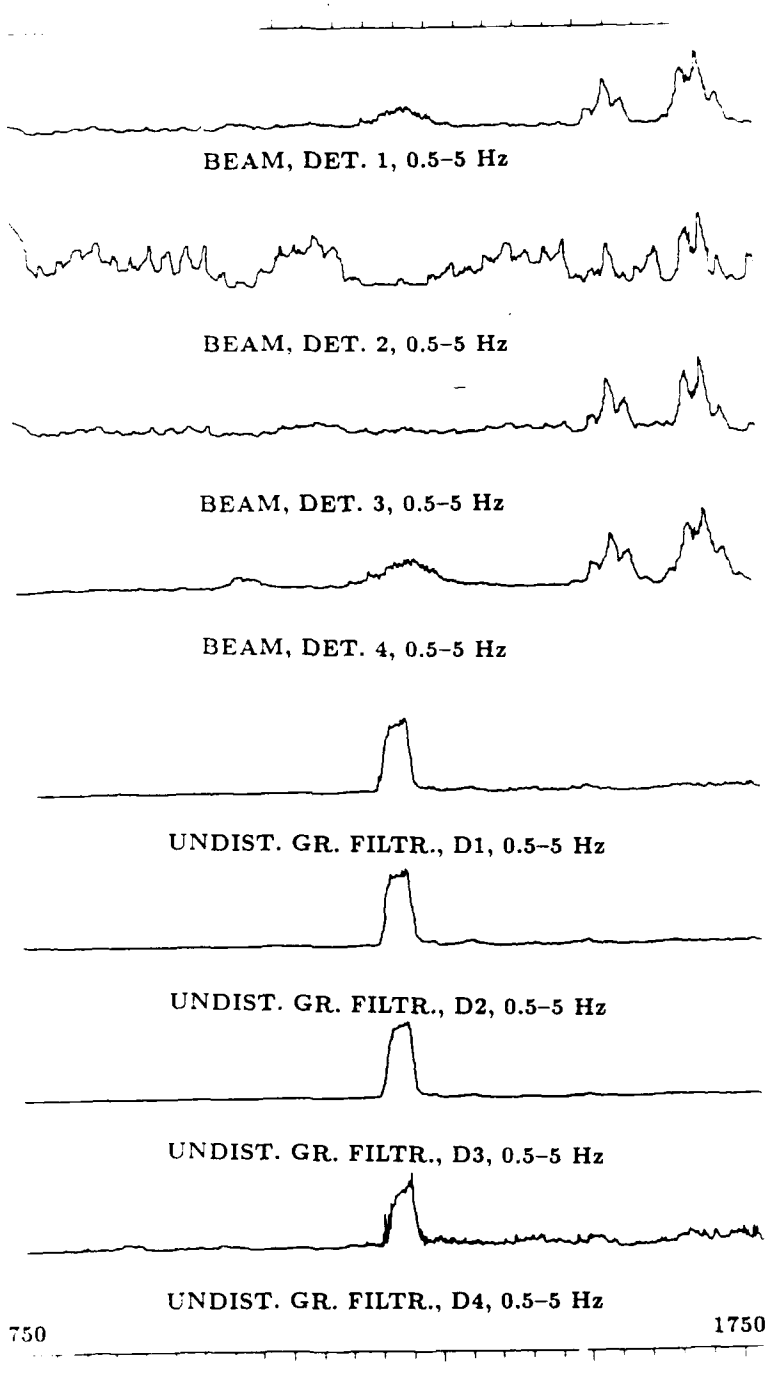
BEAM, DET. 1, 0.5–5 Hz
BEAM, DET. 2, 0.5–5 Hz
BEAM, DET. 3, 0.5–5 Hz
BEAM, DET. 4, 0.5–5 Hz
UNDIST. GR. FILTR., D1, 0.5–5 Hz
UNDIST. GR. FILTR., D2, 0.5–5 Hz
UNDIST. GR. FILTR., D3, 0.5–5 Hz
UNDIST. GR. FILTR., D4, 0.5–5 Hz
750
1750

Fig. 7.7.8

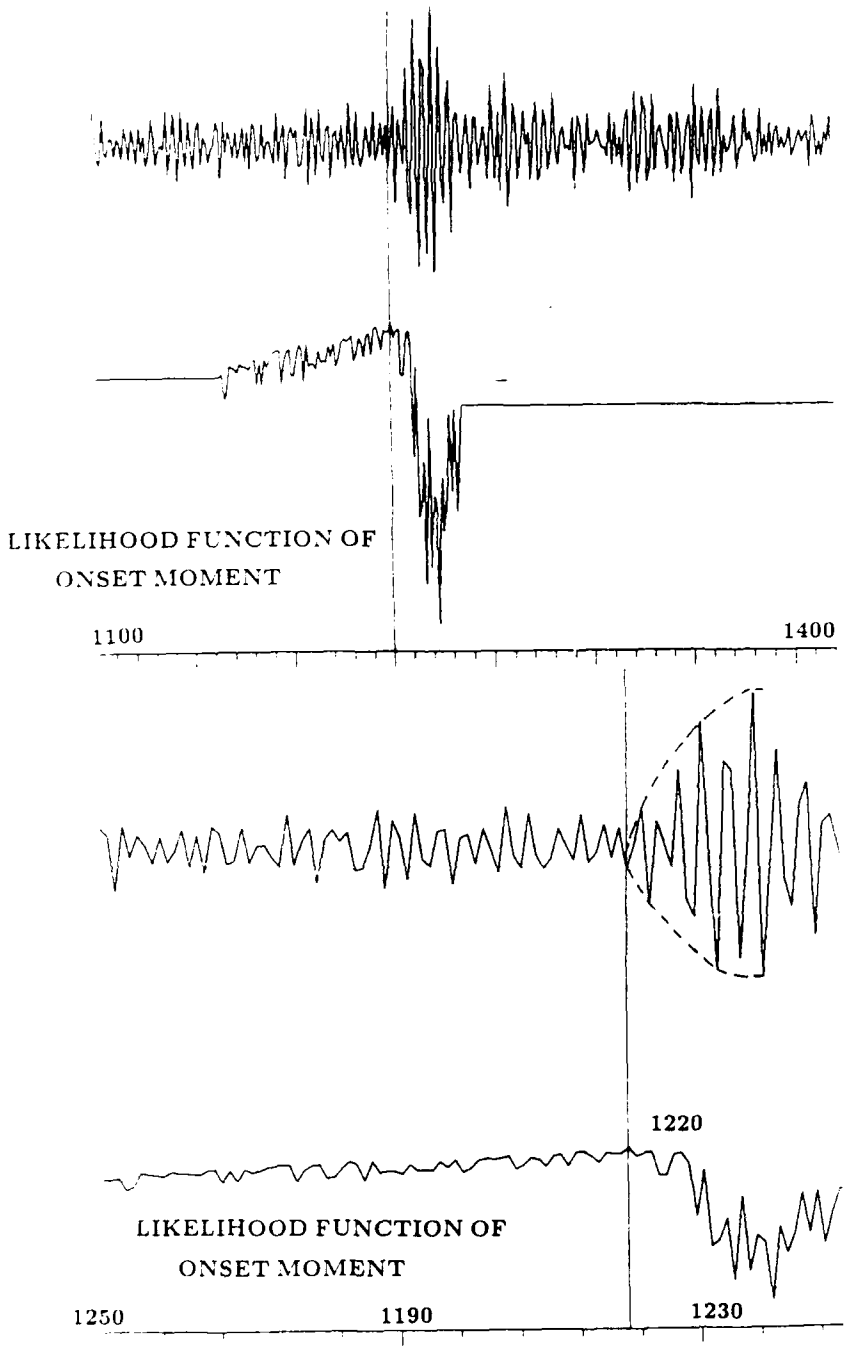
LIKELIHOOD FUNCTION OF
ONSET MOMENT
1100
1400
1220
LIKELIHOOD FUNCTION OF
ONSET MOMENT
1250
1190
1230

Fig. 7.7.9

APPENDIX
Statistically optimal event detection using array data

Let us assume that the noise $\xi_t = (\xi_{1t}, \ldots, \xi_{mt})^T$ at the m receivers of the array is a multidimensional Gaussian time series with zero mean and matrix power spectral density $F(\lambda), \lambda \in [0, 2\pi]$ and that the signal is represented as a Gaussian scalar process $\mu u_t(\Theta)$ at the seismic event source. The power spectral density of $u_t(\Theta)$ is denoted $g_\Theta(\lambda), \lambda \in [0, 2\pi]$, where Θ is an unknown vector parameter. The medium transfer functions are assumed to be linear. Then the observations $x_t = (x_{1t}, \ldots, x_{mt})^T$ become multidimensional Gaussian time series and have the form $G_t * \mu u_t + \xi_t$ and it is easy to write down the likelihood function $w(X_N \mid \mu, \Theta)$ for the moving window observations $X_N = (x_1^T, \ldots, x_N^T)^T$. Here $G_t = (G_{1t}, \ldots, G_{mt})^T$ is the vector impulse response function of the media along the paths from the seismic source to the receivers; $*$ is the sign of convolution. Then the hypothesis H_0 is that $\mu = 0$ and hypothesis H_1 is that $\mu \neq 0$. We consider the function $w(X_N \mid 0)$ to be known through adapative esitmation. If the unknown signal parameters have an *a priori* distribution $P(\Theta)$, then the best (Bayesian) test for testing these hypotheses (providing the least average signal miss probability for a given false alarm probability) has the form:

$$q(X_N) = \begin{cases} 1 \text{ (signal is present)} & \text{if } \rho(X_N) > k_\alpha \\ 0 \text{ (signal is absent)} & \text{if } \rho(X_N) < k_\alpha \end{cases} \tag{1}$$

where

$$\rho(X_N) = \int_\Theta \frac{w(X_N \mid \mu^2, \Theta)}{w(X_N \mid 0)} \, dP(\Theta) \tag{2}$$

Here, k_α is the detection threshold, determined on the basis of the given false alarm probability α.

It is practically impossible to devise an on-line algorithm on the basis of the statistic (1) when the distribution $P(\Theta)$ is arbitrary. But in the important particular case of weak signal detection, where the SNR, μ^2/σ^2, is sufficiently small and the moving window size N is sufficiently large, the statistic $\rho(X_N)$ can be simplified. As it is shown in Kushnir and Lapshin (1984), if the likelihood ratio $w(X_N \mid \gamma\sqrt{N}, \Theta)/w(X_N, 0)$ in (2) is replaced by its exponential approximation, i.e., the statistic $\rho(X_N)$ in (2) is replaced by the more computationally convenient statistic

$$r(X_N) = \int_\Theta exp\{\gamma\Delta(X_N, \Theta) - \frac{\gamma^2}{2}\Gamma_N(\Theta)\} dP(\Theta) \tag{3}$$

the asymptotic error probability limits for the test (3), $\mu^2 = \gamma/N, N \to \infty$, stay constant.

The functions $\Delta(X_N, \Theta)$ and $\Gamma_N(\Theta)$ in (3) have the following forms

$$\Delta(X_N, \Theta) = \frac{1}{2\sqrt{N}} \sum_{j=1}^{N} g_j(\Theta) \mid W_j^* x_j \mid^2 - g_j(\Theta) V_j, \quad \Gamma_N(\Theta) = \frac{1}{4N} \sum_{j=1}^{N} g_j(\Theta) V_j,$$

where $\Delta(X_N, \Theta)$ is an asymptotically sufficient statistic of the observations X_N, and

$$W_j^* = G^*(\lambda_j) F^{-1}(\lambda_j), \qquad V_j = W_j^* G(\lambda_j), \qquad g_j(\Theta) = g_\Theta(\lambda_j)$$

$\Gamma_N(\Theta)$ is the Fisher information quantity, divided by N.

$G(\lambda)$ is the Fourier transform of G_t.

$x_j = \frac{1}{\sqrt{N}} \sum_{t=1}^{N} x_t exp(i\lambda_j t)$ is the discrete Fourier transform of the observations X_N.

$\lambda_j = \frac{2}{N} \pi j$.

$F(\lambda)$ is the matrix power spectral density of the noise ξ_t.

For calculation of the integral (3) in analytic form we will assume that:

$$g_\Theta(\lambda) = 1 + \sum_{k=1}^{P} c_k cosk\lambda, \qquad \Theta = (c_1, \ldots, c_P)^T \tag{4}$$

where $c_k = 2E\{u_t u_{t+k}\}/E\{u_t^2\}$ is the autocorrelation of the source signal.

We further assume that the *a priori* distribution $P(\Theta)$ in (3) is Gaussian:

$$dP(\Theta) = \{(2\pi)^P \, det B\}^{-1/2} \; exp\{-\frac{1}{2}(\Theta - b)^T B^{-1} (\Theta - b)\} \tag{5}$$

Then we have

$$log\{r(x_N)\} = K + \gamma(\Delta_0 - \Delta^T A b) + \frac{1}{2}\Delta^T A \Delta + \frac{1}{\gamma}\Delta^T A B^{-1} b = K + r_\gamma(x_N) \tag{6}$$

where K is a constant independent of X_N, $\Delta = (\Delta_1, \ldots, \Delta_P)^T$,

$$\Delta_0 = \frac{1}{2\sqrt{N}} \sum_{j=1}^{N} \mid W_j^* x_j \mid^2 - V_j$$

$$\Delta_k = \frac{1}{2\sqrt{N}} \sum_{j=1}^{N} (\mid W_j^* V_j \mid^2 - V_j) cos(k\lambda_j)$$

$$\delta = (\delta_1, \ldots, \delta_P)^T$$

$$\delta_k = \frac{1}{4N} \sum_{j=1}^{N} V_j^2 \cos(k\lambda_j)$$

$$A = (\Gamma + \gamma^{-2} B^{-1}) = (B\Gamma + \gamma^{-2} I)^{-1} B$$

$$\Gamma = [\frac{1}{4N} \sum_{j=1}^{N} V_j^2 \cos(m\lambda_j)\cos(n\lambda_j); \quad m, n \in \overline{1, P}]$$

Thereby, the asymptotically optimal Bayes test for array detection of seismic signals with unknown spectrum is:

$$q_\gamma(x_N) = \begin{cases} 1 \text{ (signal is present)} & \text{if } r_\gamma(x_N) > k_\alpha \\ 0 \text{ (signal is absent)} & \text{if } r_\gamma(x_N) < k_\alpha \end{cases} \tag{7}$$

where the threshold k_α is determined on the basis of the given false alarm error probability, and the fitting parameter γ is determined so as to provide the highest asymptotical efficiency for the test (Kushnir *et al*, 1983).

Let us consider in particular two important (diametrically opposite) cases, where:

1. The power spectrum parameters of the source signal are almost known:

$$\| B \| << \| \Gamma^{-1} \|$$

2. The *a priori* information about these parameters is negligible:

$$\| B \| >> \| \Gamma^{-1} \|$$

In these cases, the statistic $r_\gamma(x_N)$ of the test (7) is simplified and looks like, respectively:

$$\begin{aligned} 1) \quad r_1(x_N) &= \Delta_0 + b^T \Delta \\ 2) \; r_{2\gamma}(x_N) &= \gamma(\Delta_0 - \Delta^T \alpha) + \frac{1}{2} \Delta^T \Gamma^{-1} \Delta \end{aligned} \tag{8}$$

Calculation of the test statistic (8) can be realized in the time domain as shown in Fig. 7.7.1.